Call: RFCS-2024

Project no. **101216750**

COFA
COal to FArm

Regional Agricultural Reclamation Suitability Maps

D3.1

Funded by the European Union. Views and opinions expressed are however those of the author(s) only and do not necessarily reflect those of the European Union or European Research Executive Agency. Neither the European Union nor the granting authority can be held responsible for them.

Michaela Königová | VUHU
Lucie Tichá | VUHU
Michal Řehoř | VUHU
Kateřina Svobodová | VUHU
Marcin Maksymowicz | POLTEGOR
Makary Musiałek | POLTEGOR
Beata Merenda | POLTEGOR
Barbara Rogosz | POLTEGOR
Łukasz Pierzchała | GIG-PIB
Maria Bałazińska | GIG-PIB
Aikaterini Servou | PPC
Nikolaos Paraskevis | PPC
Christos Roumpos | PPC
Theodoros Zarogiannis | CERTH
Dimitris-Enias Liolis | CERTH
Nikolaos Koukouzas | CERTH

Version | 31.05.2026
Dissemination level | **Public**

Research Fund for Coal & Steel

Funded by the European Union

Table of contents

List of Abbreviations

BSI	Bare Soil Index
CEC	Cation-exchange capacity
CLMS	Copernicus Land Monitoring Service
ČSA	Czechoslovak Army Quarry
ČSG	Česká geologická služba (Czech Geological Survey)
ČÚZK	Český úřad zeměměřický a katastrální (Czech Office for Surveying, Mapping and Cadastre)
DEM	Digital Elevation Model
DMR 5G	Digitální model reliéfu (Digital Elevation Model 5th Generation)
ESA	European Space Agency
FVC	Fractional Vegetation Cover
HRL	High Resolution Layer
LAI	Leaf area index
LST	Land Surface Temperature
LUCAS	The Land Use and Cover Area frame Statistical survey
MARS	Multivariate Adaptive Regression Splines
MODIS	Moderate Resolution Imaging Spectroradiometer
NDBI	Normalized Difference Built-up Index
NDMI	Normalized Difference Moisture Index
NDVI	Normalized Difference Vegetation Index
NDWI	Normalized Difference Water Index
NIR	Near-infrared
R/RED	Red light
SCL	Scene Classification Map
Sen2Cor	Sentinel-2 Correction
SVM	Support Vector Machine
SWIR	Short-Wave Infrared
TIN	Triangle mesh
USDA	United States Department of Agriculture

List of Figures

1. Introduction

Selection of a suitable site for agricultural production, whether for energy crops or food production within the From COal to FArm project (COFA), is a crucial step that should consider all available information about the given area. The previous deliverable D3.2 focused primarily on soil dysfunctions, which significantly affect post-mining areas. Coal mining itself represents an extensive and destructive intervention in the landscape, and the accompanying soil dysfunctions further deepen this negative impact, making them an essential part of any territorial assessment.

D3.1 builds on this foundation and focuses on identifying the most suitable land for agricultural use. To make the selection as accurate and objective as possible, it is necessary to consider a set of relevant indicators and indices, which are described in detail in Chapters 2 and 3. The indicators are divided into two groups, main and supplementary. Main indicators in this case include terrain topography with elevation, slope, land surface temperature and water conditions. Supplementary indicators encompass, for example, vegetation cover, human pressure and land use. The combination of all these parameters enables a gradual narrowing of the selection. Some areas can be excluded as unsuitable based on the collected data, while others emerge as promising candidates for agricultural use.

Suitability maps created for this output are designed to directly follow up on other parts of the COFA project (D3.3 and D3.4). The analysis in the form of map outputs and basic characteristics of the area will serve as a basis for assessing which reclamation approaches are most suitable given the specific conditions of the substrate and the land use history in each study area. This will be reflected in D3.3. It will be also necessary to evaluate the potential of identified sites for low-carbon agricultural practices and the production of energy crops, in connection with the subsequent D3.4. The interrelations with other COFA tasks is illustrated on Figure 1.

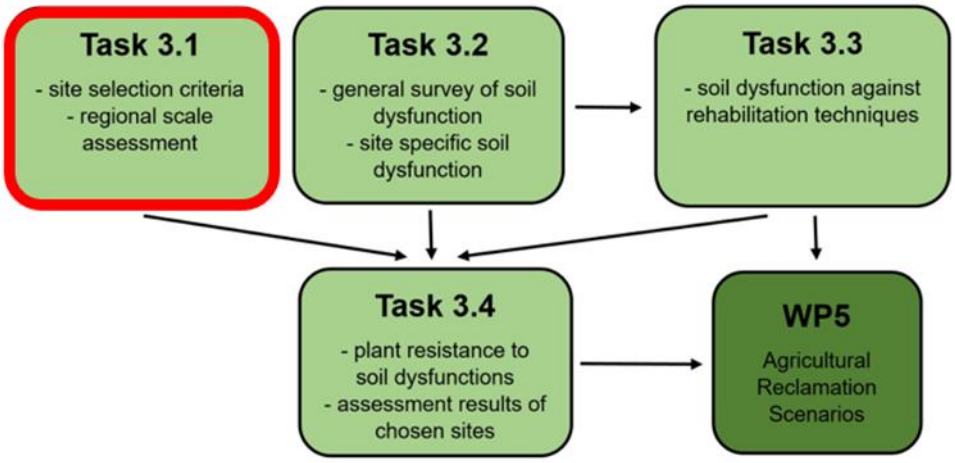

Figure 1 Interrelations with other COFA tasks

2. Main Indicators and Indices

The primary indicators represent key factors for identifying land suitable for agricultural production in post-mining areas and form the basis for initial decisions whether spoil heaps or specific parcels located on them are eligible for agricultural use. These indicators include elevation and terrain steepness, which are determined by a digital elevation model, as well as surface temperature and moisture conditions. The selection of key indicators was based on a logical assessment of the factors that need to be considered for agricultural production.

It should be noted that some of the main and supplementary indicators and indices are derived from European environmental databases, such as the Copernicus Land Monitoring Services, for which it is necessary to always specify the exact date and year of data acquisition. Since the outputs presented here serve only as a methodological proposal for a guideline on how to properly select suitable land for agricultural use, the closest available relevant dataset from 2025 was used. However, for practical application of this approach, it is essential to work with up-to-date data and to regularly update all map materials to reflect current conditions.

2.1. Digital Elevation Model (DEM)

Digital elevation models (DEMs) are a fundamental data source for terrain analysis in post-mining landscape assessments. By capturing the three-dimensional configuration of both natural and anthropogenic surfaces, DEMs enable the derivation of key morphometric parameters, most notably slope angle and elevation, which are directly relevant to evaluating land suitability for agricultural use. The analytical value of DEMs lies not only in the raw elevation values, but in their capacity to reveal subtle terrain structures that are not apparent on conventional topographic maps. This approach is central to geomorphometry, as it allows the visual identification of terraces, ground levels, anthropogenic interventions, erosional forms, and transitions between morphological units (Wood, 1996; Pike et al., 2009; Hengl, 2006).

In the context of this deliverable, DEM-derived parameters are applied across all study areas using locally available datasets. As an example of such a dataset for the Czech study area, the Digital Elevation Model of the Czech Republic, 5th generation (DMR5G), was used. DMR5G is a detailed digital representation of both natural and anthropogenic terrain, based on elevations of discrete points arranged in an irregular triangular network (TIN), with coordinates X, Y and H (altitude). Vertical accuracy reaches approximately 0.18 m in open terrain and 0.3 m in forested areas (ČÚZK, 2016). The model was created through airborne laser scanning performed between 2009–2013 and completed in 2016. It supports detailed terrain analyses, including land-consolidation projects, transport and water-management infrastructure planning, and modelling of local natural processes. It also serves as a base layer for contour generation and high-precision GIS visualizations (ČÚZK, 2016).

2.1.1. Angle of Slope

The angle of slope, derived from the digital elevation model, is an essential indicator for assessing the environmental impacts of mining. Slope influences water runoff, soil erosion and land stability—all of which affect habitat quality and biodiversity. Mining often creates steep, unstable slopes that accelerate erosion, increase topsoil loss and contribute to ecosystem degradation (Musiałek et al., 2024).

Slope is therefore crucial for sustainable land management in post-mining landscapes. Slope-based land classification helps target restoration efforts and maintain ecological balance. According to Paulo (2008) and Chodak (2013):

- **< 5°** – suitable for most agricultural crops
- **< 15°** – suitable for less intensive agriculture, e.g., grazing
- **< 35°** – suitable for forestry
- **< 60°** – forestry still possible with erosion-control measures
- **> 60°** – very unstable; requires engineering-intensive reclamation

Steep slopes exhibit high erosion risk, though south-facing steep escarpments may host valuable dry grassland habitats with high biodiversity (Musiałek et al., 2024).

For agricultural reclamation on spoil heaps, gentle slopes (< 4–7 %) are generally preferred because they allow better infiltration, reduce stagnation and prevent erosion.

Slope-based classification therefore enables mining companies and land managers to design restoration strategies that respect the natural terrain capacity and support long-term ecological recovery.

2.1.2. Elevation

Wood (1996) emphasizes that DEMs, particularly slope and steepness, allow for a much more sensitive characterization of surface morphology than elevation alone, as they capture spatial variations and surface gradients. Pike et al. (2009) add that combining multiple geomorphometric parameters in a single map (e.g., edge highlighting + colour scale + brightness gradient) provides a significantly more informative picture of landforms and their hierarchy. Hengl (2006) builds on this idea, demonstrating that the use of distinct colour scales and methods that highlight local changes in the terrain can make even subtle surface shapes visible, which would remain hidden in commonly simplified elevation models.

In the context of post-mining landscape assessment, elevation analysis is therefore employed not as a standalone parameter, but in combination with slope and additional terrain derivatives. Together, these indicators help identify terrain that is morphologically stable and spatially suitable for agricultural reclamation.

2.2. Land Surface Temperature (LST)

Land surface temperature (LST) represents the temperature of the Earth's surface and reflects the exchange of energy between the land surface and the atmosphere. It is a key variable in remote sensing studies because it is closely linked to surface energy balance, land cover, and climatic processes. LST is commonly derived from thermal infrared satellite data, and its accuracy strongly depends on correct characterization of the surface radiative properties, as well as atmospheric conditions. Due to its spatial detail, LST is widely applied in studies of urban heat islands, land degradation, and environmental impacts of human activities (Parastatidis et al., 2017).

2.3. Water Conditions

2.3.1. Scene Classification Map

The Scene Classification Map (SCL) is one of the key outputs of the atmospheric correction processor Sen2Cor, designed to classify basic surface types and assess the quality of Sentinel-2 imagery. According to Main-Knorn et al. (2017), SCL is produced by an algorithm developed for the European Space Agency (ESA) and categorizes pixels into twelve classes, such as vegetation, bare soil/desert, water, clouds or snow (Figure 2).

Documentation from Copernicus further explains that the primary purpose of SCL is to distinguish between clear, cloudy and water-related pixels, serving as a support tool rather than a full land-cover map. Recent versions of Sen2Cor continue to refine the accuracy of SCL and incorporate adjustments to Sentinel-2 product specifications, including updated class naming and integration of new auxiliary datasets (ESA Release Notes, 2024).

Value	Scene Classification	HTLM color code	Color
0	No Data (Missing data)	#000000	
1	Saturated or defective pixel	#ff0000	
2	Topographic casted shadows (called "Dark features/Shadows" for data before 2022-01-25)	#2f2f2f	
3	Cloud shadows	#643200	
4	Vegetation	#00a000	
5	Not-vegetated	#ffe65a	
6	Water	#0000ff	
7	Unclassified	#808080	
8	Cloud medium probability	#c0c0c0	
9	Cloud high probability	#ffffff	
10	Thin cirrus	#64c8ff	
11	Snow or ice	#ff96ff	

Figure 2 Scene Classification Map colour legend. Source: Copernicus / ESA

2.3.2. Normalized Difference Moisture Index (NDMI)

The Normalized Difference Moisture Index (NDMI) measures vegetation moisture using reflectance in the NIR and SWIR spectral bands (Equation 1). The concept of using NIR–SWIR reflectance differences to estimate vegetation water content was first introduced by Gao (1996), who demonstrated that SWIR reflectance responds strongly to changes in internal leaf water content, while NIR reflectance is affected mainly by leaf structure and dry biomass.

$$NDMI = \frac{NIR - SWIR}{NIR + SWIR} \quad [1]$$

According to Copernicus/Sentinel Hub, combining NIR and SWIR helps reduce the influence of leaf structure and dry matter, improving the accuracy of vegetation moisture assessment. NDMI effectively captures variations in water content in tree canopies and herbaceous vegetation, with decreasing SWIR reflectance indicating increasing water content.

For Sentinel-2 imagery, NDMI is widely used to monitor vegetation stress, drought, and forest disturbances. Taloor et al. (2021) highlight NDMI's suitability for hydrological studies, moisture assessments and identifying spatial differences in water availability within landscapes.

2.3.3. Normalized Difference Water Index (NDWI)

The Normalized Difference Water Index (NDWI) was introduced by McFeeters in 1996 as a method designed to enhance open water surfaces in remotely sensed data. The index utilizes a combination of the green band and near-infrared radiation, based on the principle that water strongly absorbs light in these parts of the spectrum. NDWI thus suppresses the influence of soil and vegetation, enabling better identification of water bodies and potentially allowing assessment of their turbidity. However, the method is sensitive to the presence of built-up areas, which may exhibit spectral properties similar to water, potentially leading to their erroneous classification as water surfaces (McFeeters, 1996; Musiałek et al. 2024). The Copernicus web tool states that NDWI values above 0.5 are typically considered water bodies, vegetation reaches lower values, and built-up areas range around 0 to 0.2.

The present study confirms the importance of NDWI in analyzing changes in water resources, particularly in areas experiencing significant water level fluctuations or long-term drought. Mahmood et al. (2025) applied NDWI to monitor drought conditions in major lakes in Iraq, analyzing changes in the extent of three key lakes over the period 1987–2014, supplemented by classification of current conditions using SVM (Support Vector Machine) on Sentinel-2 imagery. The results revealed significant changes in both the shape and extent of water bodies; for example, Lake Razzazah lost approximately 67% of its surface area between 2000 and 2014. NDWI was employed as a key indicator for quantifying changes in water levels and for supporting the design of water management measures, confirming its versatile applicability in hydrological and environmental studies (Mahmood et al. 2025).

3. Supplementary Indicators and Indices

In addition to the main indicators and indices, a set of supplementary indicators and indices can also be employed to assess the suitability of land in post-mining areas for agricultural production. These include soil texture, vegetation Index (NDVI), urban pressure (HRL) and erosion risk assessment. None of these indicators individually represents a primary determining factor. However, their combined use provides valuable supplementary information that helps to refine the overall assessment of the agricultural potential of landscapes affected by previous mining activity.

3.1. LUCAS Topsoil Survey and USDA Soil Textural Triangle

The *LUCAS Topsoil Survey* (Land Use and Cover Area frame Statistical Survey) database was used to map soil physical properties at the pan-European scale. Several key soil characteristics were modelled using hybrid methods, particularly *regression kriging*. For these datasets, topsoil texture and other derived physical properties were predicted. The regression models relied, among other inputs, on remotely sensed data from the MODIS (Moderate Resolution Imaging Spectroradiometer) sensor, whose high temporal resolution makes it possible to capture vegetation response patterns that reflect soil properties. This information can then be used to refine the spatial mapping of soil features (Ballabio et al., 2016).

Following this physical-property mapping phase, a subsequent study by Ballabio et al. (2019) focused on soil chemical properties, including pH, CEC, $CaCO_3$ content, nitrogen, phosphorus, potassium, and other elements. The authors used Gaussian Process Regression, a method that enables modelling uncertainty and incorporating prior knowledge through covariance functions.

A major methodological contribution was also provided by Montanarella (2013), who described in detail the procedures of the LUCAS Topsoil Survey and created a robust continental database of nearly 20,000 soil samples. This study provided standardized procedures for sampling, laboratory analyses, and other methodological frameworks for subsequent modelling of soil physical and chemical characteristics.

Ballabio et al. (2016) additionally addressed approaches for predicting *interrelated* soil properties such as texture. This requires advanced techniques such as the MARS algorithm (Multivariate Adaptive Regression Splines). Model validation using cross-validation (a test which checks how well the model works with new data) showed that the LUCAS dataset is suitable and reliable for mapping soil properties. The models explained approximately half of the variation in soil texture, with errors typically ranging between 4 and 10 % (Ballabio et al., 2016).

Two of the most widely used field tools for soil classification are the USDA Soil Texture Triangle and the Munsell Soil Color Book. Both tools support particle size analysis. The Munsell Color Book development is well documented (Simonson, 1993), whereas the USDA texture triangle evolved over decades. Milton Whitney (1911) published the first graphic delineation of soil texture classes, originally eight categories. Davis & Bennett (1927) expanded the triangle to ten classes (clay loam and sandy clay). In 1938, the USDA revised the upper boundary of the clay fraction to align with the international system. The modern version of the texture triangle was published in 1951 (Soil Survey Staff, 1951) and includes 12 texture classes (University of Minnesota Soil Judging Team, 2014). LUCAS provides laboratory-measured proportions of sand, silt, and clay, allowing direct derivation of USDA texture classes.

3.1.1. Basic Characteristics of Grain Size Categories

Sand particles may consist of quartz or fragments of silicate rocks and feldspars. The sandy fraction ensures good soil drainage, as water infiltrates quickly between particles. Soils with high sand content are permeable and well-aerated, but they also dry out rapidly in dry weather. Their sorption capacity is low (Šarpatka, 2014).

Silt consists of medium sized particles, between sand and clay. It is commonly found in soils formed on loess. Silt contributes to favourable physical properties and an optimal balance between water and air content (Šarpatka, 2014).

Clay belongs to the fraction with very small particle size and high specific surface area. Fine colloidal clay has a surface area approximately 10,000 times larger surface area than medium-sized sand particles. Clay strongly influences soil porosity, water and air regime, and nutrient availability within the sorption complex. Consequently, it also affects the soil's biological component (Šarpatka, 2014).

Various grain-size classification systems exist, but they generally agree that particles < 2 mm form the soil fine earth fraction. Subdivisions within the fine earth differ only slightly between classification systems (Table 1). United States Department of Agriculture (USDA) texture is illustrated in Figure 3.

Table 1 Grain size fractions in individual classifications (mm; Šarpatka, 2014)

	BSI (British standards Institutions)	ISSS (International Society of Soil Science)	USAD (United States Department of Agriculture)	KPP (Koplexní průzkum půd – ČR)
Clay	< 0,002	< 0,002	< 0,002	< 0,001
Silt	< 0,06	< 0,02	< 0,05	< 0,05
Sand	< 2,0	< 2,0	< 2,0	< 2,0

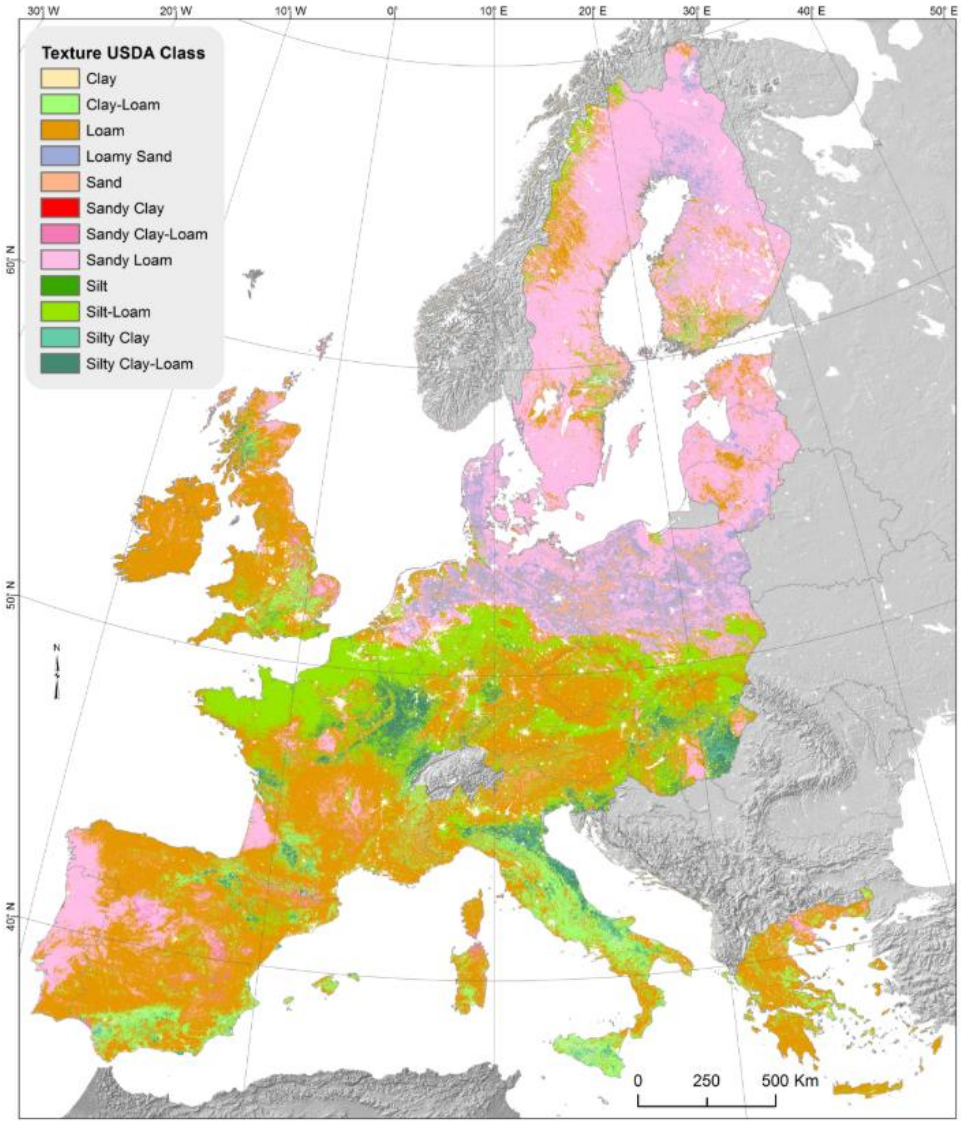

Figure 3 Texture USAD Class for Europe. Source: esdac.jrc.ec.europa.eu

3.2. Vegetation Conditions

3.2.1. Normalized Difference Vegetation Index (NDVI)

The Normalized Difference Vegetation Index (NDVI) is one of the most widely used indicators of vegetation health and biomass in remote sensing. It was first clearly defined by Kriegler et al. (1969), who observed that live vegetation strongly reflects near-infrared radiation (NIR) while absorbing red light (RED) due to chlorophyll. NDVI uses a simple ratio to express the contrast between high NIR reflectance and low RED reflectance (Musiałek et al., 2024). Rouse et al. (1973) later introduced NDVI into satellite practice.

Carlson & Ripley (1997) showed that NDVI correlates with fractional vegetation cover (FVC) and leaf area index (LAI). Variations in NDVI reflect differences in leaf optical properties and canopy structure, supporting its use as a proxy for vegetation productivity.

Huang et al. (2021) provided a comprehensive overview of NDVI applications, confirming its robustness and long-term comparability despite known limitations (e.g., saturation in dense vegetation, soil background influence, atmospheric effects).

NDVI values range from –1 to +1 (Figure 4):

–1 to –0.1 → water surfaces
–0.1 to +0.1 → bare soil, rock, snow
0.2 to 0.4 → grasslands, shrublands
0.6 to 1.0 → dense, healthy vegetation

NDVI range	HTLM color code	Color
NDVI < -0.5	#0c0c0c	
-0.5 < NDVI ≤ 0	#eaeaea	
0 < NDVI ≤ .1	#ccc682	
.1 < NDVI ≤ .2	#91bf51	
.2 < NDVI ≤ .3	#70a33f	
.3 < NDVI ≤ .4	#4f892d	
.4 < NDVI ≤ .5	#306d1c	
.5 < NDVI ≤ .6	#0f540a	
.6 < NDVI ≤ 1.0	#004400	

Figure 4 NDVI colour legend. Source: Copernicus / ESA.

NDVI remains a foundational index used for ecosystem monitoring, agricultural assessment, drought detection, productivity modelling, and land-cover change analysis, supported by decades of literature (Kriegler et al. 1969; Rouse et al. 1973; Carlson et Ripley 1997; Huang et al. 2021). The NDVI calculation is defined in Equation 2; for Sentinel-2 in Equation 3 (Copernicus / ESA).

$$NDVI := \texttt{Index}(NIR, RED) = \frac{NIR - RED}{NIR + RED} \quad [2]$$

$$NDVI := \texttt{Index}(B8, B4) = \frac{B8 - B4}{B8 + B4} \quad [3]$$

The Copernicus Land Monitoring Service (CLMS) is highly suitable for monitoring NDVI due to globally available, regularly updated products with a 10-day temporal resolution and ~300 m spatial resolution. CLMS supports environmental monitoring, drought assessments, and long-term vegetation trend analyses (Swinnen et al., 2021).

3.2.2. Bare Soil Index (BSI)

BSI combines blue, red, near-infrared (NIR), and shortwave infrared (SWIR) spectral bands to capture the variability of the soil surface. The SWIR and red bands are used to quantify the mineral composition of the soil, while the blue and NIR bands suppress the influence of vegetation (Rikimaru et al., 2002; Mzid et al., 2021). The index is calculated according to the formula: **BSI = ((SWIR1 + Red) − (NIR + Blue)) / ((SWIR1 + Red) + (NIR + Blue))**. BSI is a combination of NDVI and the Normalized Difference Built-up Index (NDBI) and constitutes a spectral index that enhances the detection of exposed soil surfaces and uncultivated areas by exploiting soil reflectance characteristics. Values range from −1 to 1, where a higher value indicates the barest soil (Rikimaru et al., 2002). Pixels with a BSI value above 0.021 are classified as bare soil (Diek et al., 2017). The threshold for bare soil extraction may, however, vary between 0.02 and 0.08 depending on the study area and the data used (Diek et al., 2017; Mzid et al., 2021; Vaudour et al., 2021). The index is applied particularly in the mapping of areas potentially affected by land degradation and soil erosion (Salas et Kumaran, 2023).

3.3. High Resolution Layer Imperviousness (HRL Imperviousness)

The High-Resolution Layer Imperviousness (HRL Imperviousness) is a key component of the Copernicus Land Monitoring Service, mapping the extent of artificial, sealed surfaces such as roads, buildings or infrastructure with spatial resolution of 10 m and 100 m. The layer provides harmonized European-scale data on the percentage of surface sealing (0–100 %), which is essential for monitoring urbanization, assessing runoff patterns, flood risk, soil function loss, and heat-island effects.

HRL Imperviousness supports urban planning, land-use management and environmental assessment by showing how human activity alters landscapes. Strand (2022) confirmed the accuracy of HRL Imperviousness in environmental monitoring, while Lefebvre et al. (2016) demonstrated how Sentinel-2 data can be used to efficiently update and refine this layer.

4. Study Areas Description

The selected indicators and indices, designed to support the identification of post-mining sites suitable for agricultural reclamation, are applied below to individual partner countries (the Czech Republic, Greece, and Poland). These countries have a long tradition of coal mining and are also actively involved in the reclamation of mining-affected areas. Deliverable D3.1 aims to identify the most suitable land and reveal its potential within the context of the COFA project.

For the Czech Republic, the area of interest is the Most Basin; for Greece, the Ptolemaida Mining Area, and for Poland, the Konin Lignite Basin.

The use of a methodological proposal for assessing the suitability of land for agricultural use, developed within the COFA project, is purely theoretical in nature, and the authors bear no responsibility for reliable feasibility.

4.1. Most Basin (CZ)

The Most Basin is the largest brown coal basin in the Czech Republic located in northwestern Bohemia (Figure 5). Its geological history together with intensive lignite mining have significantly influenced the landscape, soil structures, and ecological stability in the region. An extensive network of spoil heaps has been created as a result of mining. These spoil heaps are nowadays the main subject of reclamation and research activities.

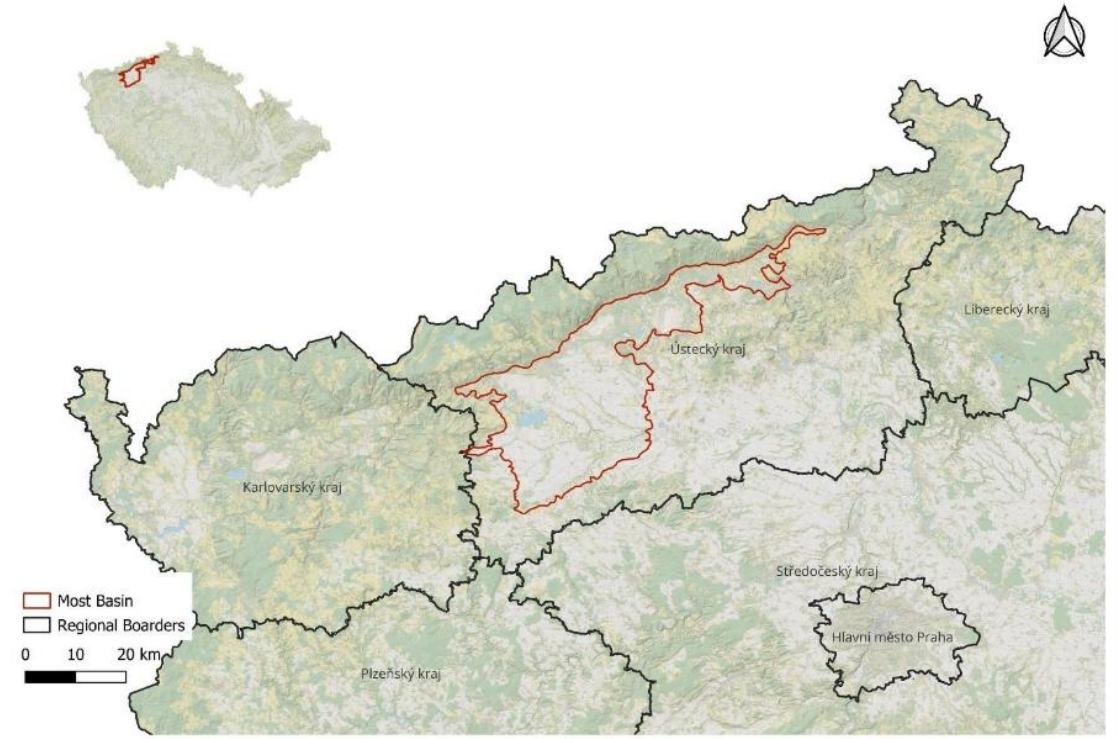

Figure 5 Location of the Most brown coal basin in the Czech Republic. Source: QGIS

4.1.1. General Characteristics of the Most Basin

Intensive brown coal mining has radically transformed the landscape of the Most Basin (Figure 6). An extensive network of open-pit mines, dozens of meters deep, has been created there. Once mining operations cease, these areas are subject to reclamation, which takes various forms depending on local substrate conditions and land-use objectives, including forestry, agriculture, hydric reclamation or succession. Mining also disrupted the hydrological regime, for example, in the city of Most it was necessary to continuously drain water, which lowered the groundwater level, and after pumping ceased, new lakes began to form in the pits, such as Lake Most, 71 metres deep, which was gradually flooded between 2008 and 2020. (Lipský, 2022; DIAMO, 2025).

From a geological perspective, overburden consists primarily of Tertiary clays, claystones, and sands. In some places, gravel layers overlie Quaternary loess and the original topsoil. The topsoil was temporarily removed during mining and later returned. However, in most reclaimed areas, we encounter anthropogenic soils. These soils were formed by mixing of materials from various depths and they differ significantly in structure and properties from the original agricultural soils. They are often physically unbalanced—the alternation of heavy clayey materials with permeable sands causes an uneven water regime. These soils tend to be poor in nutrients and organic matter and are characterized by extreme chemical properties. Acidity is a particularly serious problem: sulphides (especially pyrite in coal shales) are commonly found in exposed rocks, which oxidize into acidic sulphate compounds. This leads to a sharp drop in pH, often below 4, and to the release of hazardous elements into the soil. Consequently, extremely acidic and phytotoxic substrates form on many spoil heaps in the Most Basin, which results in the withering of sensitive plants, leaf chlorosis, and overall stunted vegetation growth (Řehoř et al., n. d.).

Another notable phenomenon, on the other hand, is the salinization and alkalization of some spoil heaps. At the Nástup Tušimice quarry, the overburden, in some places, contained gypsum, which, combined with the influence of limestone fly ash, led to increased soil salinity and an extremely alkaline pH. Highly alkaline substrates are also unsuitable for most plants—they cause a deficiency of available micronutrients and require subsequent chemical neutralization during reclamation efforts (Řehoř et al., n. d.).

A distinctive feature of the North Bohemian Most basin is that mining takes place at four geologically very different sites, which requires a selection of appropriate reclamation methods. At the Bílina open pit mine and, to some extent, in Vršany, the greatest problem is posed by the overburden of the coal seams. This overburden contains a high proportion of sandy material, but also very high levels of coal matter (approx. 5%) and sulphur (approx. 3%). The result is extremely acidic soils, which, when present on the surface, create phytotoxic areas requiring special reclamation procedures. Conversely, the soils at the Libouš and ČSA sites are generally more suitable. However, even there, especially at Libouš, we find substrates with an extremely high clay content. When placed in the topsoil horizons of reclaimed areas, these create sterile surfaces whose treatment requirements are entirely different from those of the acidic and phytotoxic substrates at the Bílina and Vršany mines (Řehoř, 2007).

This mosaic of geological conditions results in a diverse range of spoil soils with varying properties, which form the topsoil layers of both the outer and inner spoil heaps of open-pit mines. This, in turn, makes the reclamation of these areas exceptionally challenging, as it must always respect the specific characteristics of the particular substrate and location (Řehoř, 2007).

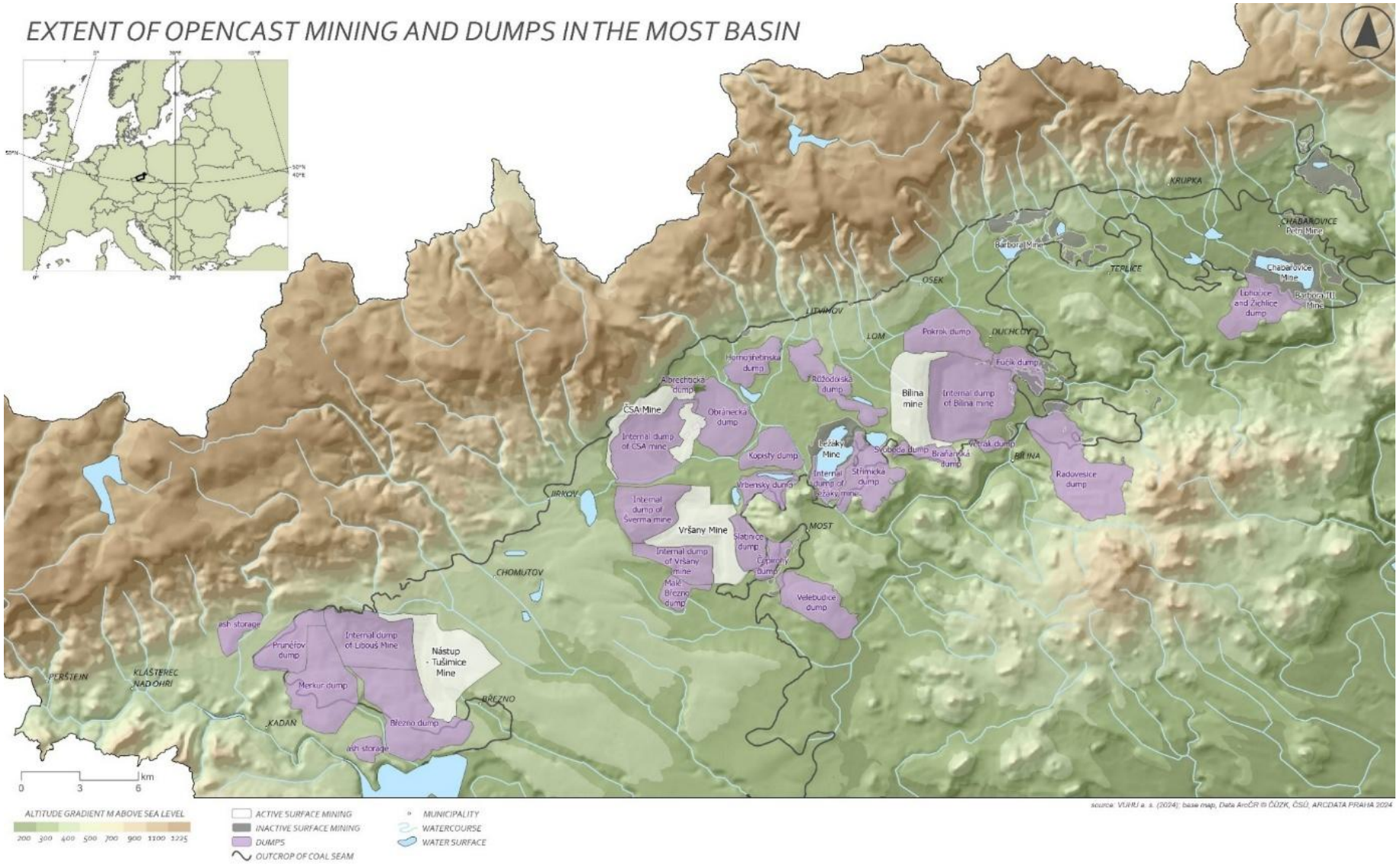

Figure 6 Actual situation of mining and reclamation in the Most Basin. Source: QGIS

4.1.2. Geological Development of the Most Basin

The Most Basin was formed during the Tertiary period, when its development began to take shape in the Lower Oligocene as a result of Alpine orogenic movements affecting the Bohemian Massif. Its further development was significantly influenced by the uplift of the Ore Mountains, the simultaneous formation of the Bohemian Central Mountains and the Doupov Mountains, which manifested themselves in a gradual subsidence of the basin floor. These geodynamic processes caused a gradual subsidence of the basin floor, which subsequently began to fill with thick layers of sandy and clayey sediments of Tertiary age (Grünbaum, 2011; Chlupáček et al., 2002).

The Lower Miocene was characterized by a warm and humid climate, which created conditions for the formation of extensive swamps accumulating organic matter. During the period between 22 and 17 million years ago, this matter reached a thickness of up to 500 m, and its subsequent diagenesis led to the formation of extensive brown coal deposits in the Most Basin. The main brown coal seam, reaching a thickness of 25–45 m in most of the area, was formed by the transformation of sedimented peat in Tertiary swamps. In places where rivers flowed into the peat-forming environment, coal formation was suppressed and the seam is replaced by river or delta sediments (Grünbaum, 2011).

The end of Miocene sedimentation subsequently resulted in the tectonically induced collapse of the basin and its elevation division during the Quaternary period. This period was characterized by alternating cold ice ages and warm interglacial intervals, which led to the intensive denudation of less resistant rocks and the formation of a relief similar to today's state. While the Žatec part of the basin is characterized by a higher contribution of sand and clay, the central area between Litvínov, Osek, Duchcov, Lom, and Mariánské Radčice represents the main coal center of the basin (Grünbaum, 2011).

The geological map of Most Basin is in Figure 7, legend in Annex 1.

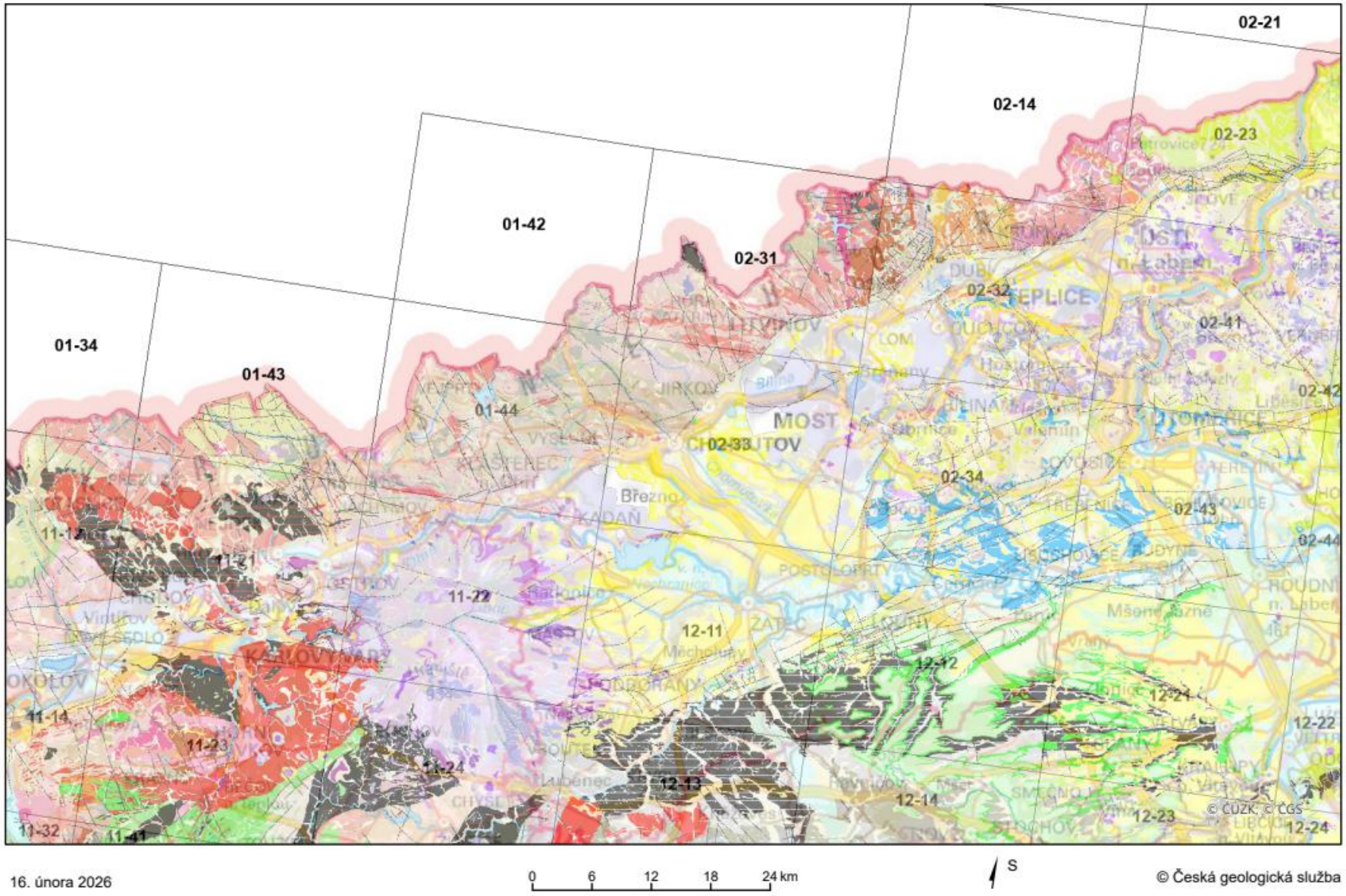

Figure 7 Geological map of the Most Basin. Legend in Annex 1. Source: Czech Geological Survey (ČGS)

4.1.3. Soil Characteristics of the Most Basin

- **Soil Texture According to USDA Classification**

The soil texture map based on the USDA classification (Figure 8) covers the entire territory of the Czech Republic and shows a marked predominance of loamy soils (Loam), depicted in orange colour, which form the most extensive areas, particularly in the central part of the country and in many of the more fertile lowlands. In higher and more rugged areas, Silt-Loam and Clay-Loam soils (green and light green shades) predominate, occurring continuously, for example, in the border mountain ranges. In several locations, particularly towards the northeast, southeast, and in local enclaves, Sandy Loam and Loamy Sand (pink and gray-blue areas) also occur, often in smaller, irregular blocks. In some places, smaller occurrences of Silt and finer textures such as Silty Clay Loam are also evident, although these types do not form extensive continuous units. The overall picture of the map thus shows that the Czech Republic is pedologically diverse, but loamy soils are the dominant texture, while fine-textured and sandier soils occur primarily in peripheral or geologically specific areas.

The same assessment applies to the Most Basin area; loamy soils (Loam) dominate, in this case primarily in the Ore Mountains range. Silt-Loam and Sandy Loam features are visible only from the foothills of the Ore Mountains. Silt and Silty Clay Loam are also visible in some places.

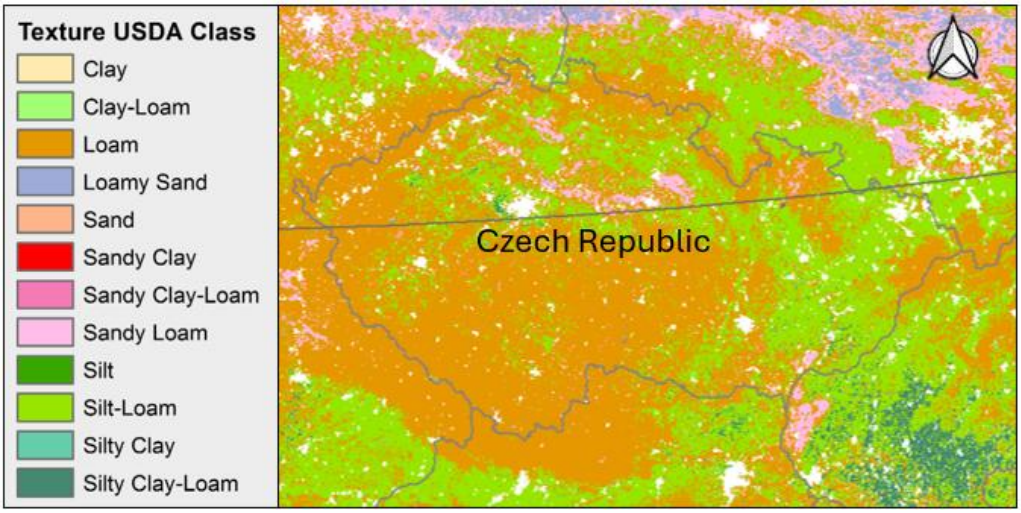

Figure 8 Texture USAD Class for Czech Republic. Source: esdac.jrc.ec.europa.eu

- **Pedological Map from the Czech Geological Survey**

The pedological map (Figure 9; legend in Annex 2) of the Most Basin shows a highly heterogeneous soil cover, reflecting the diverse composition of sediments and topography, as well as intensive human intervention. The central part of the basin is dominated by loamy or clay-loamy soils formed on loess and loess clays, which constitute the most fertile parts of the landscape. In areas with tertiary lake sediments or clayey coal-bearing layers (4.1.2), heavier clay soils prevail, often with poorer permeability. Around spoil heaps and reclaimed areas, anthropogenically formed soils of variable composition are evident, there texture depends on the type of deposited material.

Compared to the lowland basin, the adjacent Ore Mountains range exhibits a markedly different pedological profile. The soils here are predominantly sandy-loamy to loamy cambisols, developed on acidic crystalline rocks which are typical for this mountain range. With increasing elevation, skeletal soils become more common, these are prone to higher erosion and have lower fertility. Along the foothills of the Ore Mountains, a clear transition is evident between the fine-textured soils of the Most Basin and the coarser, more podzolized soils of the mountain range. In general, it can be said that the Most Basin is pedologically composed primarily of loamy textures, while the Ore Mountains transition into sandy, skeletal mountain soils.

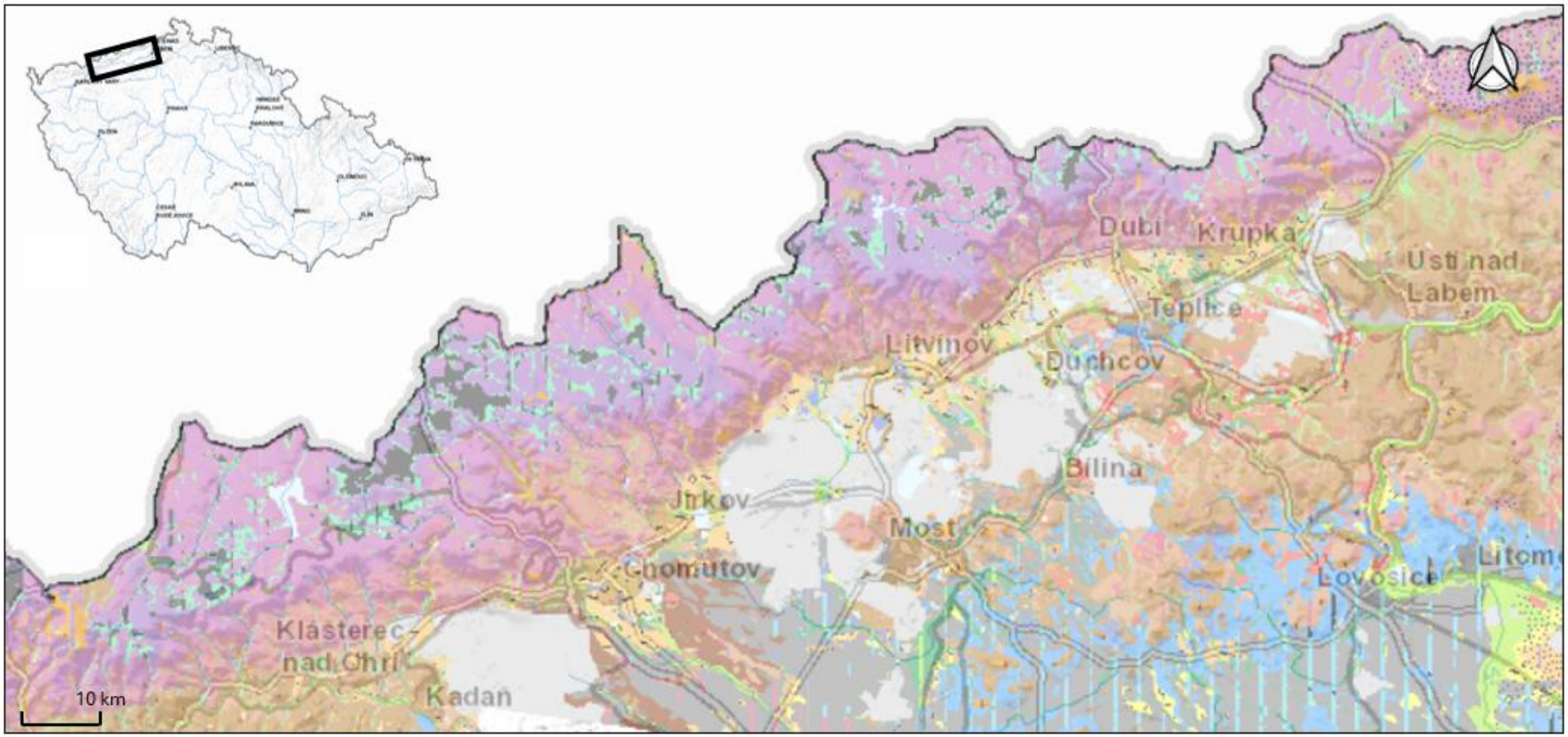

Figure 9 Pedological map of the Most Basin. Legend in Annex 2. Source: Czech Geological Survey (ČGS)

4.1.4. Reasons for Selecting Sites of Interest in the Most Basin

The majority of the Most Basin is formed by the largest brown coal deposits in the Czech Republic. Soil dysfunctions there are present in areas left to natural succession and on already technically reclaimed surfaces (as mentioned in D3.2). The Radovesice and Střimice spoil heaps are typical examples of this condition and were selected to illustrate the diversity of soil types, different approaches to reclamation, and varying degrees of phytotoxicity.

Both monitored spoil heaps are located outside the Ore Mountains belt, and therefore no input of metamorphites occurs here, nor does subsequent soil contamination by arsenic (a risk in the areas of the ČSA mine and Doly Nástup Tušimice), which would otherwise automatically exclude agricultural reclamation, particularly food production due to the accumulation of this hazardous element in biomass. Nevertheless, the area cannot be considered suitable even for energy crop cultivation. The main limiting factor is the risk of contaminated residual waste which would arise during subsequent biomass processing, where the environmentally safe management would pose a significant challenge. Potential use of these sites could therefore only be considered in the case of targeted phytoremediation measures. However, within the framework of the given project, this option can only be regarded as a secondary or supplementary objective, not as the primary one.

Sufficient long-term data and research results are available for both spoil heaps, enabling a qualified assessment of their properties and development trends. A particularly important source of information is the documentation and outputs from the REECOL project (RFCS-funded “Ecological Rehabilitation of post mining areas”, 2022–2025), upon which the COFA project can build and partially refer to within the relevant scope.

The Střimice site (former Ležáky mine) represents an exceptionally heterogeneous area burdened by a wide spectrum of soil dysfunctions, including erosion, acidification, and phytotoxicity. In the past, numerous reclamation interventions of varying types and success rates have been carried out here, including the application of reclamation additives (particularly bentonite from the Red Hill quarry), tree planting with variable outcomes, agricultural and hydric reclamation, measures with a recreational function, and the leaving of certain areas to spontaneous succession. This combination of different interventions, soil conditions, and developmental trajectories makes the Střimice site an exceptionally valuable area for experimental and long-term research, which is already receiving increased professional attention.

Selected parts of the area exhibit soil properties comparable to those in certain parts of the ČSA mine area, which is currently being prepared for restoration primarily through spontaneous succession. At the same time, research focused on the cultivation of the potential energy crop Miscanthus × giganteus is already underway here, allowing the Střimice site to serve as a reference and comparative area for evaluating the effectiveness of various reclamation and management approaches in similarly challenging experimental conditions.

The Radovesice spoil heap ranks among the most significant reclaimed and successional sites in the Czech Republic, with long-term documented positive results. Although certain dysfunctions occur here, they are less pronounced compared to the Střimice site. The site demonstrates considerable potential for agricultural reclamation, which has already proven successful in practice. Thanks to the achieved stability of the soil environment and the successful outcomes of previous interventions, the Radovesice spoil heap can serve as a reference site for evaluating the feasibility and success of experimental solutions under comparable conditions.

Both spoil heaps thus represent a striking and methodologically valuable contrast. On one side stands the Střimice spoil heap, characterised by a high degree of soil dysfunctions and phytotoxicity, posing a significant challenge for meaningful and sustainable land use. On the other side lies the Radovesice spoil heap, which has shown promise from the outset, has been successfully reclaimed, and currently exhibits optimal conditions for agricultural use.

Also noteworthy is the fact that the straight-line distance between these two fundamentally different sites is approximately seven kilometres (in a straight line). This clearly illustrates the remarkable spatial variability of the Most Basin landscape, heavily influenced by mining activity, and emphasizes the importance of locally specific reclamation approaches.

The variability of these sites was deliberately chosen to enable the evaluation of various forms of post-mining soil dysfunctions and to gain a broader overview of potential issues not only in the monitored areas but across the Most Basin as a whole.

The fact that both sites have already undergone some phase of reclamation or spontaneous succession makes it possible to assess their current development and evaluate whether and if, under certain conditions, they could be suitable for energy crop cultivation in the future. Both areas with minimal dysfunctions and those burdened by severe dysfunctions must be considered, as even severely dysfunctional soils may, following targeted reclamation measures, acquire specific productive potential. In some cases, the potential is even higher on severely dysfunctional sites than on less dysfunctional sites which are primarily designated for food production.

- **Factors Influencing Site Selection – Topografy, Land Surface Temperature and Character of the Areas**

The Kopisty spoil heap, Hornojiřetín spoil heap, the internal spoil heap of the Vršany mine, and the adjacent Březno spoil heap are characterised by pronounced slope gradients and significant terrain relief (Figure 10; Figure 11; Figure 12). It is also evident that the spoil heaps in the vicinity of the Vršany mine exhibit elevated land surface temperature (LST) values, as is likewise apparent at the Nástup Tušimice and ČSA mine sites and their surrounding spoil heaps (Figure 13). For these reasons, the aforementioned areas were excluded from the selection of the most suitable post-mining sites for agricultural production.

The Nástup Tušimice and ČSA mine sites are furthermore problematic regarding their location at the foot of the Ore Mountains (Figure 11), from which metamorphites via runoff. As a result, there is an elevated probability of arsenic soil contamination in these areas, which further disadvantages their use for agricultural purposes.

Although the Pokrok and Fučík spoil heaps do not exhibit significantly elevated LST values and their slope gradients are not critically limiting (the terrain relief of the Fučík spoil heap is somewhat more varied) (Figure 13; Figure 11; Figure 10), these sites have already largely undergone substantial reclamation interventions. At the same time, only a limited number of suitable successional areas are present here, which were also subject to analysis within the framework of the project.

At the Pokrok site, a succession area of steppe character is present. However, its topographic conditions are not particularly suitable for the intended use (Figure 11). A successional area is also identified at the Fučík spoil heap, characterised by dense vegetation cover, similarly to a considerable part of the spoil heap itself. It would therefore be undesirable for the purposes of the project to disturb or destroy this relatively stabilised and ecologically valuable area.

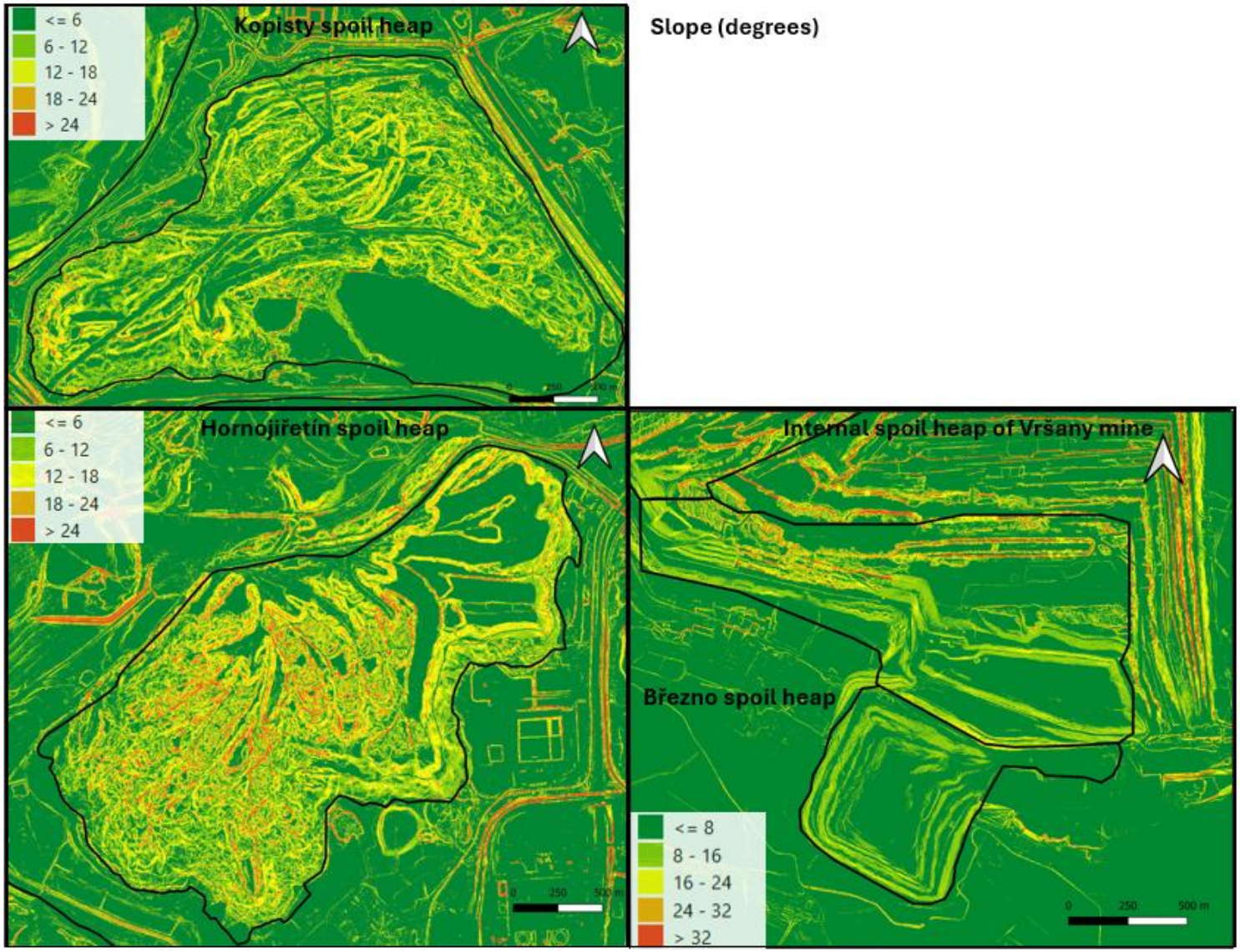

Figure 10 Slope of the Kopisty, Hornojiřetín, and Březno spoil heaps and Internal spoil heap of Vršany mine. Source: QGIS

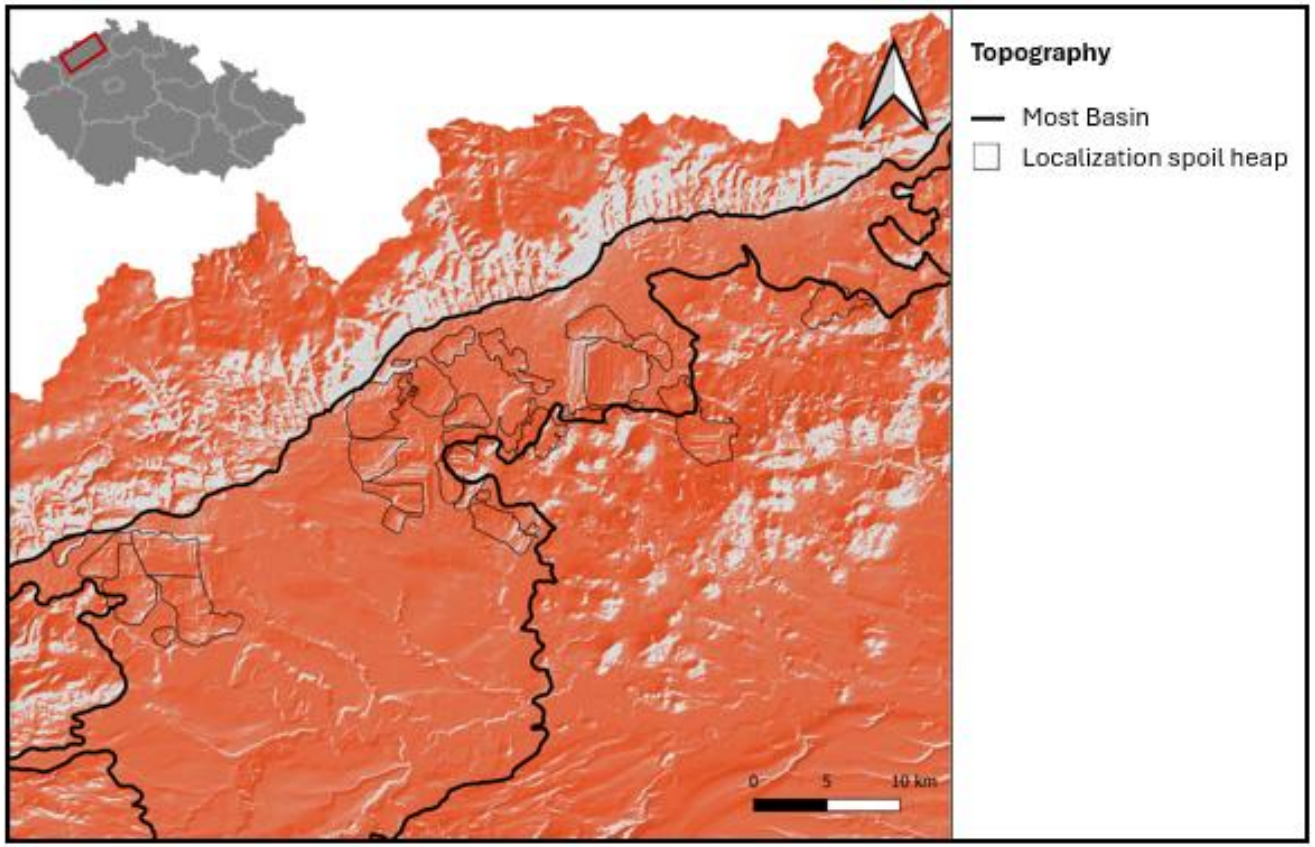

Figure 11 Topography of the terrain of Most Basin with indicated spoil heaps. Source: QGIS

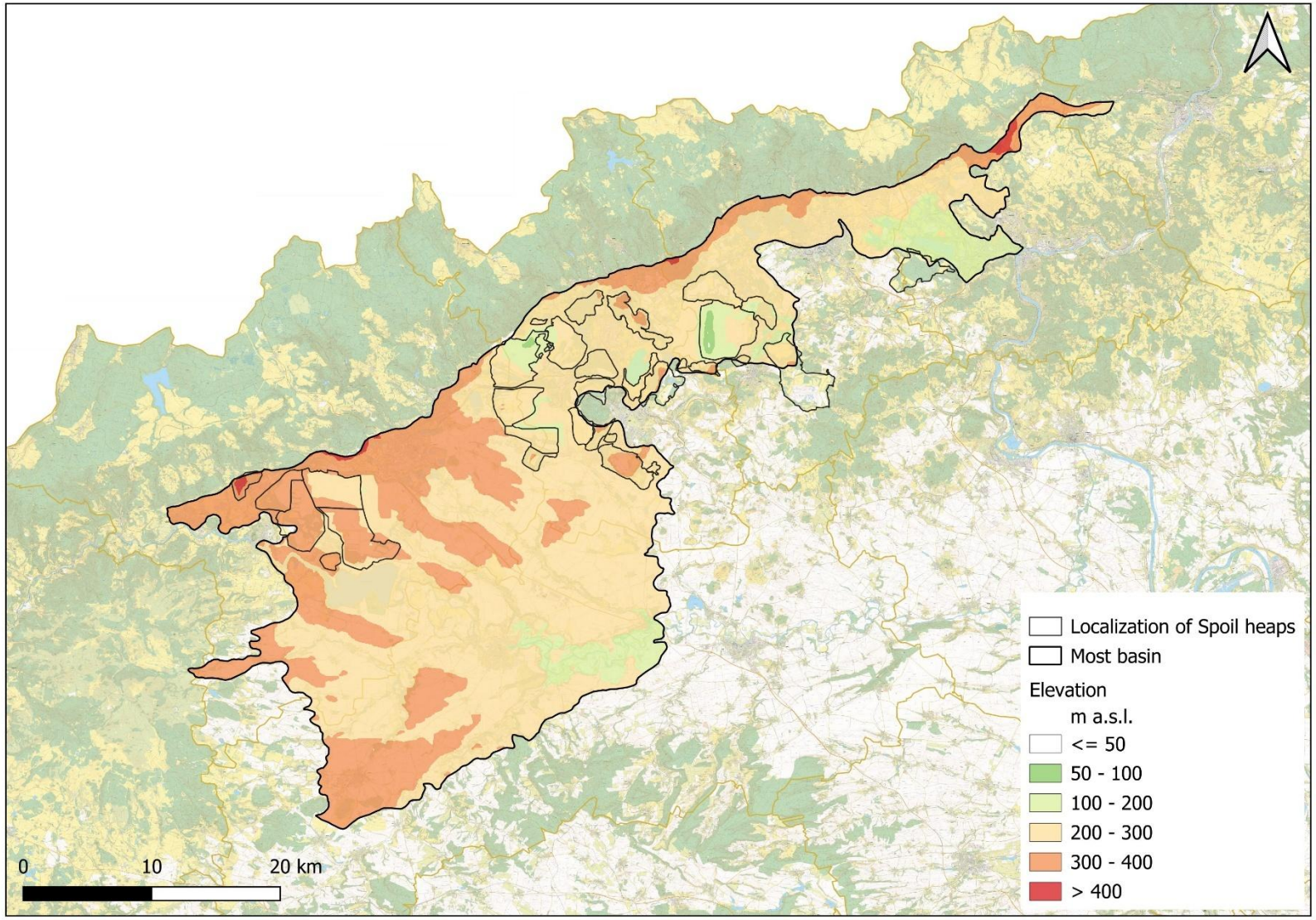

Figure 12 Elevation of the Most Basin with localization of spoil heaps. Source: QGIS

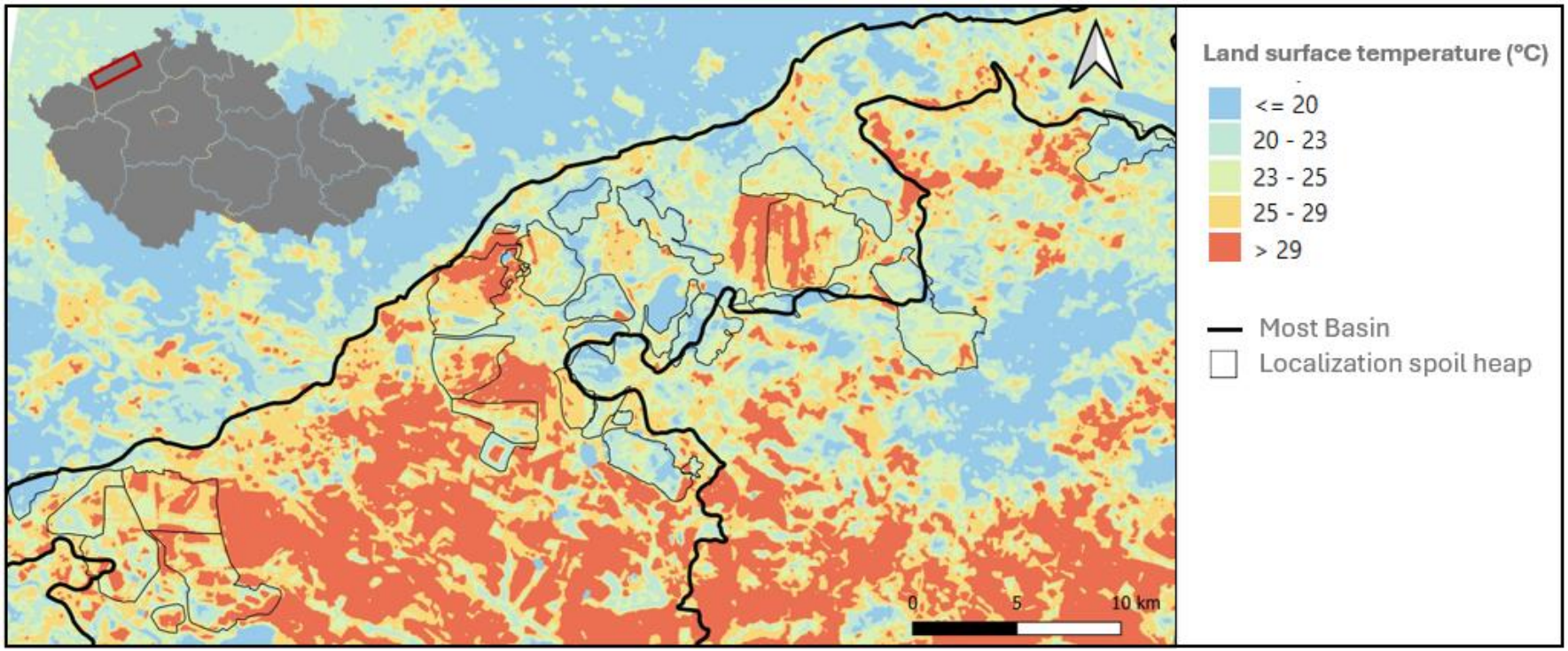

Figure 13 Land surface temperature of Most Basin with indicated spoil heaps, September 2025. Source: QGIS, landsatlst.appspot.com

4.1.5. Study area 1: Radovesice Spoil Heap

4.1.5.1. Characteristics of Radovesice Spoil Heap

The Radovesice spoil heap (Figure 14) is the largest spoil heap of the Severočeské Mines company. The construction of the dump began in 1964, and the placement of overburden was completed in 2003. Nowadays technical reclamation is practically completed. The pedological characteristics of the overburden soils at the Bílina quarry, deposited on the surface of the spoil heap, were highly unfavorable. The area was dominated by sterile sands that posed a safety hazard; to a lesser extent, there were dusty clays, and in rare cases, phytotoxic soils from stratified layers were present (Fraštia and Řehoř, 2014; Řehoř, 2022).

The first phase of the Radovesice spoil heap reclamation began in 1986 with the afforestation of a 30-hectare area (Fraštia et Řehoř, 2014; Řehoř, 2022). Marls were used to create a root zone. The spoil heap consisted of unsuitable overburden clays and quartz sands containing pyrite admixtures (Luxa, 1997). The second phase involved creating extensive marl deposits over an area of 120 ha. This was followed by the Radovesice III–Radovesice XVII phases. With the exception of experimental plots that were left to natural succession (Radovesice XVII), marl was used in all cases to create a rooted horizon (Fraštia et Řehoř, 2014; Řehoř, 2022).

Two sites covering 20 ha and 32 ha (Radovesice XVIIA and Radovesice XVIIB) were established as experimental sites for natural succession. Currently, these are long-term succession monitoring sites in the Most Basin and among the largest in the Czech Republic. On the reclaimed areas of the Radovesice spoil heap, forestry reclamation and other types of reclamation predominate, due to the creation of a recreational area for the town of Bílina. Agricultural reclamation is focused on the older, adjacent Jirásek spoil heap (Fraštia et Řehoř, 2014; Řehoř, 2022).

The application of marl and marlstone was primarily driven by availability, low costs, and the need to stabilize the sandy spoil body. This is not a common method. Consequently, even greater demands were placed on the correct methodology for applying marl and marlstone. According to a pedological survey, the application rates were adjusted over time. Today, high-quality forest reclamation is evident in the Radovesice I and Radovesice VI areas. The choice of reclamation method can be considered successful (Fraštia et Řehoř, 2014; Řehoř, 2022).

The research succession plots were established primarily for the long-term monitoring of naturally evolving soil properties. From a pedological perspective, the topsoil horizon of these plots can be considered stable, and its quality is similar to that of reclaimed surfaces. However, it should be noted that the experimental succession plots were selected based on a thorough pedological survey in locations with the highest-quality soils and low sand content (Fraštia et Řehoř, 2014; Řehoř, 2022).

- **Experimental Area Radovesice I**

This is a 30-hectare reclaimed site where marl and marlstone were applied. The site was established in 1991 and is the oldest monitored experimental site in the Most Basin. Originally, the site was dominated by spoil consisting of sandy clays and sands (Řehoř, 2007). The initial site preparations were completed in 1991, and today the site features mature forest reclamation (Fraštia et Řehoř, 2014; Řehoř, 2022).

- **Experimental Area Radovesice VI**

The 44-hectare reclaimed area was established in the western part of the Radovesice spoil heap. Marl was again applied here, and the original soil consisted of sandy loam and sand. Today, the area is aesthetically diverse, with a balanced mix of forest reclamation, grass planting, and hydrological reclamation (Fraštia et Řehoř, 2014; Řehoř, 2022).

- **Experimental Area Radovesice XVIIA**

This is a northern succession site covering an area of approximately 20 hectares. The dominant soil type is a heterogeneous mixture of brown clay, gray clay loam, and gray sandy clay loam with a higher content of brown clay. Brown-gray kaolinitic-illitic clays are also found here. The southern boundary of the area is formed by so-called sand dunes. Furthermore, there are several small water bodies and wetlands, as well as two large natural reservoirs (Řehoř, 2007; Fraštia et Řehoř, 2014; Řehoř, 2022).

- **Experimental Area Radovesice XVIIB**

The 32-hectare southern succession plot is similar to the experimental northern succession plot (Radovesice XVIIA). In the eastern part, sandy soils are present, which also form the boundary of the site. There are natural water bodies and small-scale wetlands here (Řehoř, 2007; Fraštia and Řehoř, 2014; Řehoř, 2022).

- **Former Quarry Jirásek**

Adjacent to the Radovesice spoil heap is the older, already reclaimed Jirásek site, where reclamation work began as early as 1973. Initially, only the slopes were reforested, primarily due to irregular subsidence. In the northern part of the Jirásek area near the village of Světec, 16.5 hectares were initially reclaimed; after 1983, afforestation continued on additional slopes covering 52.7 hectares. Once the subsidence had ceased, work began on restoring the plains at the individual levels and bringing in topsoil. On the first level, 100 ha were restored for agricultural use, and on the second, 77.6 ha. Silvicultural management is currently underway in the forested areas (Luxa, 1997).

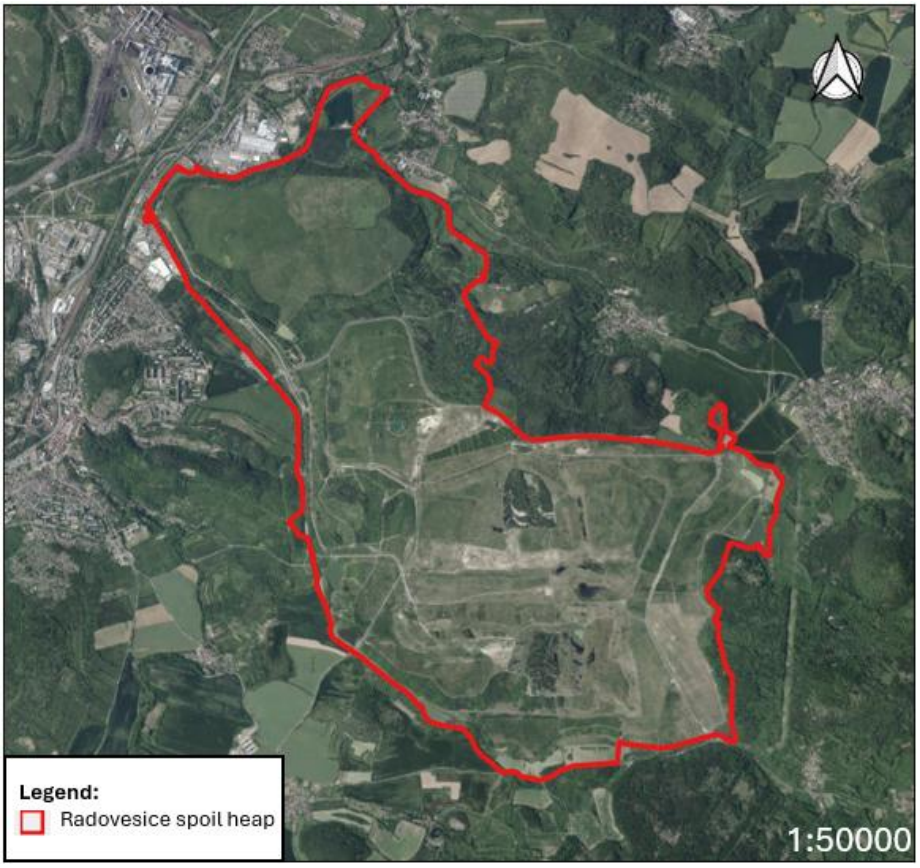

Figure 14 Radovesice spoil heap. Source: QGIS

- **Applied Reclamation Measures**

Due to unsuitable soil conditions, marl and marlstone were applied, this approach was chosen primarily for reasons of availability, low cost, and the need to stabilize the sandy spoil heaps. Since this is not a commonly used method, high demands were placed on the proper methodology for applying marl and marlstone. Based on long-term monitoring of the entire area, application rates were adjusted over time (Řehoř, 2022; Řehoř et al. n.d.).

Marlstone is a rock that is effectively used, particularly in improving the anti-erosion properties of texturally heterogeneous spoil soils in the Bílina region. Compared to, for example, loess clays, marls and marlstones have poorer soil properties, which are primarily influenced by a high content of calcite and, in unweathered rock, also by the skeleton. Weathered marlstones are mostly moderately to strongly water-retentive and weakly to moderately porous (Čermák and Ondráček, 2006). The only mined marlstone site in the Most Basin area consists of Cretaceous marlstones forming the geological surface of an erosional valley in the bedrock of the Radovesice spoil heap (Řehoř, 2007).

Today, high-quality forestry reclamation is evident in most of the reclaimed areas. The chosen reclamation method appears to be successful. This is currently the only application of marl and marlstone in the Most Basin (Řehoř, 2007). If similar post-mining areas face comparable soil dysfunctions in the future, the use of marl and marlstone could be considered as an alternative, but only after a thorough pedological survey and proper determination of application rates.

4.1.5.2. Use of Digital Elevation Model of Radovesice Spoil Heap

The digital elevation model shows that the Most Basin lies beneath the Ore Mountains (Figure 15). The Radovesice spoil heap has a significantly more rugged relief in the areas of succession, with the most rugged section located in the strip that separates these areas. In contrast, the older, predominantly agricultural part of the Jirásek spoil heap is characterized by a predominantly flat terrain.

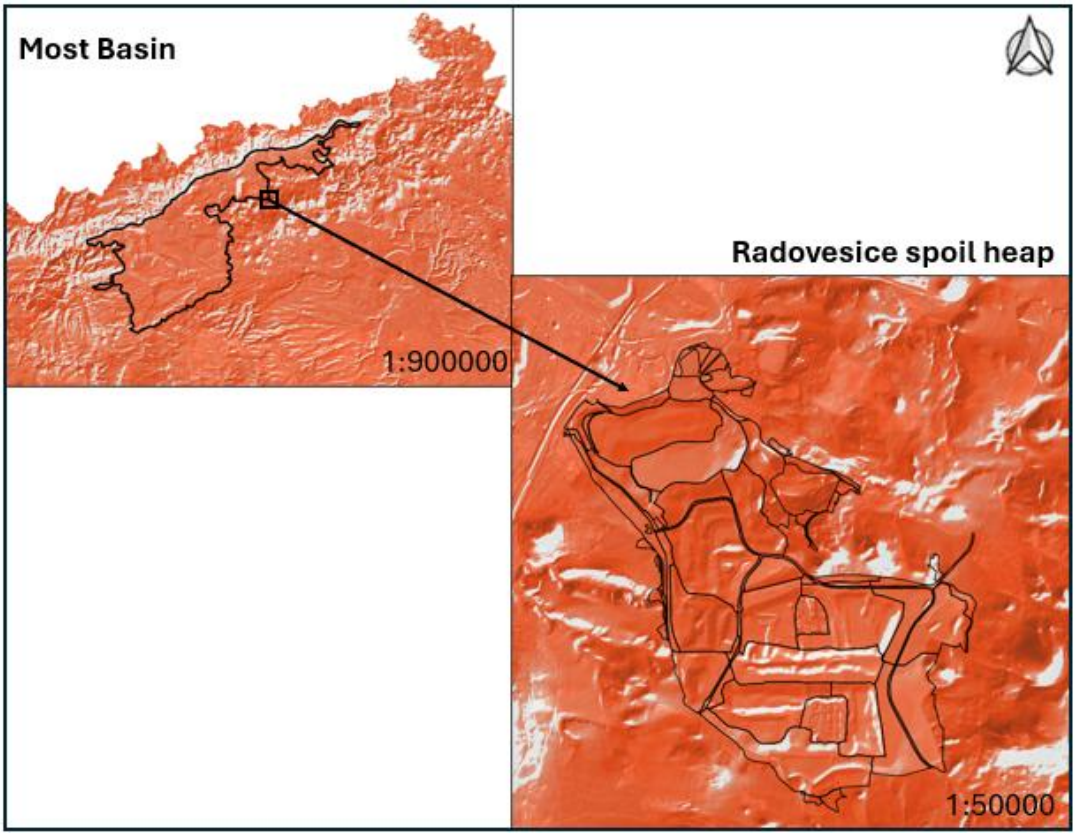

Figure 15 Digital Elevation Model of Most Basin and Radovesice spoil heap. Source: QGIS

- **Elevation of Radovesice Spoil Heap**

Figure 16 shows the elevation of the Radovesice spoil heap and its surrounding area. The northern, reclaimed part of the heap lies at lower elevations, while the successional areas and their surroundings are situated at higher elevations. Within the Radovesice spoil heap area, elevation does not exceed 400 m a. s. l., the nearest significantly higher point is Kloč Hill, which reaches over 700 m a. s. l.

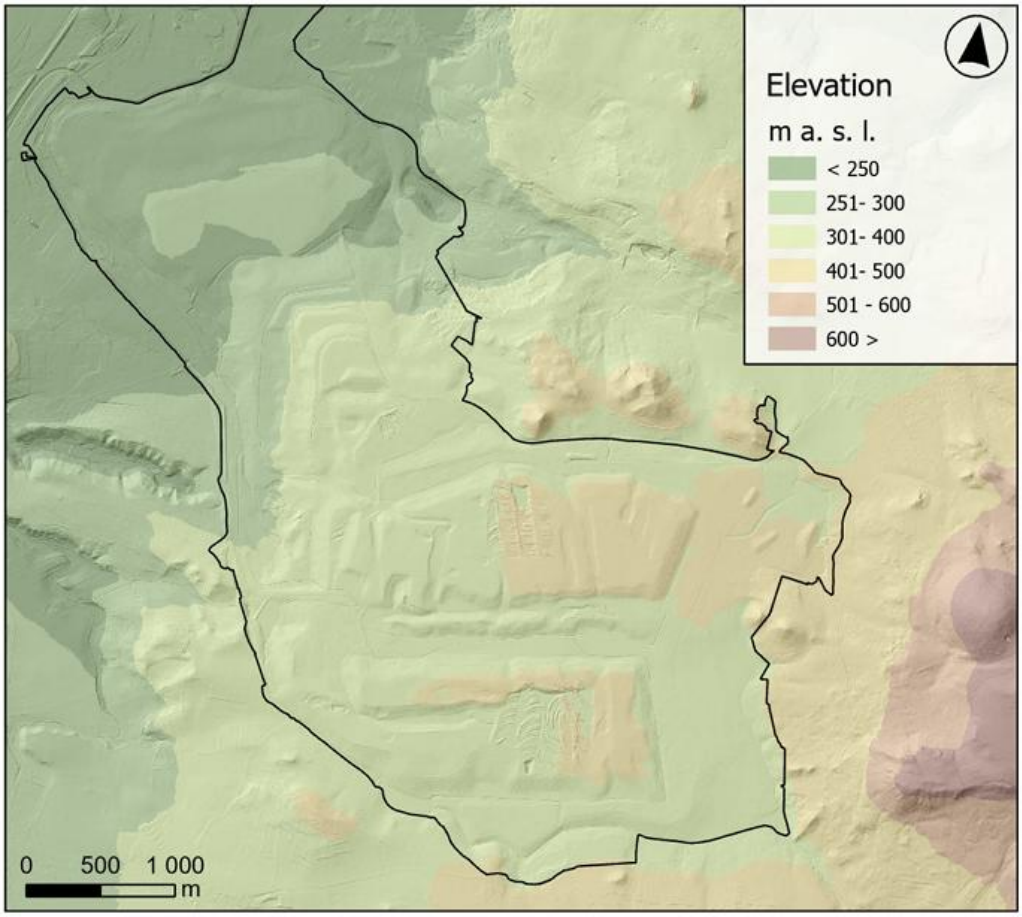

Figure 16 Elevation of Radovesice spoil heap. Source: ArcGIS

- **Steepness of Slopes at Radovesice Spoil Heap**

As the digital terrain model suggests (Figure 17), more pronounced slopes appear primarily in the succession areas and in their immediate surroundings. The greater slope of the terrain in these areas is not surprising, as no terrain modifications have taken place here. A relatively significant slope is also evident in the area below the Jirásek spoil heap, even though reclamation of the 'other' type has already been completed in this part and the area otherwise has a mostly modified character.

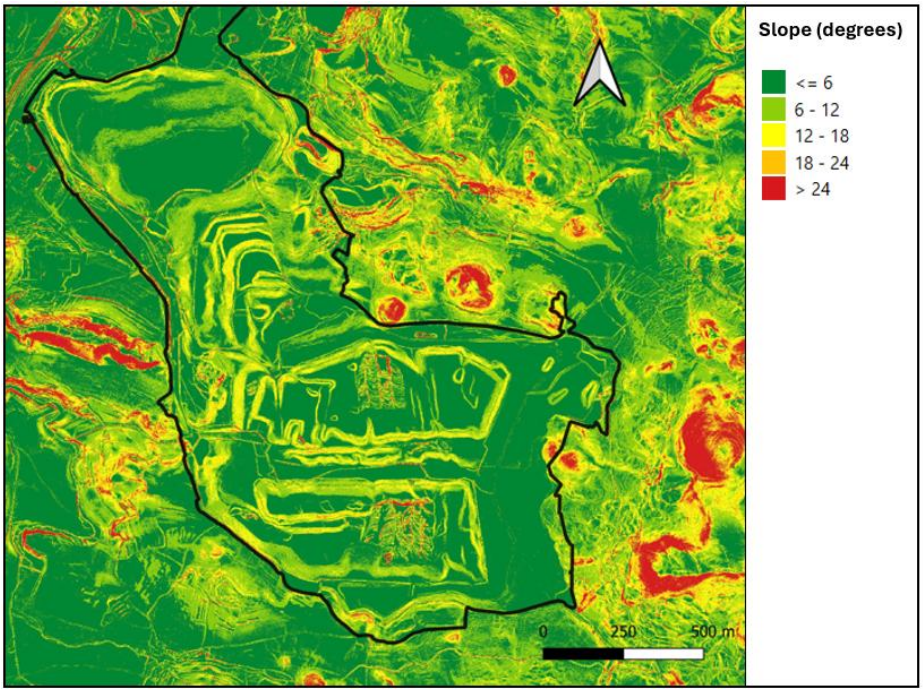

Figure 17 Slope of Radovesice spoil heap. Source: ČÚZK, QGIS

4.1.5.3. Situation at the Radovesice Spoil Heap

In the northern part of the map (Figure 18) lies the former Jirásek spoil heap, where agricultural reclamation now predominates, supplemented by forestry reclamation, hydrological reclamation occurs to a lesser extent. The Radovesice spoil heap is primarily in the active phase. Other reclamation predominates here, followed by forest reclamation and then agricultural reclamation. Smaller water bodies are more prevalent here than at the Jirásek spoil heap. It should be noted that the "other" category also includes the experimental succession areas Radovesice XVIIA and Radovesice XVIIB.

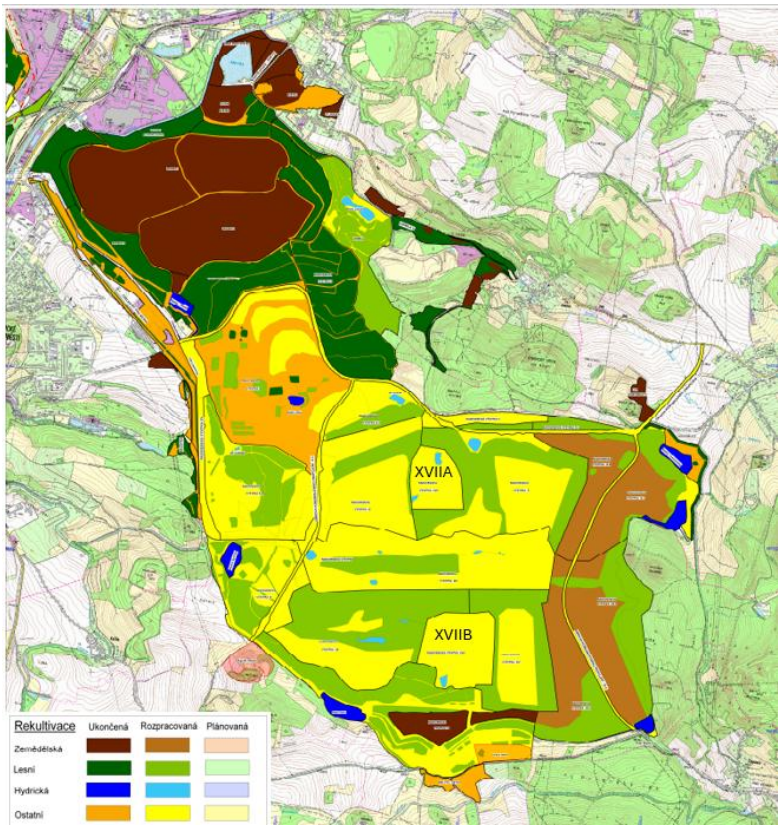

Figure 18 Land use of Radovesice spoil heap

4.1.5.4. Water Conditions of Radovesice Spoil Heap

- **Scene Classification Map of Radovesice Spoil Heap**

The map below (Figure 19) shows a scene classification map. The image clearly shows that vegetation dominates the area. Areas without vegetation cover are also visible, though to a lesser extent, particularly in the southern and southeastern parts. Small bodies of water are also visible, mainly at the edge of the polygon.

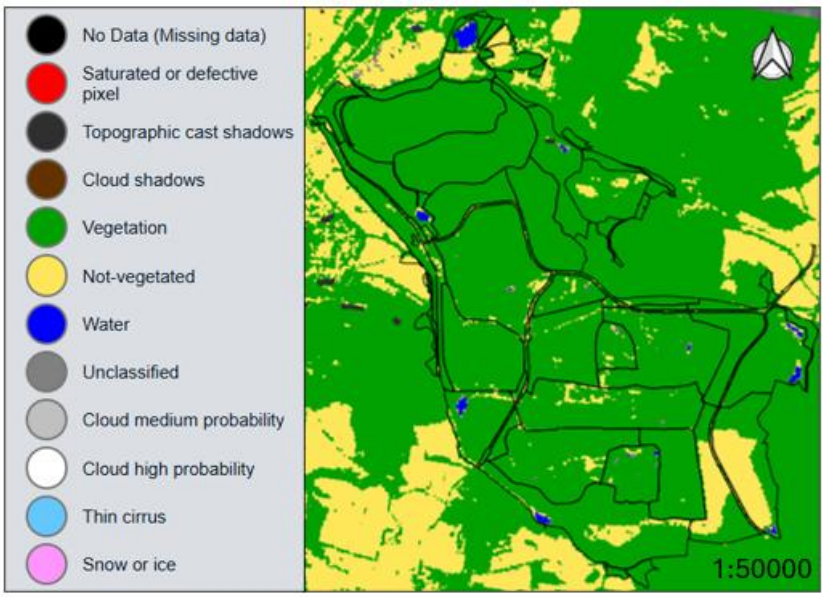

Figure 19 Scene classification map for Radovesice spoil heap, September 2025. Source: copernicus.eu, QGIS

- **NDMI Index of Radovesice Spoil Heap**

Figure 20 shows the “Radovesice spoil heap” site visualized using the NDMI (Normalized Difference Moisture Index), which reflects vegetation moisture. The colour scale on the left shows NDMI values ranging from –0.8 (red/orange) to >0.8 (dark blue). Dark blue areas (higher than 0.24 to >0.8) represent vegetation with high water content, i.e., wetter and healthier stands. Light blue to turquoise shades (around 0.032) indicates moderate vegetation moisture. Yellow and light orange areas (around 0 to –0.032) correspond to dry stands or vegetation with reduced water reserves. Red and dark orange areas (NDMI below –0.24) indicate very low vegetation moisture, or surfaces with almost no vegetation (bare soil, waste rock, anthropogenic surfaces). The map therefore does not show water as such, but rather the health and hydration of the vegetation cover. In the case of the Radovesice spoil heap, the pattern shown indicates that a significant portion of the area has low to moderate moisture content, while only some parts exhibit significantly moist vegetation (dark blue areas).

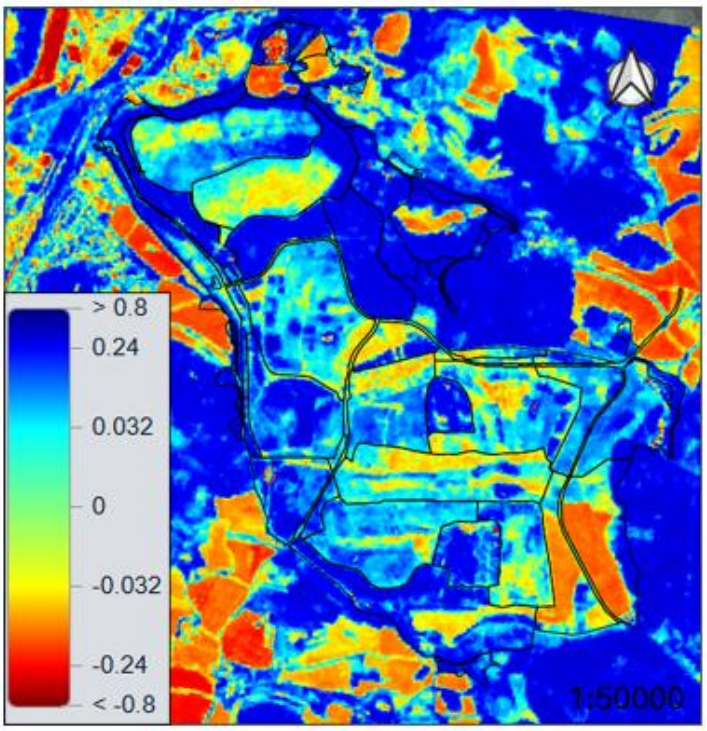

Figure 20 NDMI index for Radovesice spoil heap, September 2025. Source: copernicus.eu, QGIS

- **NDWI Index of Radovesice Spoil Heap**

The map (Figure 21) displays NDWI (Normalized Difference Water Index) values, which are used to identify water bodies and wet surfaces. Blue areas (NDWI near 0.8) represent water bodies or very wet surfaces—visible on the map mainly as small ponds and retention areas. Green shades ranging from 0 to < -0.8 correspond to vegetation and unpaved surfaces with normal moisture levels. Light green and very light white areas (NDWI around 0) indicate dry surfaces, such as fields, post-harvest meadows, or bare soil. The map thus allows for a clear distinction between water bodies (blue) and the surrounding landscape (green) and provides an overview of moisture conditions in individual parts of the territory.

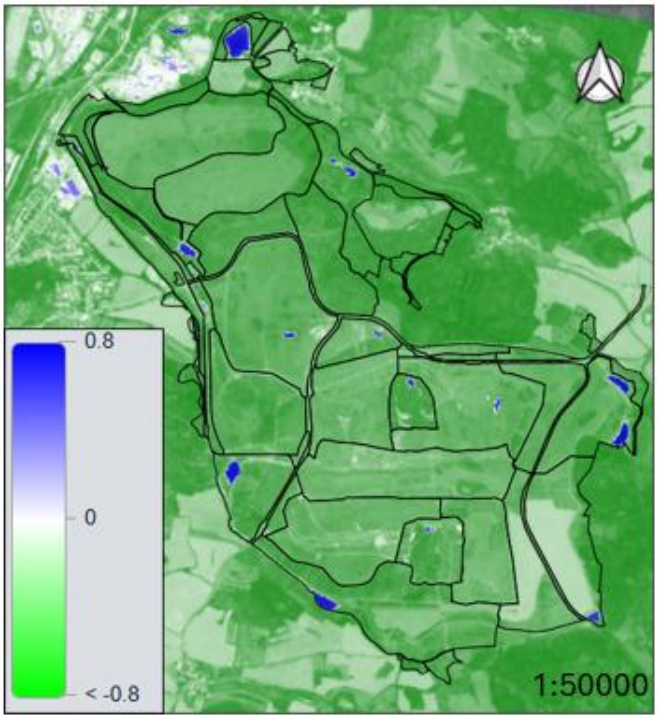

Figure 21 NDWI index for Radovesice spoil heap, September 2025. Source: copernicus.eu, QGIS

4.1.5.5. Urban Pressure of Střimice Spoil Heap

- **HRL Imperviousness of Radovesice Spoil Heap**

On the map (Figure 22) the impervious areas are highlighted in dark red, while the surrounding landscape (forests, meadows, fields) is shown in various shades of green. The dark red clusters correspond to urban and suburban development, roads, and other artificial surfaces. The highest concentration is visible in the centre of the map, where the main urbanized core of the city of Bílina is located. Smaller red areas scattered across the landscape represent smaller surrounding villages, industrial facilities, or local built-up areas. Green areas indicate natural or undeveloped territories, such as forests, fields, meadows, or open spaces. The map thus allows for a quick assessment of the extent of urbanization, the density of development, and the distribution of impervious surfaces within a given area.

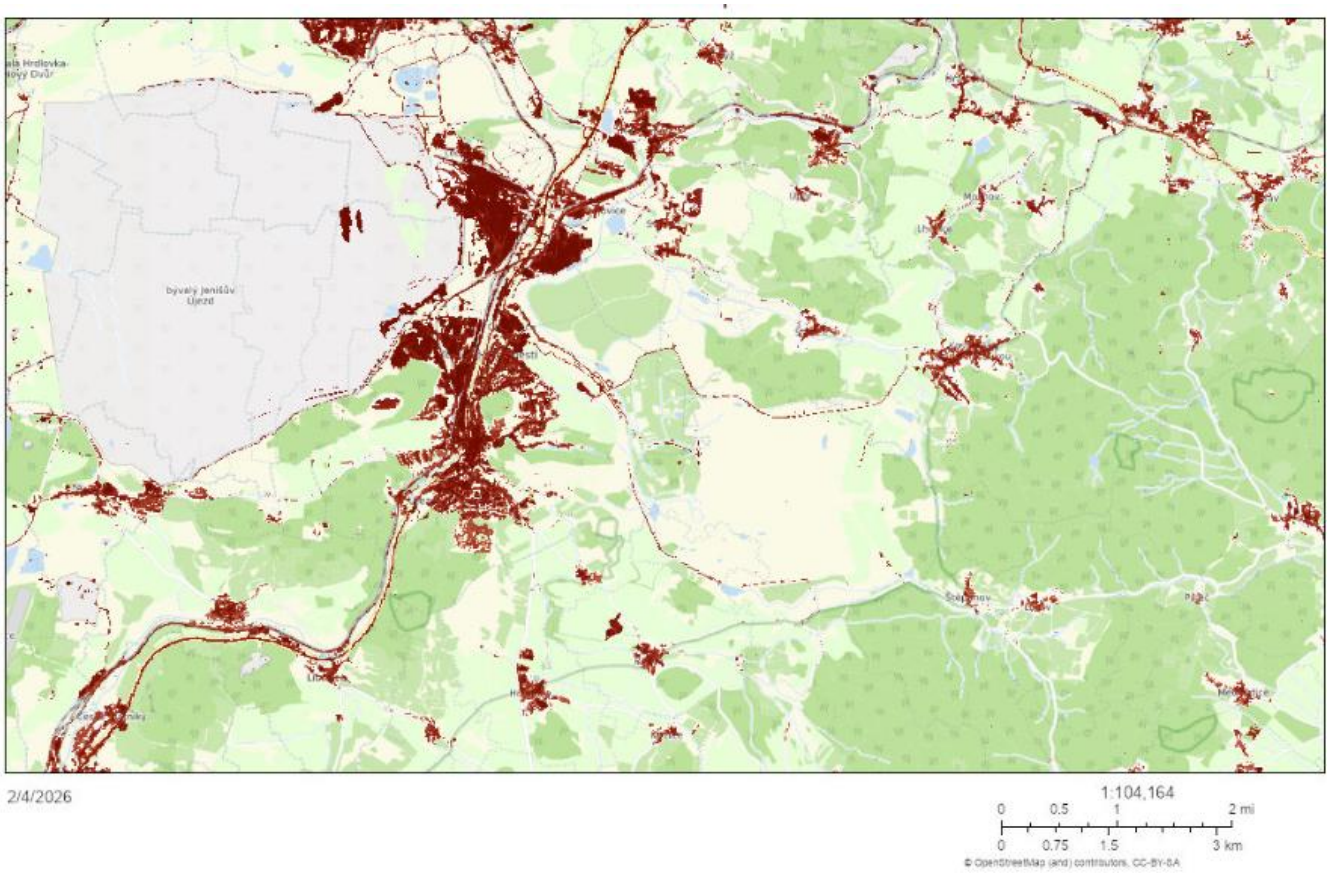

Figure 22 HRL Imperviousness for Radovesice spoil heap. Source: copernicus.eu

4.1.5.6. Vegetation Conditions of Radovesice Spoil Heap

- **NDVI Index of Radovesice Spoil Heap**

Figure 23 shows a map based on NDVI (Normalized Difference Vegetation Index) values, which indicate the abundance and vitality of vegetation. Dark green areas (NDVI around 0.6–1) represent dense, healthy vegetation, likely forest stands or fully established lawns. Lighter shades of green (NDVI 0.2 to approx. 0.4) correspond to sparser vegetation, agricultural areas, or recently mowed/cultivated areas. These areas are most prominent in the southeastern part of the study area of the Radovesice spoil heap. Yellow to light gray areas (NDVI around 0 to -0.1) indicate minimal vegetation cover, such as dry meadows, roads, or disturbed areas. Dark gray to black areas (NDVI -0.2 to -1) are areas without vegetation cover, such as water bodies, roads, or other artificial surfaces. For the area of interest, the gray to black areas represents small water bodies. It is evident that the Radovesice spoil heap is dominated by denser vegetation cover, i.e., values in the range of NDVI 0.2–1.

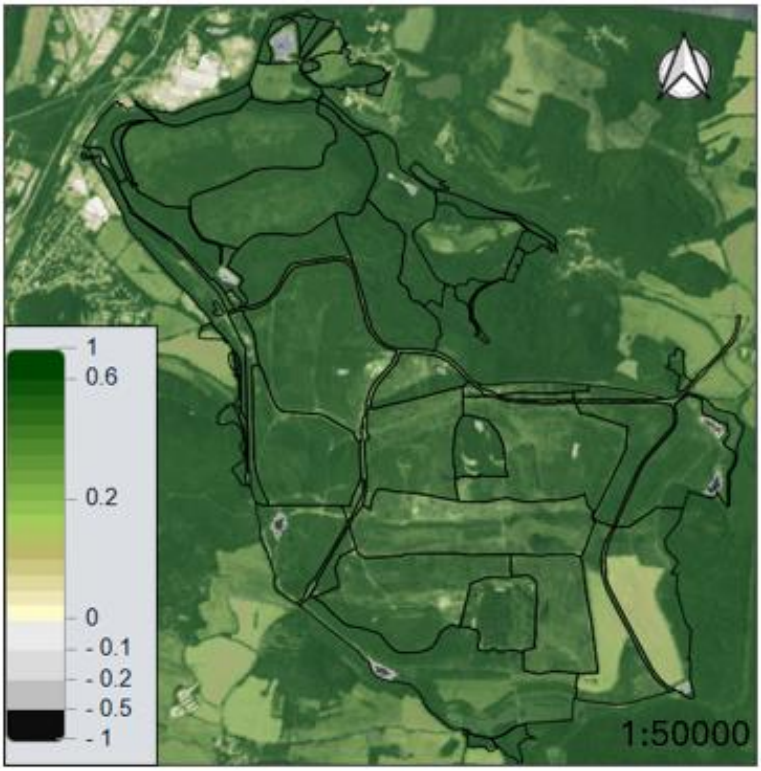

Figure 23 NDVI index for Radovesice spoil heap, September 2025. Source: copernicus.eu, QGIS

- **BSI Index of Radovesice Spoil Heap**

The BSI map (Figure 24) displays the Bare Soil Index values for the Radovesice spoil heap and its surroundings. The study area is dominated by values in the range of −0.28 to −0.02 (medium green) and −0.02 to 0.23 (light green/turquoise), indicating a prevailing vegetation cover with limited bare soil exposure. Light beige areas with values of 0.23–0.49, corresponding to partially exposed soil or sparse vegetation, are scattered across the polygon, with a more pronounced occurrence in the central and eastern parts of the heap. Areas with values above 0.49 (brown), representing the highest bare soil fraction, are largely absent within the polygon. Dark green areas (≤ −0.28), indicating dense vegetation or moisture, are visible particularly in the northern part of the study area. Overall, the BSI confirms that the Radovesice spoil heap is well vegetated, with only localised patches of bare or sparsely covered soil, consistent with the advanced stage of reclamation at this site.

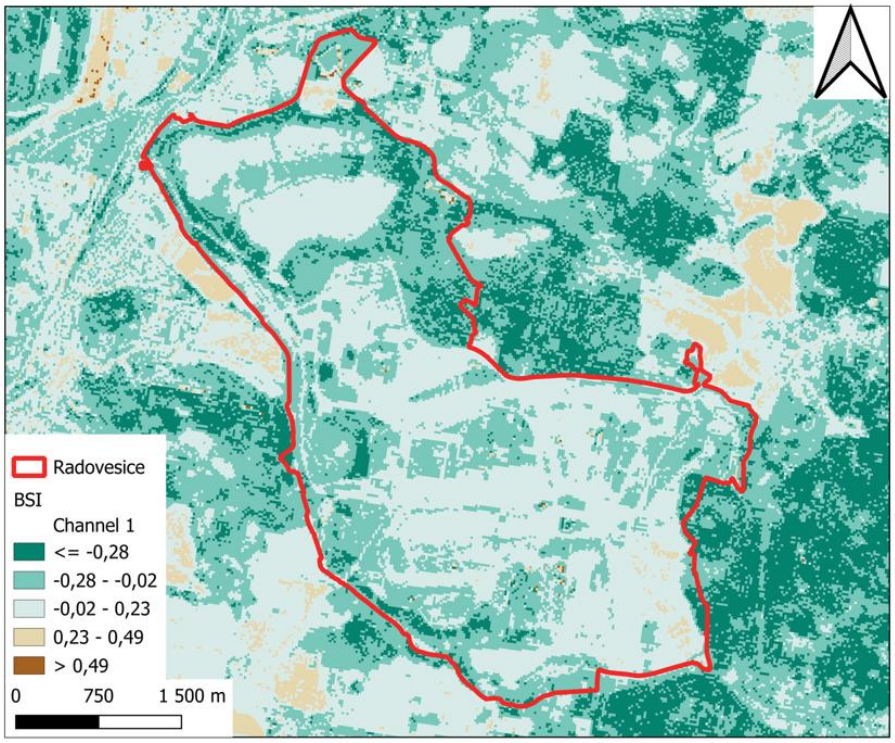

Figure 24 BSI for Radovesice spoil heap, September 2025. Source: QGIS, copernicus.eu

4.1.5.7. Proposed Areas for Energy Crops on the Radovesice Spoil Heap

From the available map data, it follows that the most suitable location appears to be the one situated in the southern to southeastern part of the area of interest (Radovesice XVI), that is, in the lower half of the maps. This is a section where “other” reclamation is planned in the future (Figure 18), which is suitable for these purposes. The NDMI index shows medium moisture values (light blue to green shades) (Figure 20). The area is therefore neither too wet nor too dry. At the same time, the NDWI index indicates that the nearest water bodies are in Radovesice XVIIB (Figure 21). However, the available aerial images also record a water body near the selected area of interest (Figure 14). The NDVI index shows medium vegetation cover without dark green forest stands (Figure 23). The dense vegetation cover would be a shame to remove for the cultivation of energy crops, because such areas exhibit too favourable properties, which are more suitable for food cultivation or for leaving forest stands.

In contrast, areas with too low vegetation cover do not appear suitable either, as soils might be too degraded, indicating low water availability. It is advisable to choose the NDVI index – predominantly “moderately” green, which means classified as vegetated agricultural land without extreme deforestation. DEMG5G indicates a slope primarily on the eastern side of the area (Figure 15-Figure 17), which in the future can also serve as an anti-erosion measure. HRL Imperviousness indicates that there is no urbanization in the immediate vicinity (Figure 22). There are only roads nearby, and the closest city with high human activity is Bílina. It is located from the northwest to the west side of the selected area. The chosen area is neither too wet, nor too dry or disturbed, and at the same time it is not forested or situated on a steep slope, which makes this area optimal for growing energy crops.

Another suitable option is a plot of land located in the eastern part of the spoil heap, which has a boomerang shape (Radovesice IX) (Figure 18). In the future, the plot is planned for agricultural use which makes it a promising alternative. The NDWI index here reaches moderate values (light blue to turquoise) (Figure 21), so the area is neither dry nor excessively wet. Conversely, the NDVI index shows high values, indicating the vegetation is in a good condition (Figure 23), which is also confirmed by the Scene classification map (Figure 19). BSI index also shows that the spoil heap is relatively densely covered with vegetation, which confirms advanced forest reclamation in the

surroundings (Figure 24). The slope and overall topography of the terrain are favourable (Figure 15-Figure 17). The nearest human settlements are at a sufficient distance. The closest to the area is the village of Kostomlaty pod Milešovkou.

4.1.6. Study Area 2: Střimice Spoil Heap

4.1.6.1. Characteristics of Střimice Spoil Heap

The Střimice spoil heap is located near the town of Most (Figure 25) and was established between 1959 and 1973 (Řehoř et al. 2024). The spoil heap is divided into two parts. The first successional part, covering an area of 2 ha, is the peripheral area of the Střimice landfill. The second part of the Střimice spoil heap is a reclaimed area covering 10 ha. Research began here in 1992 (Řehoř, 2007).

- **Experimental Area Střimice I**

The experimental plot Střimice I, with an area of 2 ha, was enclosed in a small, uncultivated peripheral part of the Střimice landfill. Research on it has been ongoing since 1998. The predominant soil type is a heterogeneous mixture of overlying soils from the coal seams of the Bílina surface mine. Sandy-clay loams and sands with a significant admixture of coal and siderite also dominate here. The area is extremely acidic and phytotoxic. On the surface, a remarkable development of erosion rills with a depth of up to several meters is visible. The extremely acidic nature of the environment creates inhospitable conditions for vegetation. Therefore, its representation is minimal, but rare acidophilic species may occur here (Řehoř, 2007).

- **Experimental Area Střimice II**

The experimental area of Střimice II is located on the upper part of a reclaimed landfill where bentonite was used. It is an experimental area covering 10 hectares. Research here began in 1992. Bentonite was applied here to improve the surface of unsuitable, phytotoxic landfill soils and to create a rooting soil horizon. At the same time, forest reclamation was carried out here (Řehoř, 2007).

In the past, forest reclamation without previous special surface preparation also took place on the Střimice spoil in the area of the M. Gorkij I. mine in 1967. However, due to toxic substances that penetrated into the surface zone, the planting mostly died out. At the same time, significant erosion negatively affected the spoil heap. In 1974, reclamation work was resumed. Bentonite from the nearby Red Hill quarry was spread on the surface in fifty-centimeter layers. After plowing, the area was grassed and later reforested. In 1988, an agricultural reclamation was built on the spoil heap plain. A total of 80 ha was forested, and 63 ha of fields were created, and on a prepared area of 26 ha a new airport was built (Luxa, 1997).

Near the village of Braňany, on the old spoil heap of Svoboda quarry, which was closed in the 1960s, both agricultural and forestry reclamation were carried out. However, due to the extreme acidity of the sandy soils on the surface of the spoil heap, a later adjustment of the top horizon was made by incorporating loess soils (Luxa, 1997).

Figure 25 Střimice spoil heap. Source: QGIS

- **Applied Reclamation Measures**

Bentonites are rocks of Tertiary age that have versatile reclamation uses, primarily in improving the chemical, physical, and anti-erosion properties of soils (Čermák and Ondráček, 2006). The only significant area where bentonites can be found is in the Most Basin, and they are extracted on the Braňany site near the town of Most and Rokle near Kadaň (Řehoř, 2007; Čermák and Ondráček, 2006). These are rocks that retain water very well, are highly porous, and when mixed with other spoil soils, they also exhibit considerable loosening ability (Čermák and Ondráček, 2006). In the history of Czech reclamation, this was the first significant use of bentonites as a reclamation additive. However, their application for future purposes is limited due to high financial costs (Řehoř, 2007).

Loess clays are an important category of selectively hidden soil-forming substrates of Quaternary origin. The carbonate content in “true” loess reaches more than 5%, while in loess clays it is less than 3%. Loess clays in the Most Basin are characterized by a higher content of physical clay, and in this territorial region they also constitute the most significant category of fertile soils used primarily for forestry reclamation. The soils are structureless, retain water well, and are rather less porous (Čermák and Ondráček, 2006). Loess and loess clays form discontinuous layers in the forefields of the Bílina and Vršany surface mines. In terms of both reserves and quality, the situation is better in the Vršany area. Loess layers reach a thickness of 1–2 m, exceptionally 8 m. Significant loss reserves were also identified in the forefield of the former Chabařovice surface mine near the city of Ústí nad Labem. However, hydraulic reclamation has taken place here, so this deposit is no longer of interest (Řehoř, 2007).

4.1.6.2. Use of Digital Elevation Model at Střimice Spoil Heap

From the topographic relief map (Figure 26), it is clear the greatest diversity of terrain forms occurs around the Střimice spoil heap, especially in the area of the bird conservation area, covering 251 ha, which was established in 2025. A more varied relief is also evident on the eastern to southeastern edge of the spoil heap. Light (white) colour tones on the map represent higher elevations, for example, the Na Skalice peak near the quarry.

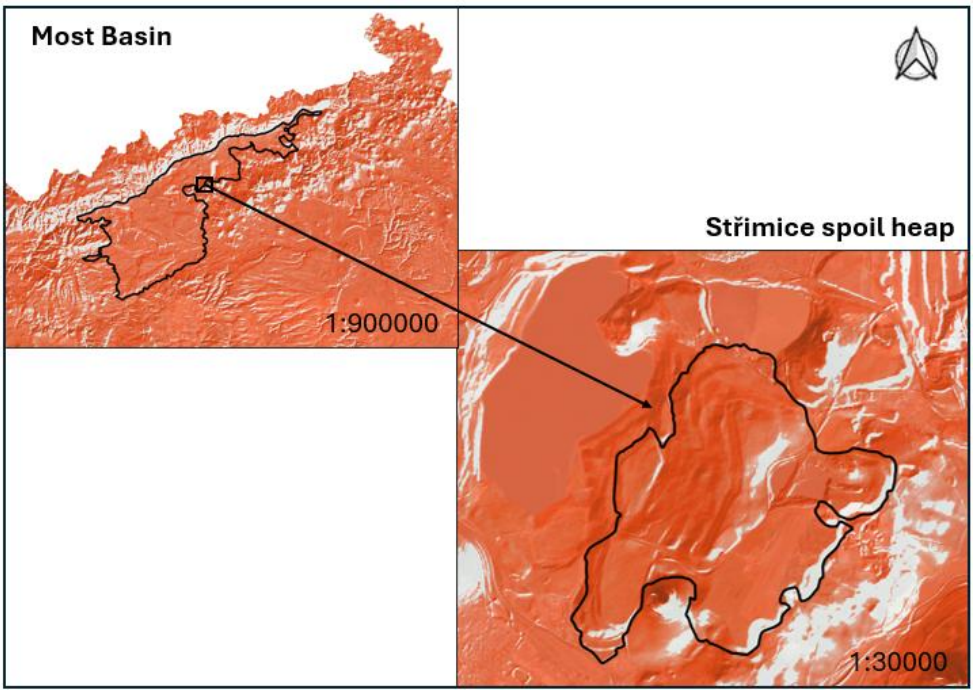

Figure 26 Digital Elevation Model of Most Basin and Střimice spoil heap. Source: QGIS

- **Elevation of Střimice Spoil Heap**

Figure 27 illustrates the elevation of the Střimice spoil heap. The western part of the heap is situated at a lower elevation, while the eastern part lies at an elevation exceeding 300 m above the sea level. The highest points in the surrounding area are Špičák Hill (400 m a.s.l.) and Zlatník Hill (520 m a.s.l.). Overall, the Střimice spoil heap is located at a higher elevation than the Radovesice spoil heap, although the difference is not significant.

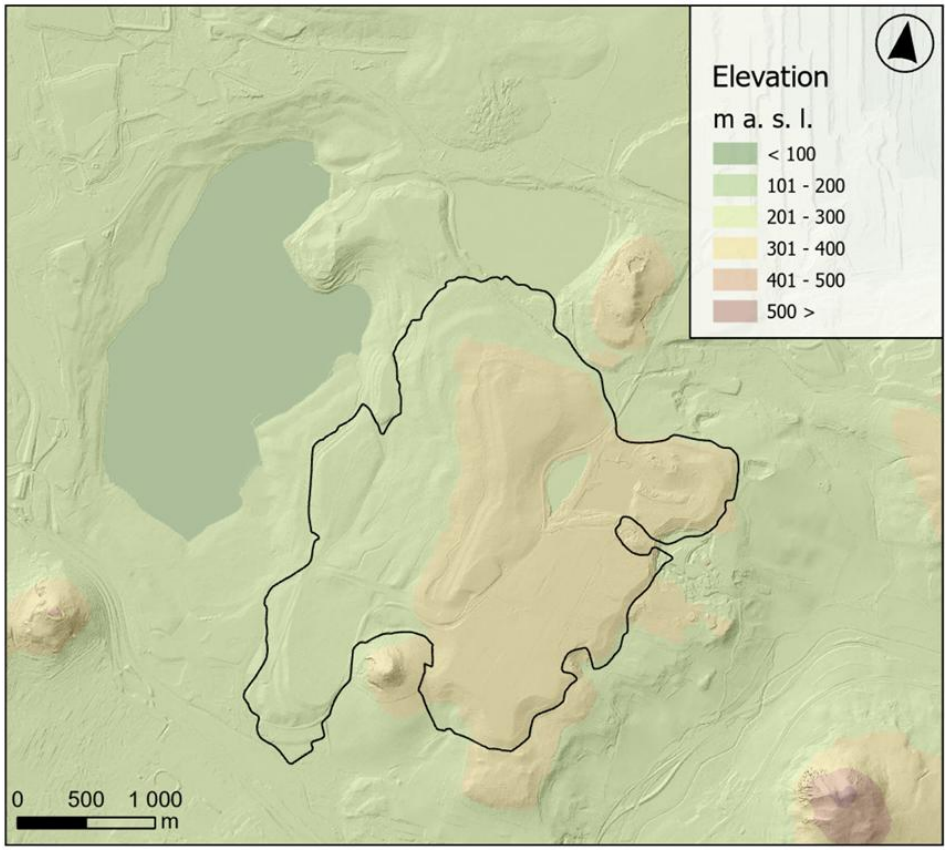

Figure 27 Elevation of Střimice spoil heap. Source: ArcGIS

- **Steepness of Slopes at Střimice Spoil Heap**

From the terrain slope map (Figure 28), it is evident that the lowest angle of the slope is in the southeastern part of the area, where Most airport is situated. Moderately sloped terrain is mainly present in the bird conservation area. The steepest slopes appear on the edges of two medium-sized water bodies – Braňany sandpits and, also near the Red Hill quarry. It is also worth mentioning the significant steep slope around Lake Most, which lies outside the marked polygon, and which was created by flooding of the former Ležáky quarry. This area is characterized not only by steep slopes but also by remarkably developed erosion rills.

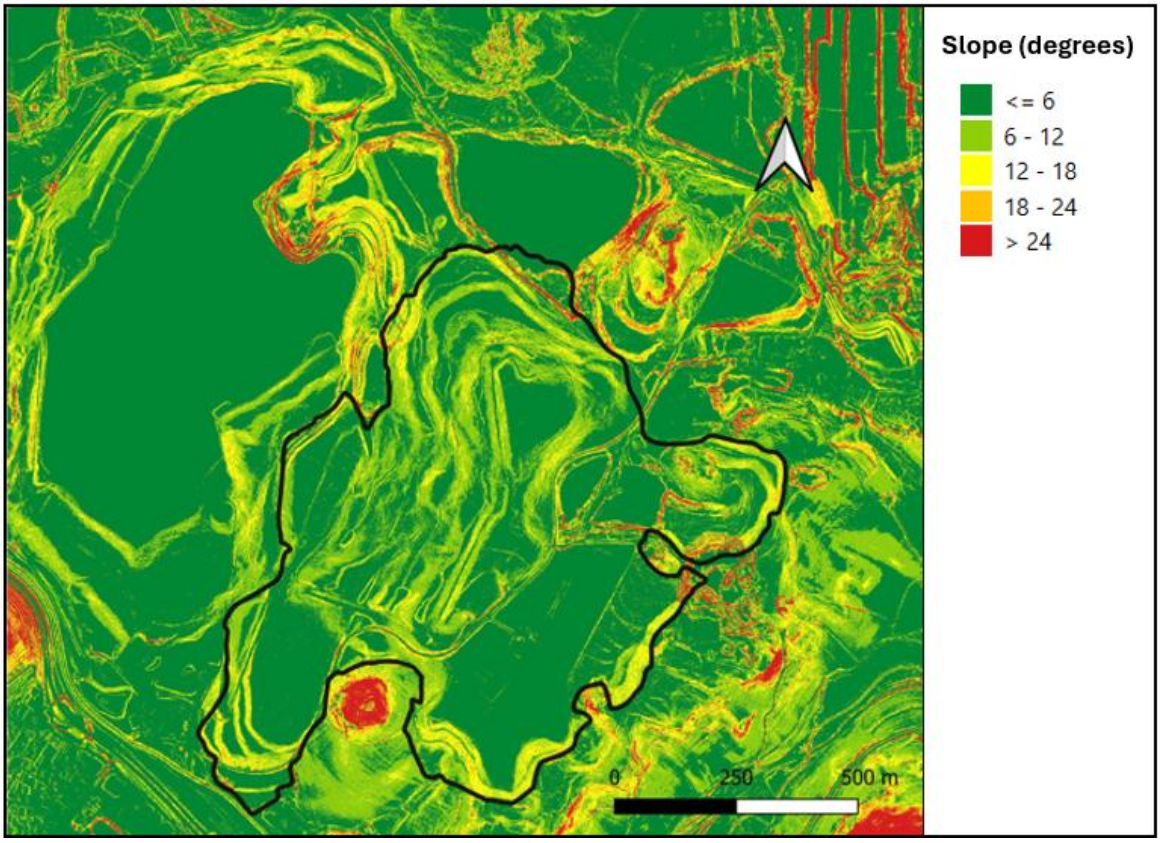

Figure 28 Slope of Střimice spoil heap. Source: ČÚZK, QGIS

4.1.6.3. Situation at the Střimice Spoil heap

The Střimice spoil heap is characterized by a diverse landscape and varied land use (Figure 29). It includes areas designated for agriculture and pastures, as well as extensive regions covered with vegetation in the form of forests. Public services are concentrated only in the eastern part, where the Most airport is located. Near the polygon, several water features can also be found. Northeast lie water bodies of the Braňany sand pits, while a smaller water reservoir can be found northeast on the west side. A significant nearby water feature is Lake Most, which was created by flooding the former Ležáky quarry. The area also includes a mining area.

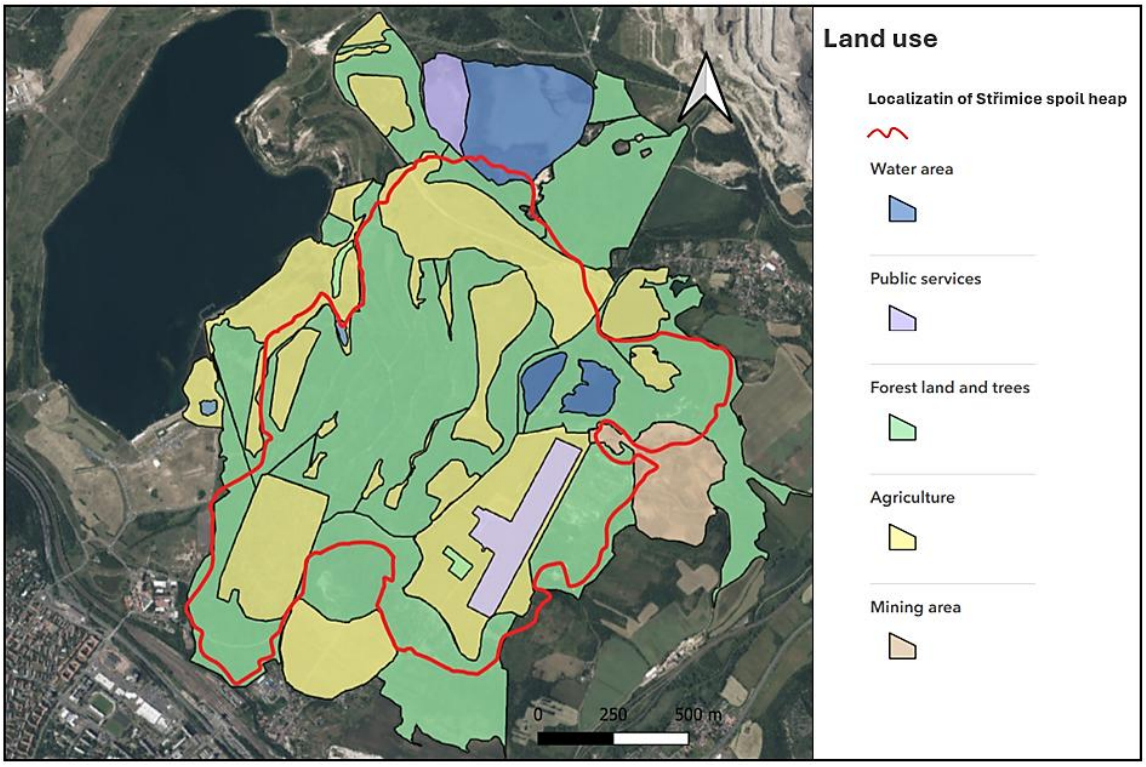

Figure 29 Situation on Střimice spoil heap. Source: ArcGIS, QGIS

4.1.6.4. Water Conditions of Střimice Spoil Heap

- **Scene Classification Map of Střimice Spoil Heap**

The map (Figure 30) shows the Scene Classification Map, from which it is apparent that vegetated areas dominate the territory again. Similar situation is at Radovesice spoil heap. To a lesser extent, non-vegetated surfaces also occur here, especially in the northern to northeastern part of the spoil heap. Water bodies in the Střimice spoil heap are represented by only two locations – the Braňany sandpits. The dark brown colouring on the map indicates cloud cover captured at the time the image was taken.

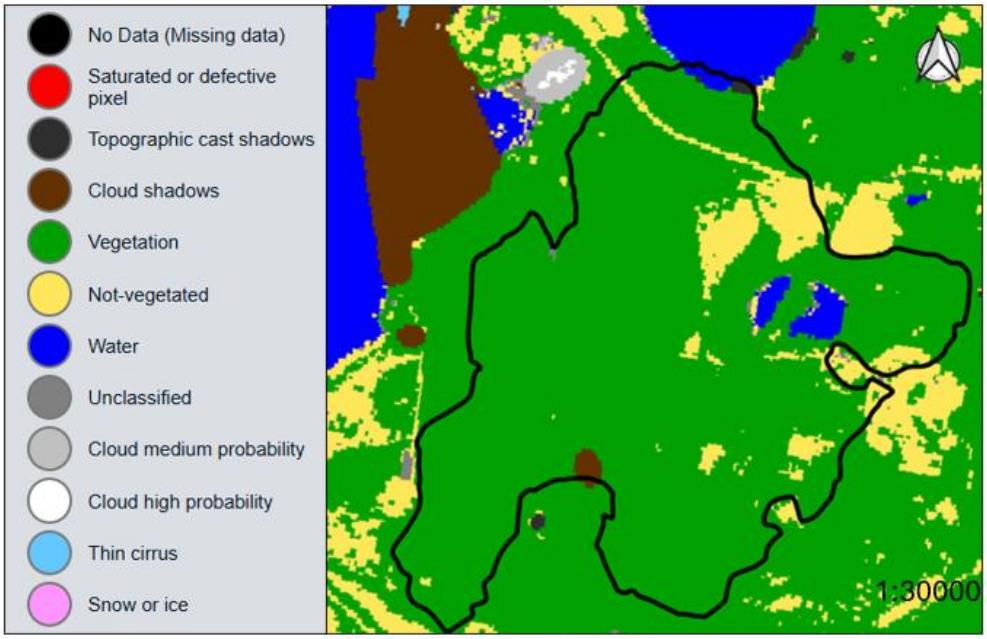

Figure 30 Scene classification map of Střimice spoil heap, September 2025. Source: copernicus.eu, QGIS

- **NDMI Index of Střimice Spoil Heap**

The map (Figure 31) captures the area of interest of the Střimice spoil heap and shows the spatial distribution of vegetation moisture. The bird conservation area within the spoil heap exhibits vegetation with high water content, which is manifested by its predominantly blue colour (NDMI >0.8). However, in the immediate surroundings, there are also areas with reduced water supply or dry vegetation, which are depicted in yellow and turquoise shades (NDMI 0.032 to -0.032). Very low vegetation moisture is especially noticeable in the eastern part of the map, where the Most airport is situated. Similarly, the northeastern edge of the spoil heap shows significantly low moisture values (-0.24 to < -0.8), which are visible on the map as a red crescent-shaped feature. Overall, it can be stated that approximately half of the Střimice spoil heap is covered with vegetation with high water content, while the other half exhibits reduced to low water content in the vegetation.

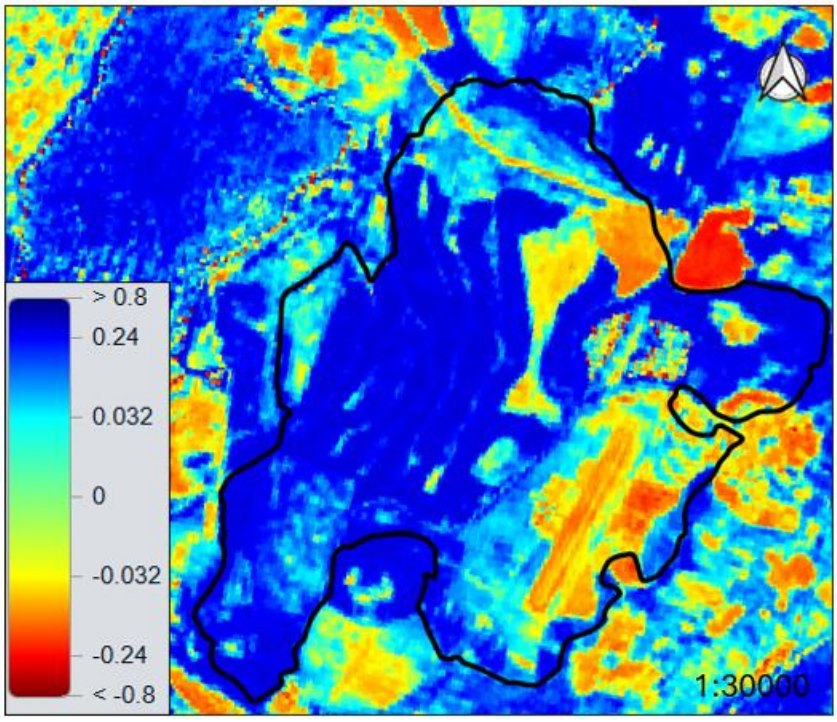

Figure 31 NDMI index of Střimice spoil heap, September 2025. Source: copernicus.eu, QGIS

- **NDWI Index of Střimice Spoil Heap**

The map (Figure 32) illustrates the NDWI index, which is used to identify water bodies and wet surfaces. Within the area defined by the polygon, there are two smaller water bodies, known as the Braňany Sandpits. Another little water feature is visible in the vicinity of the Most airport, and a small water body is also located in the bird conservation area. The immediate surroundings of these water bodies predominantly show a landscape character according to the colour scale, meaning drier or mixed surface types. A comparison shows that the Radovesice spoil heap is more diverse in small water bodies than the Střimice spoil heap. However, its surroundings prominently feature two large water reservoirs – The Lake Most and Venuše water body beneath Red Hill.

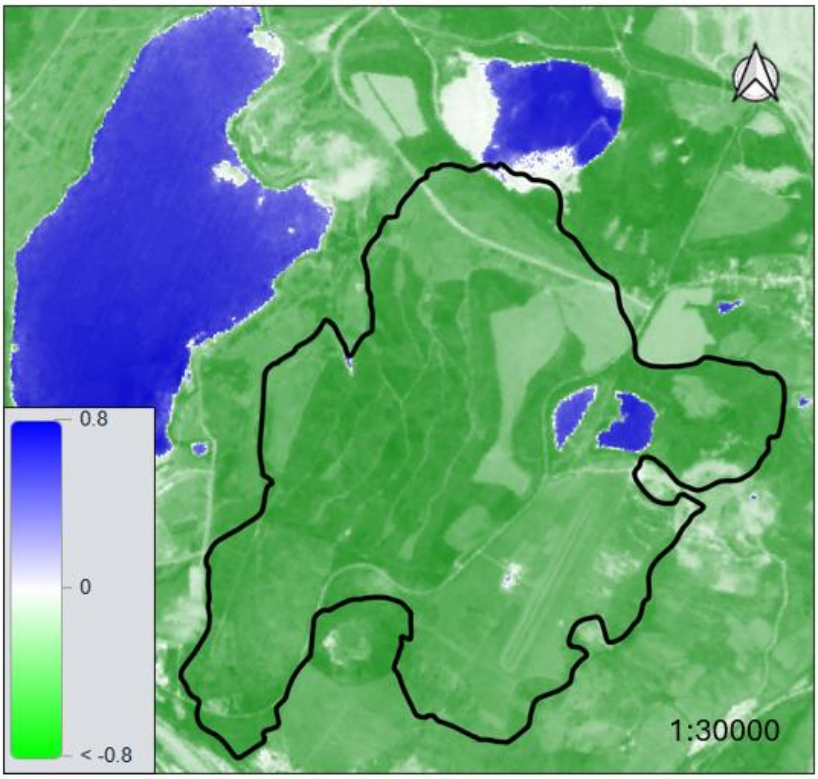

Figure 32 NDWI index for Střimice spoil heap, September 2025. Source: copernicus.eu, QGIS

4.1.6.5. Urban Pressure of Střimice Spoil Heap

- **HRL Imperviousness of Střimice Spoil Heap**

The map (Figure 33) shows the HRL Imperviousness layer, which identifies artificially sealed surfaces, that means, areas covered with asphalt, concrete, buildings, or other impermeable materials. These surfaces are highlighted in dark red colour on the map, while nature or agricultural areas are shown in various shades of green. The dominant dark red clusters represent the urban centres of nearby towns, particularly the extensive built-up area of the city of Most in the central part of the map and the adjoining urban structures of Litvínov and Bílina.

It is also visible that sealed surfaces extend along transport corridors as prominent lines, corresponding to the routes of major roads and railways in the area. In relation to the Střimice landfill, it is evident that the proportion of artificially sealed areas is minimal in its territory – more typical are only roads, service roads, and the infrastructure of Most Airport on its northern edge. The nearest larger urbanized structures are therefore mainly formed by the city of Most and smaller settlements in the surrounding area, such as Braňany at the foothills of Red Hill.

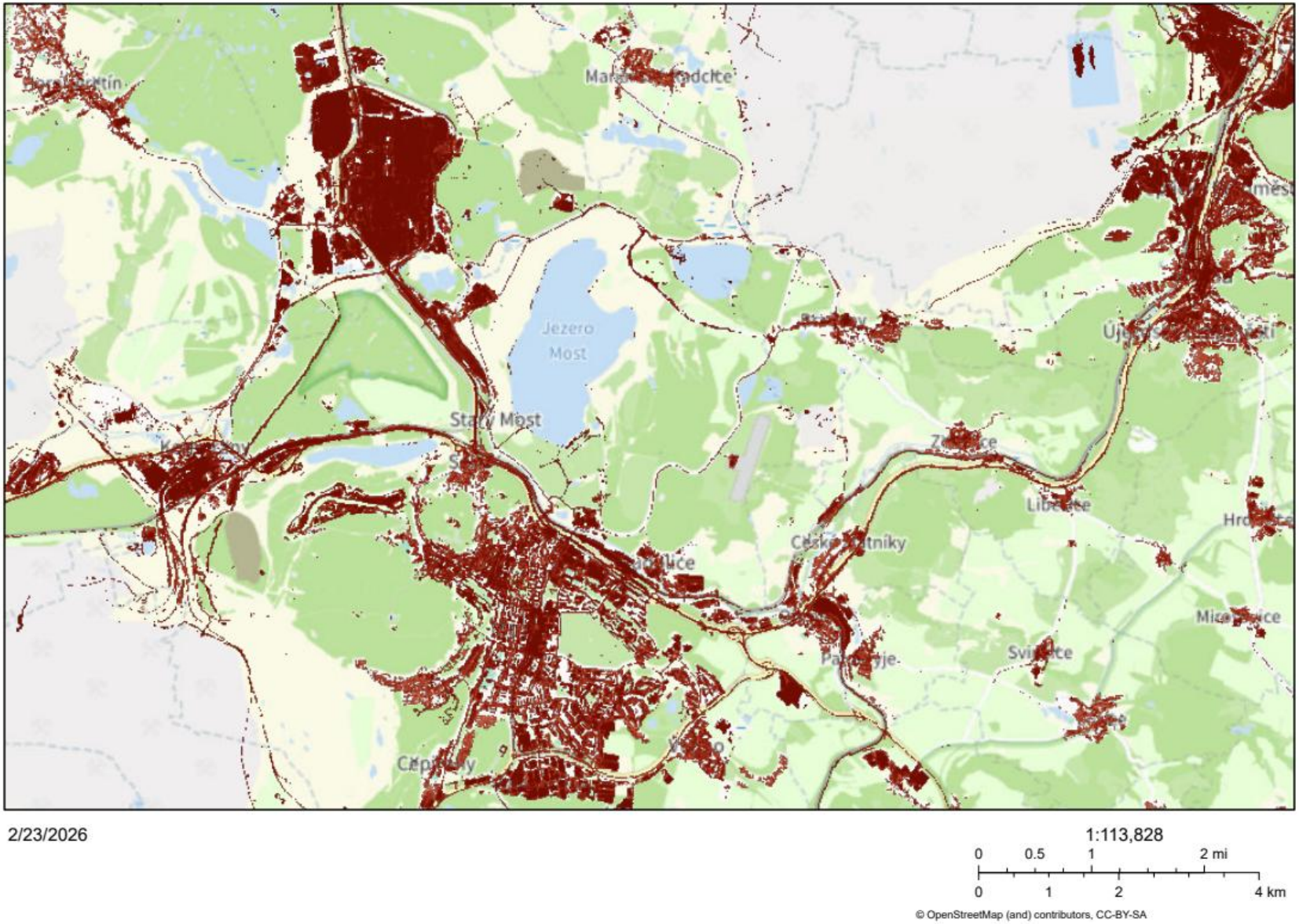

Figure 33 HRL Imperviousness for Střimice spoil heap. Source: copernicus.eu, QGIS

4.1.6.6. Vegetation Condition of Střimice Spoil Heap

- **NDVI Index of Střimice Spoil Heap**

The map based on NDVI values (Figure 34), which expresses the amount and vitality of vegetation, shows extensive dark green areas with values around NDVI 0.6–1. These values indicate very vital vegetation cover, probably composed of forests or dense grasslands. Lighter green shades (NDVI around 0.2) indicate sparser vegetation, typical especially for agriculturally cultivated lands. On the northeastern edge of the Střimice spoil heap, distinctly light brown-yellow areas with NDVI values around 0 appear, indicating minimal vegetation cover. Dark grey areas (NDVI 0 to -0.5) represent completely vegetation-free areas, in this case they represent bodies of water. Overall, the Střimice spoil heap is characterized by predominantly dense vegetation cover, which is confirmed by dominant NDVI values in the range of 0.2 to 1.

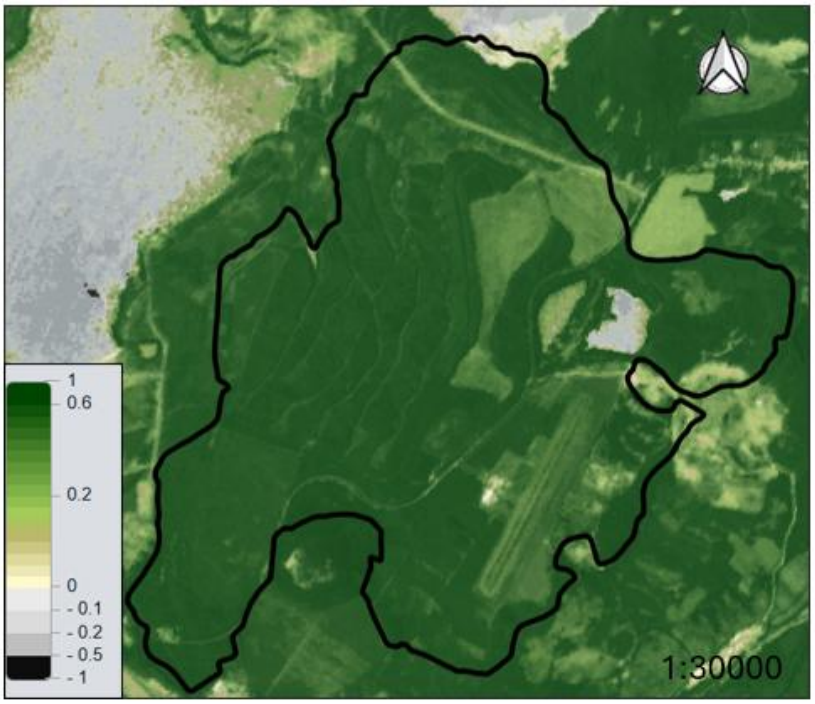

Figure 34 NDVI index for Střimice spoil heap, September 2025. Source: copernicus.eu, QGIS

- **BSI Index of Střimice Spoil Heap**

The BSI map (Figure 35) displays the Bare Soil Index values for the Střimice spoil heap and its surroundings. The majority of the study area shows values in the range of −0.28 to −0.02 (medium green) and −0.02 to 0.23 (light green/turquoise), indicating a predominance of vegetation cover over bare soil. Light beige areas with values of 0.23–0.49, corresponding to partially exposed soil or sparse vegetation cover, occur locally both within and outside the delineated polygon. Brown areas with values above 0.49, representing the highest proportion of bare soil, are visible predominantly outside the polygon, in the northeastern part of the map. Dark green areas (≤ −0.28) in the southwestern part correspond to a water body. Overall, the BSI confirms that the Střimice spoil heap is largely covered by vegetation, with areas of more pronounced bare soil occurring mainly at the margins.

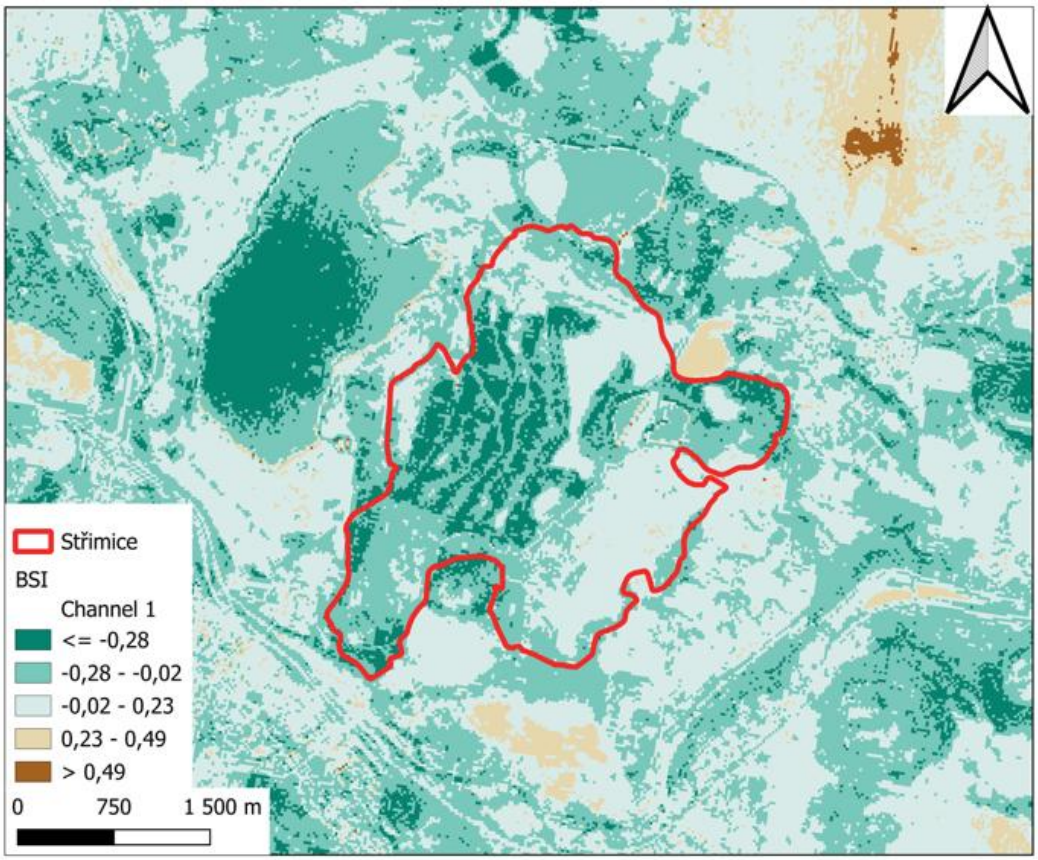

Figure 35 BSI for Střimice spoil heap, September 2025. Source: QGIS, copernicus.eu

4.1.6.7. Proposed Areas for Energy Crops on the Střimice Spoil Heap

One possible alternative use of the studied area for experimental purposes is the phytotoxic site located on the eastern edge of the spoil heap. Although the map datasets do not indicate it as an ideal location, mainly due to its higher slope and low NDMI and NDVI values (Figure 28; Figure 31; Figure 34), parts of this area may be suitable precisely for the purpose of testing the possibilities of revegetation and the utilization of highly dysfunctional soils. These strongly dysfunctional sites represent typical environments of anthropogenic spoil heap soils, for which it is desirable to assess their reclamation potential. While healthy or less dysfunctional soils are more suitable for cultivating food-producing crops, highly dysfunctional to phytotoxic soils may be prospectively used for the cultivation of energy crops, without competing with agricultural production on high-quality soils. An experiment conducted here could therefore contribute to evaluating how such inhospitable locations may be restored to functional landscape use in the long term. This can be considered in the subsequent D3.4.

Another proposed plot for cultivating an energy crop is the northernmost of the evaluated locations, situated directly on the boundary of the bird park. The NDMI index here shows light-blue to turquoise values, corresponding to a medium level of moisture and indicating no significant extremes (Figure 31). The NDWI index (Figure 32) further confirms the natural landscape character of the site, with no signs of excessive waterlogging or drying. Vegetation vitality (NDVI) also falls within a suitable range (Figure 34), and the Scene Classification Map confirms the presence of continuous vegetation cover in the area (Figure 30). The HRL Imperviousness layer indicates the nearby presence of a road, which may facilitate access to the plot (Figure 33). The site is characterized by a gentle slope (Figure 28), which should not exceed 7° (2.1.1), remaining within the acceptable limit for standard agricultural use. From the perspective of topography (Figure 26; Figure 27), moisture conditions (Figure 30; Figure 31; Figure 32), and vegetation cover (Figure 34), the location is therefore relatively well suited for the cultivation of energy crops.

The third proposed plot suitable for cultivating an energy crop is the westernmost location situated at the edge of the spoil heap. The NDMI index here shows medium values (turquoise coloration) (Figure 31), indicating balanced moisture conditions without signs of extreme waterlogging or drying. The slope gradients in this part of the area generally do not exceed 7° (Figure 28), making the plot suitable for continued agricultural use. The HRL Imperviousness product confirms that the area is not part of a built-up or technical environment (Figure 33), which increases its suitability for growing the target crops. The Scene Classification Map likewise confirms the presence of continuous vegetation cover (Figure 30). NDVI values indicate a relatively high vegetation density (Figure 34). However, based on aerial imagery (Figure 25) and NDVI values (Figure 34), it is evident that the plot is already used for agricultural purposes, meaning that potential cultivation of energy crops would not result in the loss of natural or ecologically valuable vegetation cover. The BSI index also confirms a greater presence of vegetation, while bare areas occur more at the edges of the spoil heap Figure 35).

4.2. Ptolemais Lignite Mining Area (GR)

4.2.1. General Characteristic of Ptolemais Lignite Mining Area

The Ptolemais mining area is a complex of lignite surface mines located in the Kozani province of Western Macedonia, in Northern Greece (Figure 36). In this region, the lignite mines of Public Power Corporation (PPC) have been in operation for the last 68 years, since 1958, and are now in a closure phase. It constitutes a large-scale mining operation covering an area of 148 km^2 (within the environmental permitting limit). During the period 1958-2025, a total of 1.55 billion tonnes of lignite have been produced from ten mines for electricity generation and 7,07 billion m^3 of rock have been excavated. In 2002, lignite production in the Ptolemais mines peaked at 47,24 million tonnes (Roumpos et al. 2023). In 2025, lignite production was 5.67 Mt, with excavations of 23.90 million m^3 and a stripping ratio of 3.38 m^3/t. During the long period of mining operations, new mines were opened, and exhausted mining areas were covered with waste materials from neighbouring mines. After 2013, mining operations were gradually but significantly reduced, following the increased electricity production from natural gas-fired power stations and renewable energy sources. The mining operations were mainly based on the application of continuous surface mining equipment (bucket wheel excavators, belt conveyors, and spreaders) in combination with noncontinuous mining equipment for specific earthmoving tasks.

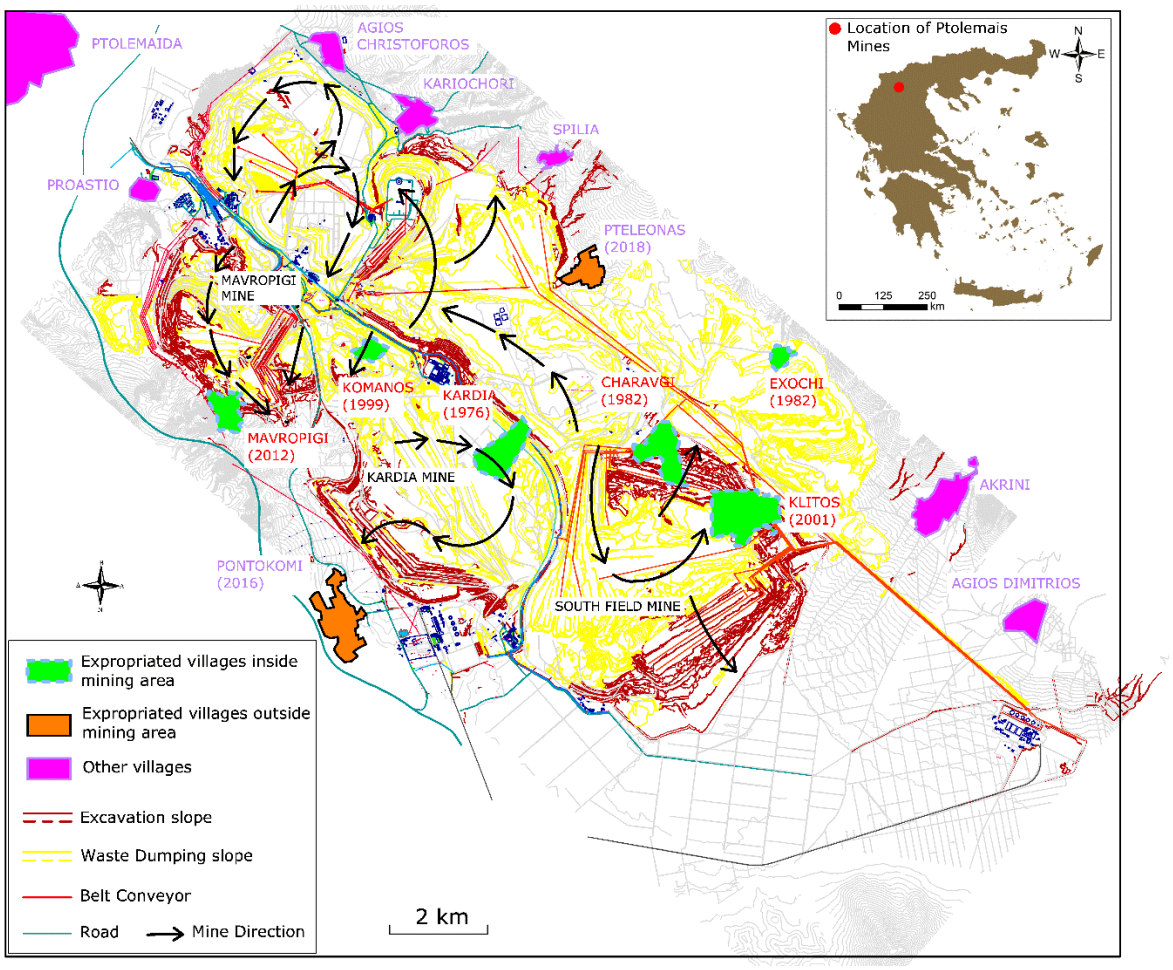

Figure 36 Location map of the Ptolemais surface lignite mines (end of 2025), including mines' direction and dates of expropriation /resettlement villages (Pavloudakis et al. 2026)

Simultaneously with the mining activities, extensive environmental reclamation work was underway. The reclaimed land has been utilized for various purposes, including the installation of RES. Currently, the only two active mines (Mavropigi and South Field) are in a closure phase, and they are expected to stop lignite production until the end of 2026, while reclamation works will continue until all required activities defined in the mine environmental permitting terms are completed (Pavloudakis et al. 2026). Figure 35 depicts the land use allocation along the Ptolemais mining area, and the latest reclamation works that have been employed in 2025. The reclaimed land of Ptolemais mining area is consisted of forest land (2080.8 ha), agricultural land (808.4 ha), graded areas (297.6 ha), graded areas for photovoltaics installation (1023 ha) and lakes (3.9 ha) (Figure 37).

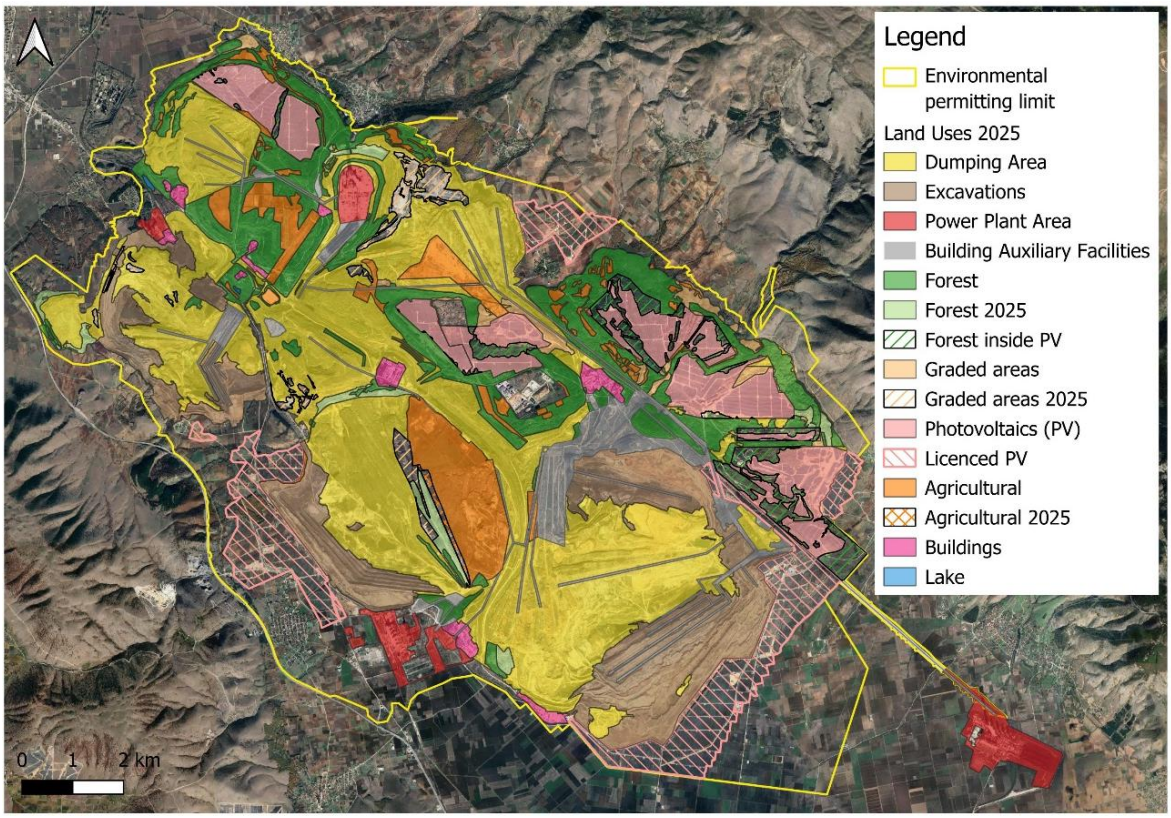

Figure 37 Land use allocation map in the Ptolemais mining area (end of 2025) (Technical report of exploitation and reclamation works in the Ptolemais mining area, 2025, PPC)

The methodology for the reclamation of the mining areas is based on the Just Transition Plan, according to which the areas inside the decarbonization core and the undisturbed areas will be suitably configured depending on the proposed land uses. The reclamation plan for the areas related to mining activities will be employed in consecutive annual phases. Each phase starts after the release of the mining area and is completed within two years. The reclamation stages are adjusted depending on the intended land use for each under-reclamation area. The methodologies followed for individual types of reclamation are described according to the Environmental Impact Assessment Study of Ptolemais and Amyntaio-Lakkia mines, 2024.

4.2.2. Geomorphology of the Ptolemais Lignite Mining Area

Figure 38 and Figure 39 show the general geomorphology of the broader area, as well as within the Environmental Permitting Limits of the Ptolemais mining area. The geomorphology of the area is characterized by mild slopes ranging from 0 to 6 degrees (Figure 40).

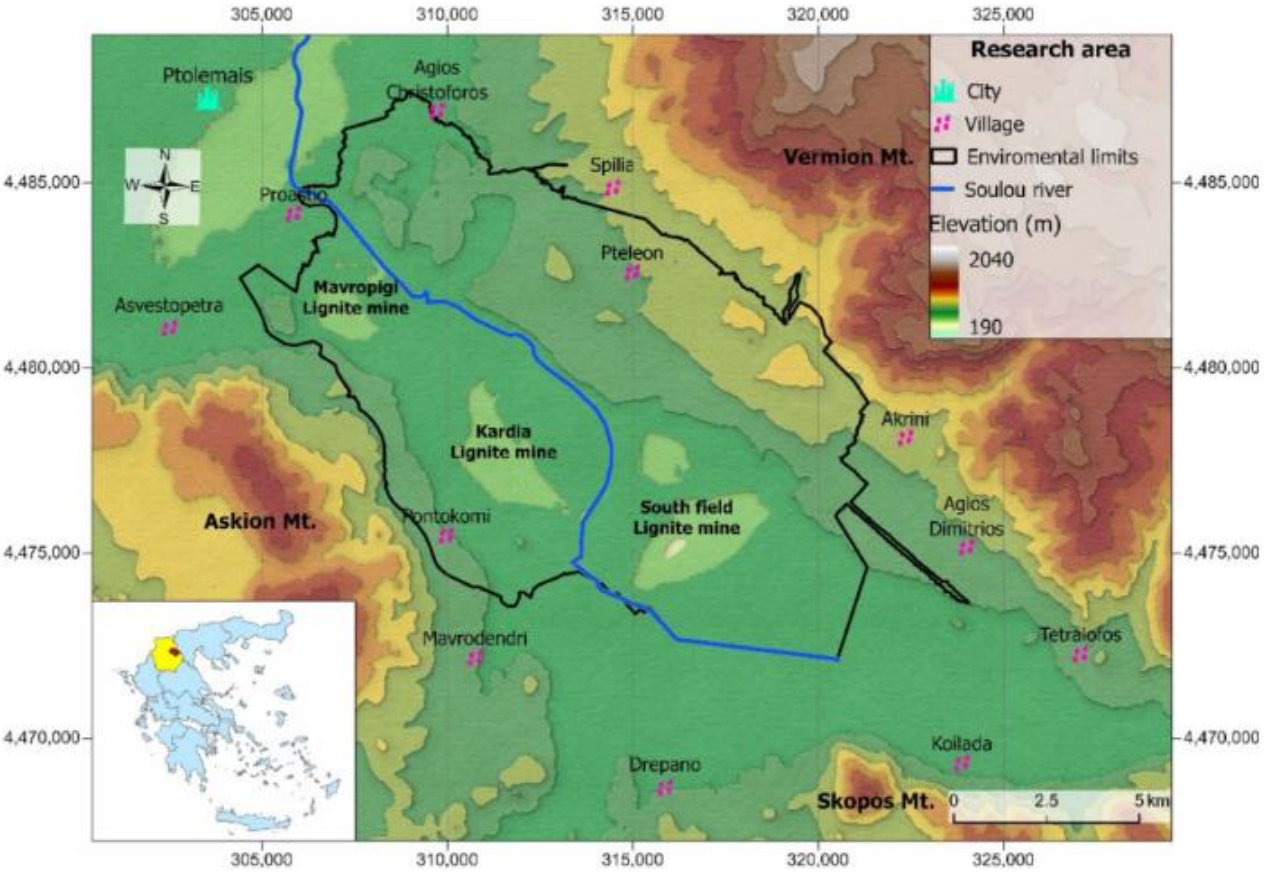

Figure 38 Elevation map of the broader area of the Ptolemais mining area where the surrounding villages and mountains are depicted

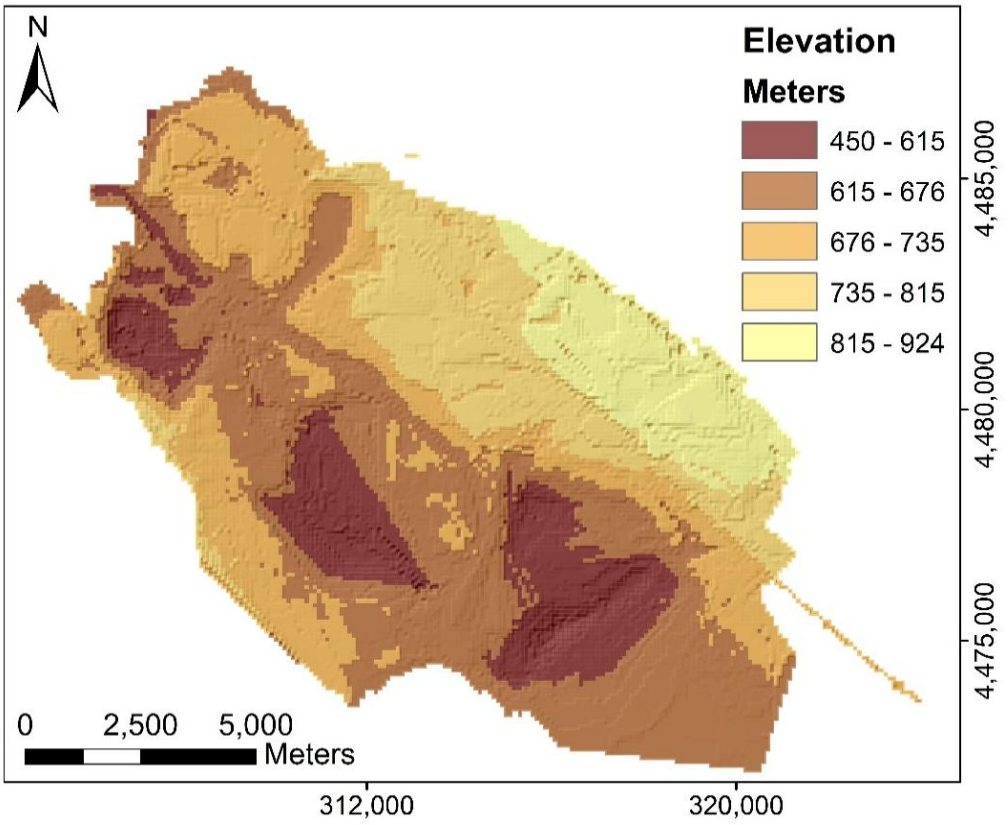

Figure 39 Elevation map of the Ptolemais mining area (Coordinate system: WGS84). Source: Servou et al. 2023.

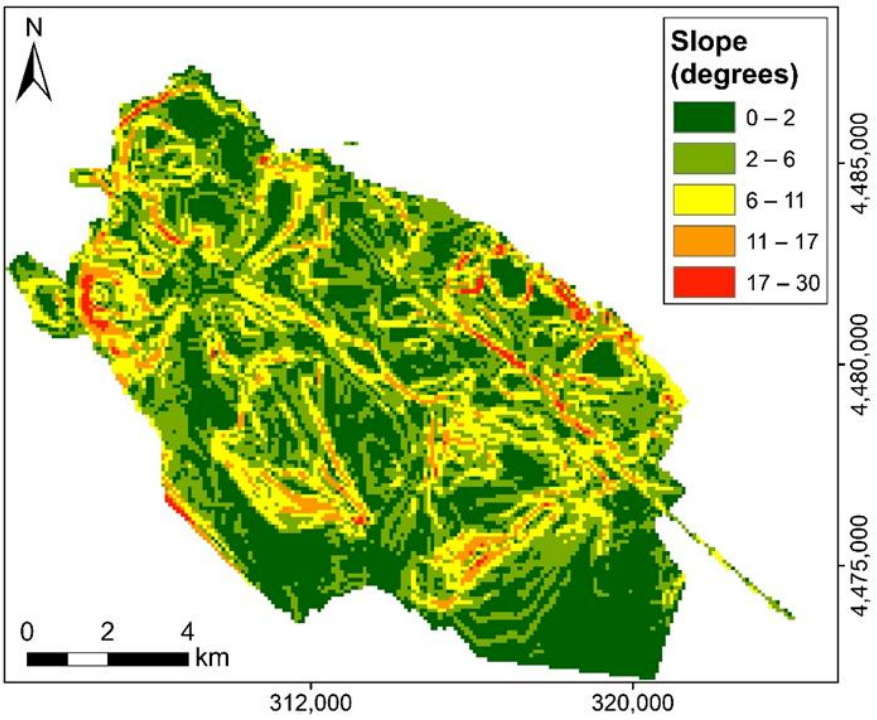

Figure 40 Slope map of the Ptolemais mining area (Coordinate system: WGS84). Source: Servou et al. 2023.

Figure 41 and Figure 42 present the distribution of the topographic wetness index and stream power index (SPI) respectively. As can be seen from the maps, there are small areas inside the mine boundary where water flow is concentrated. The spatial distribution of the SPI shows high values in the northeast and south-southwest areas of mining activity, where the water runoff and overland flow of the Vermion, Askion, and Skopos Mts. are active.

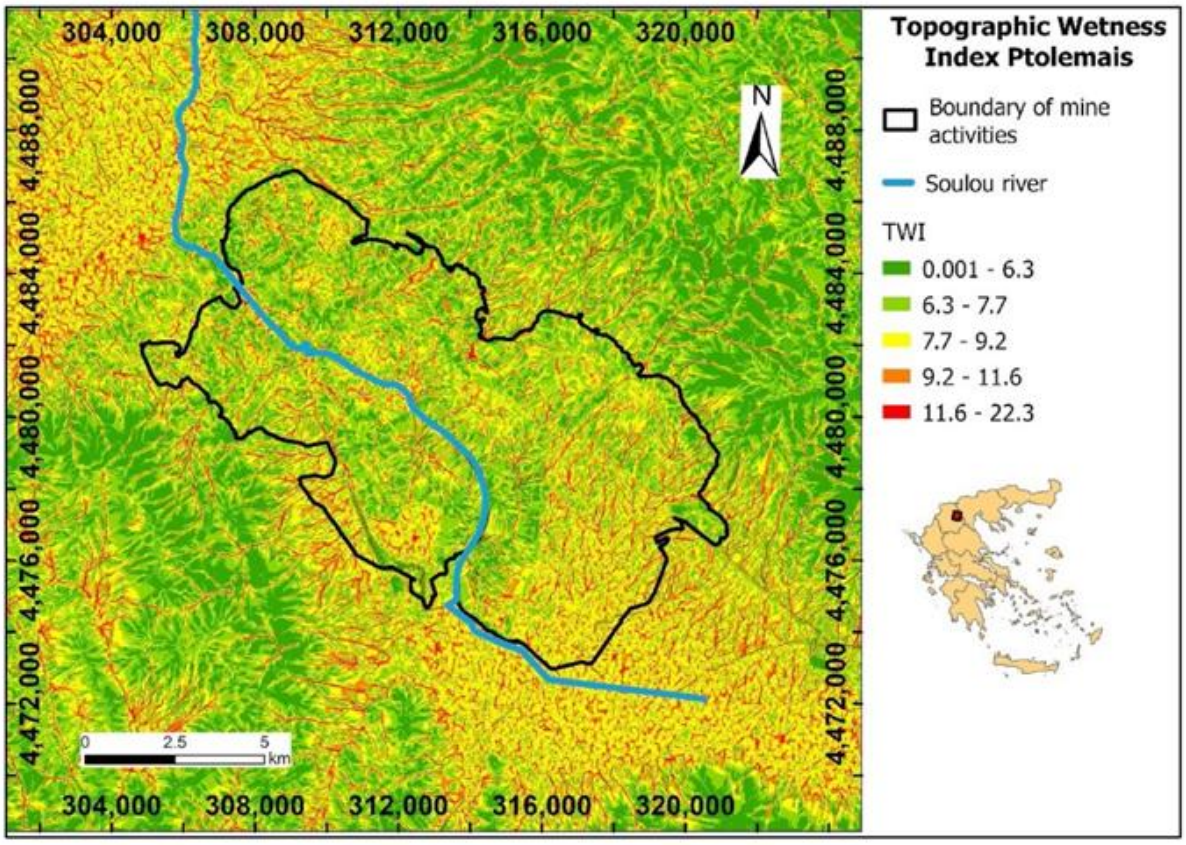

Figure 41 Spatial distribution of TWI with the combinations of two DEMs in 2022 where drainage networks are shown in red colour, (Ptolemais Basin, northern Greece). Source: Louloudis et al. 2023.

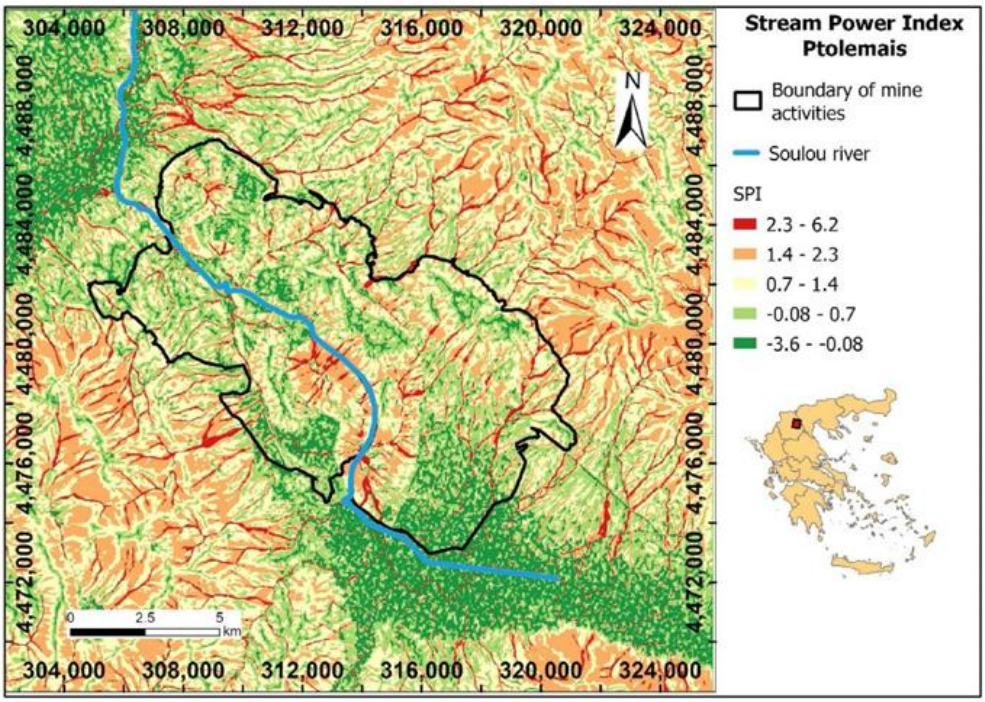

Figure 42 Spatial distribution of SPI with the combinations of two DEMs in 2022 where the high velocity of the streams is presented with red values (Ptolemais Basin, northern Greece). Source: Louloudis et al. 2023.

Figure 43, Figure 45 and Figure 46 present the distribution maps of NDVI, NDWI and MNDWI where the maximum vegetative coverage is presented. Typically, high NDVI values illustrate younger and healthier vegetation, while low values correspond to a lack of vegetation. According to Figure 43, the area of the outside waste dumping, i.e. the northern part of the South Field Lignite mine, has a vegetative cover due to the mine restoration activities. Strong evidence of young and healthy vegetation also appears in the cultivated agricultural land, as shown in the southern area of the South Lignite Mine. Figure 44 shows the NDVI allocation in August 2025 where bare soil is emerged with small patches of trees with the highest values of density observed in the surrounding crop cultivation areas. The NDWI in Figure 45 shows the water features which are accumulated in locations with a high potential for inundation, while Figure 46 shows an improved NDWI, without noise from the urban areas. Figure 47 shows the sites which are covered by ground with sparse vegetation with small concentrations of water bodies that seem to be rich in sediment. The light-colored areas show activity or waste concentration from past activity.

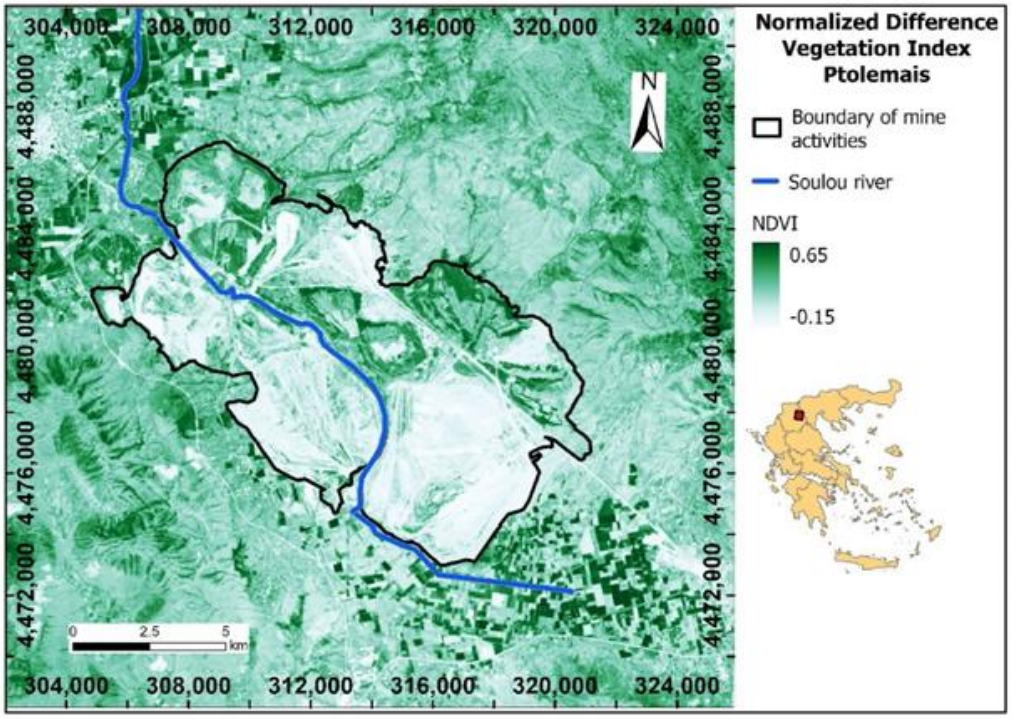

Figure 43 Spatial distribution of NDVI in July 2022 (Ptolemais Basin, northern Greece). Higher values of NDVI suggest healthy and dense vegetation while lower values non-vegetated-surfaces. Source: Louloudis et al. 2023

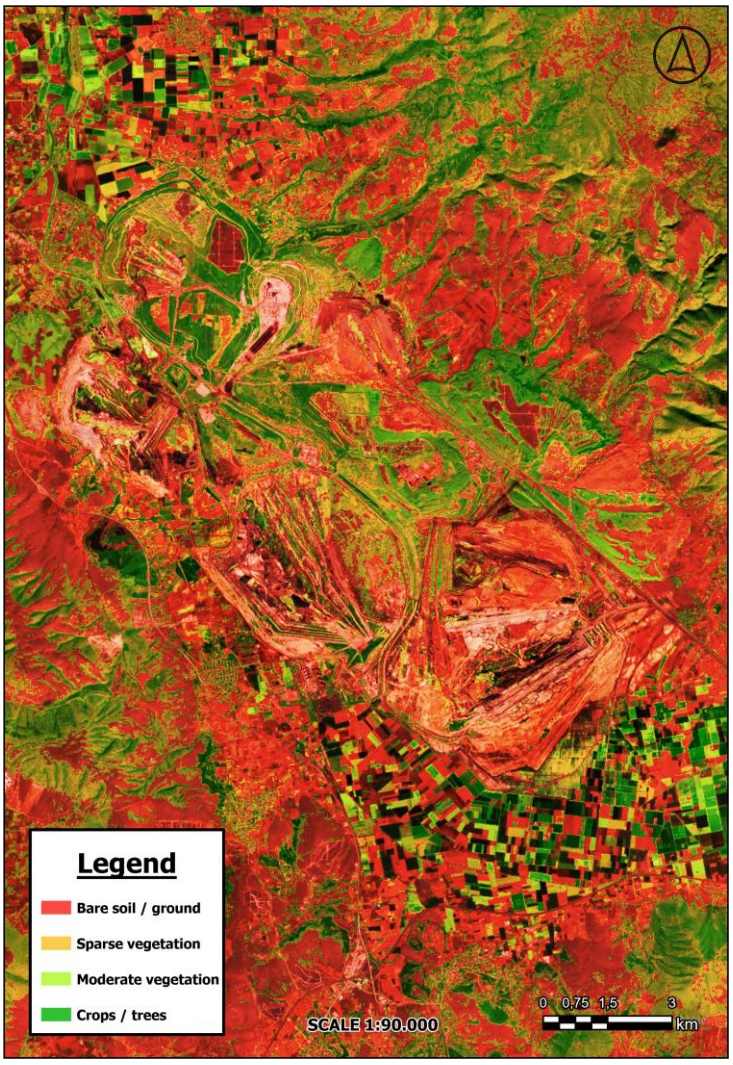

Figure 44 NDVI index for Ptolemais mine. Source: Copernicus.

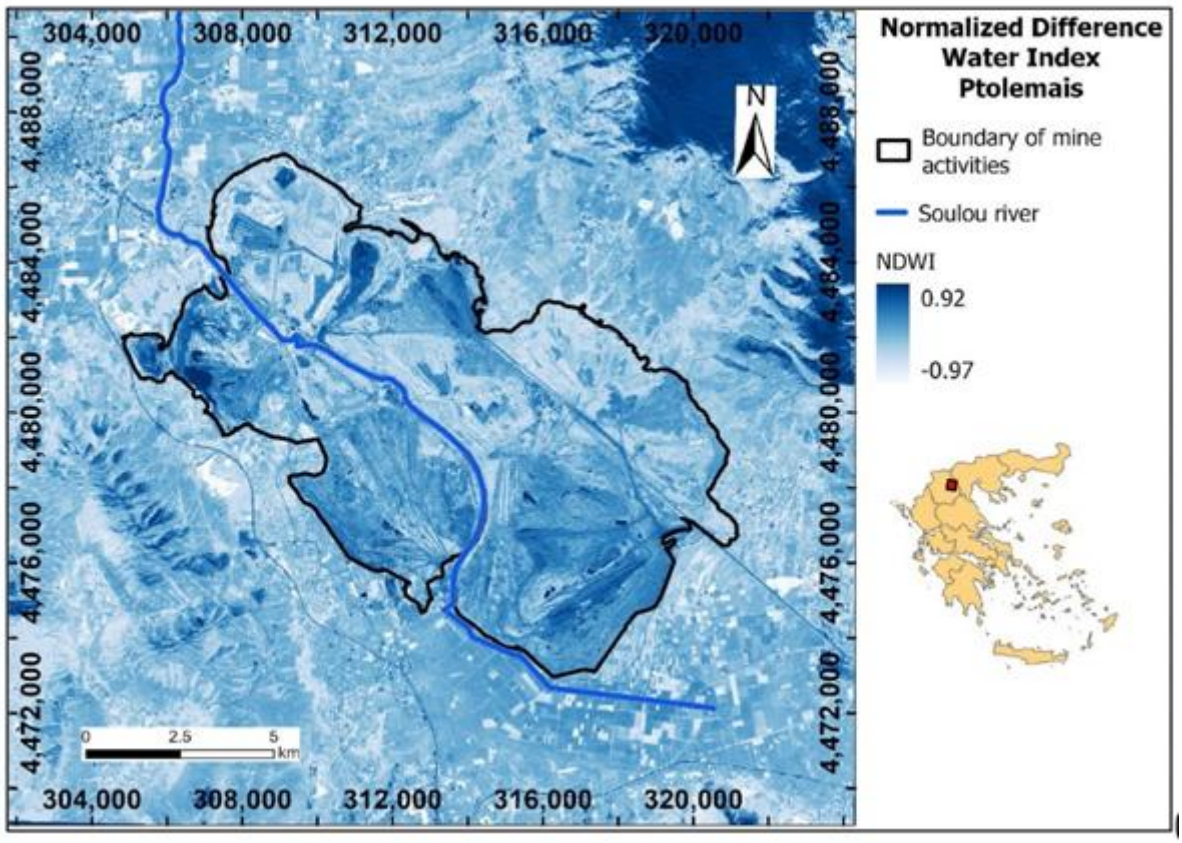

Figure 45 Spatial distribution map of NDWI, December 2021 (Ptolemais Basin, northern Greece). Water features are represented by dark blue colour. Source: Louloudis et al. 2023

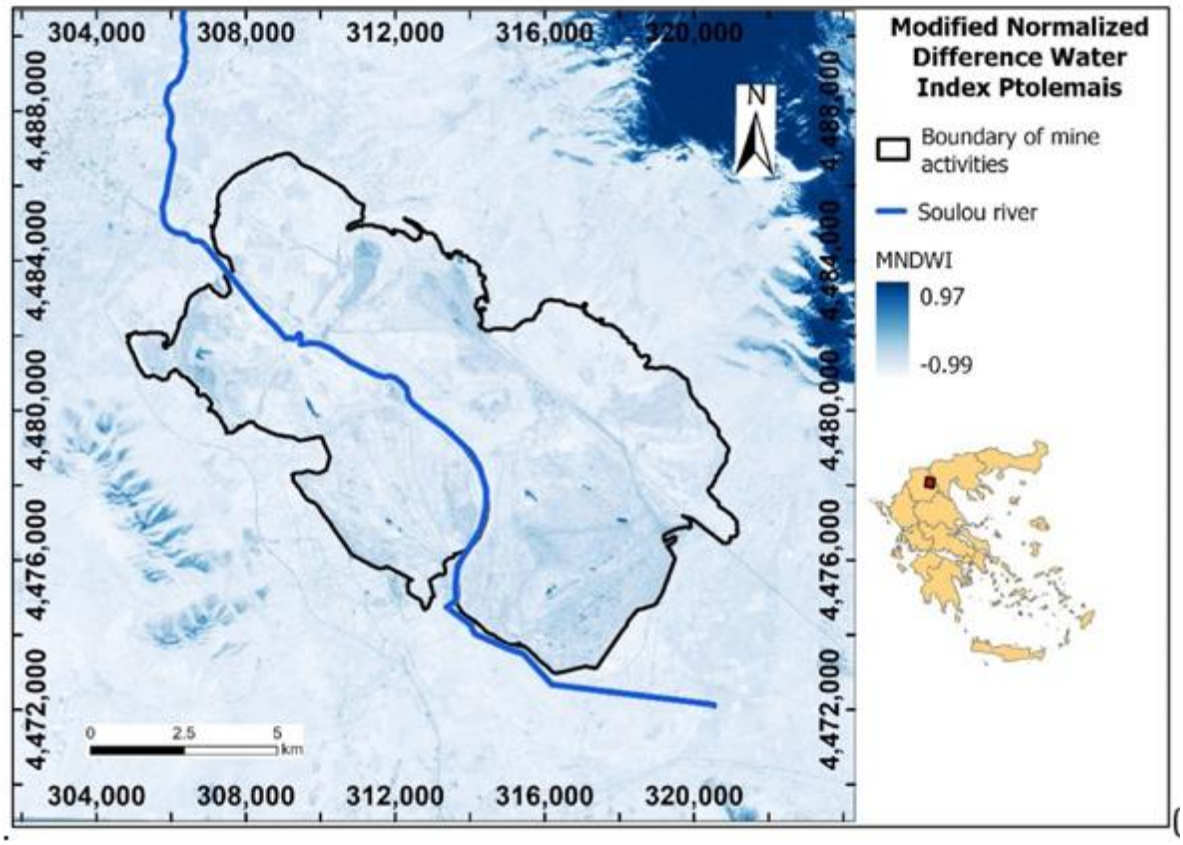

Figure 46 Spatial distribution map of MNDWI, December 2021 (Ptolemais Basin, northern Greece). Water features are represented by dark blue colour. Source: Louloudis et al. 2023.

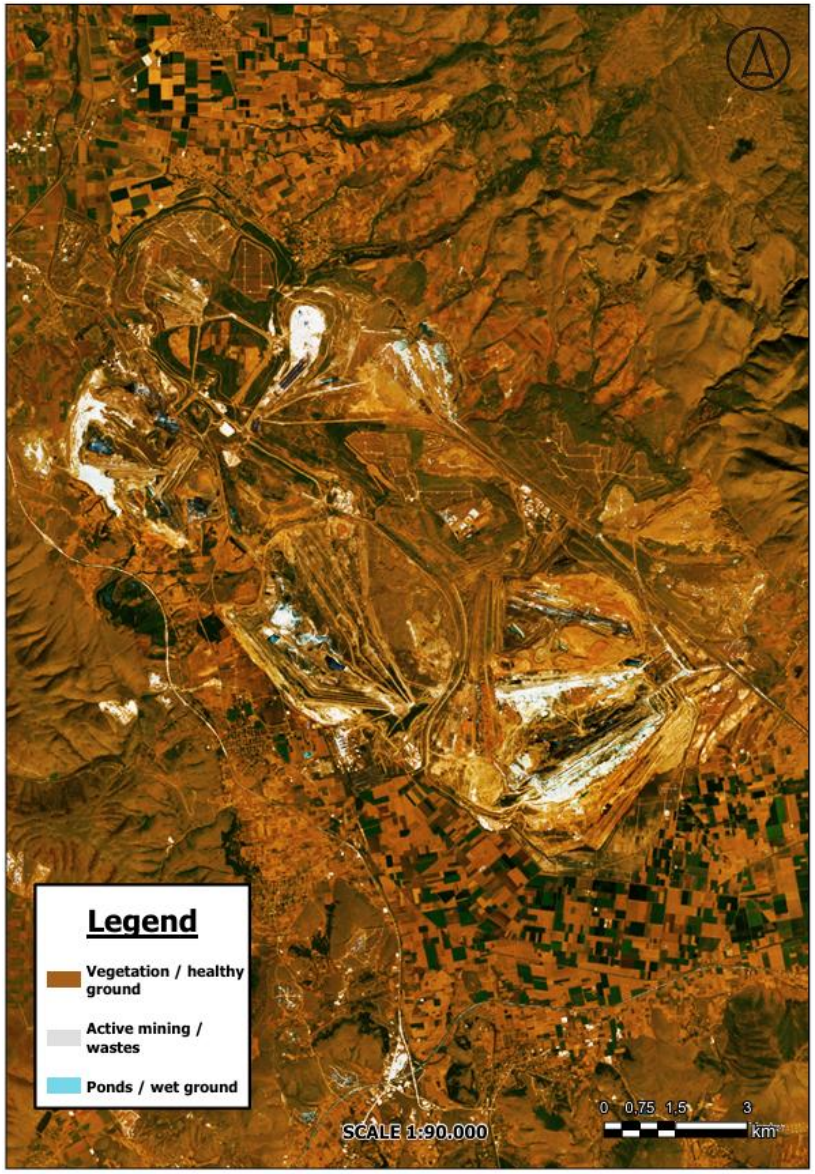

Figure 47 NDWI index for Ptolemais mine (August 2025). Source: Copernicus.

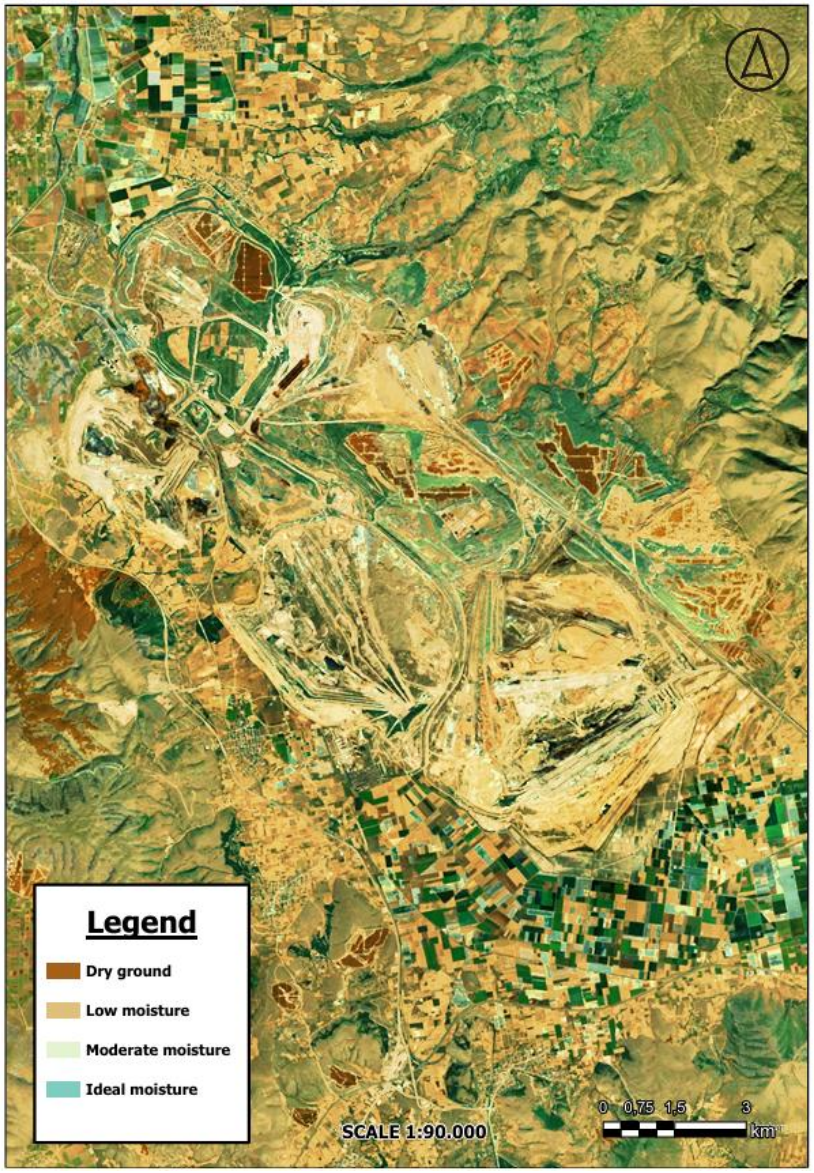

Figure 48 NDMI form Ptolemais mine (August 2025). Source: Copernicus.

The NDMI was used to determine vegetation water content by calculating the ratio between the NIR and SWIR. The area of Figure 48, as expected, display low to moderate moisture levels with higher levels in the surrounding crop cultivating areas. In addition, the water bodies found within the mines also feature low levels of moisture due to high sediment concertation.

Figure 49 presents the Land Surface Temperature spatial distribution map in July 2022, where high temperatures are observed inside the mine sites. The mean temperature value was 34 °C, while the temperature recorded at that time ranged from 9 to 45 °C.

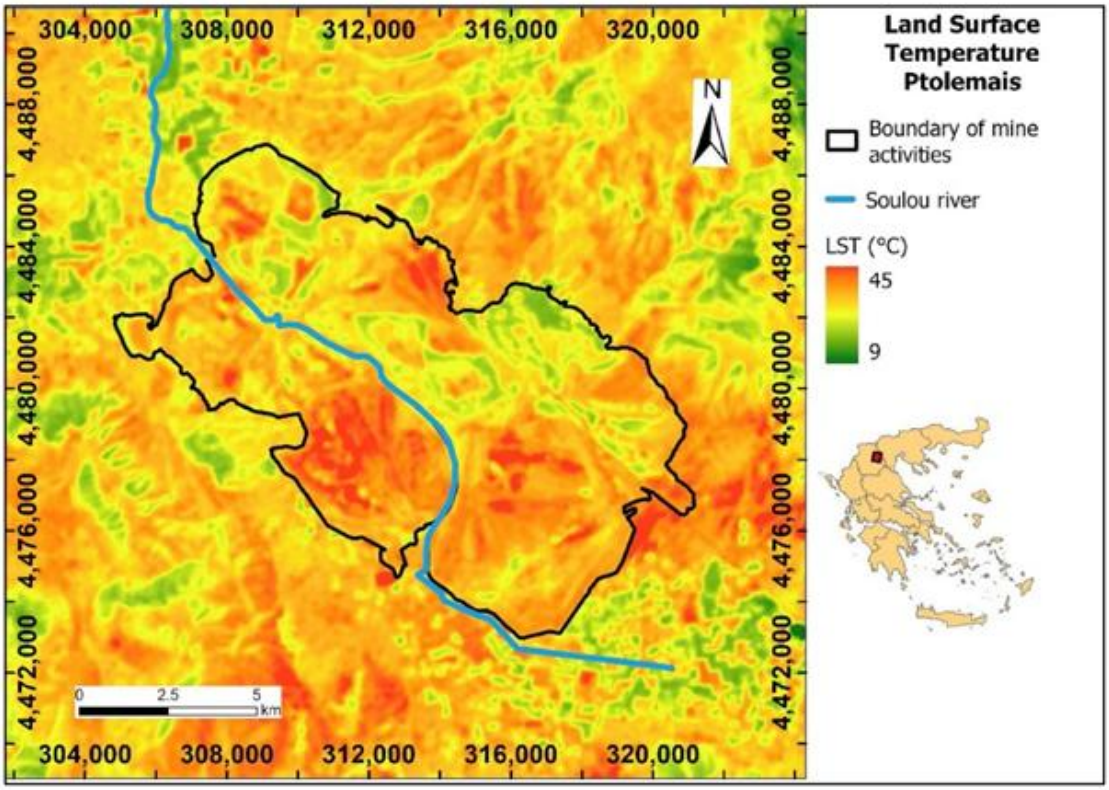

Figure 49 Spatial distribution of temperature in July 2022 (Ptolemais Basin, northern Greece). The area of mining activities is shown. Source: Louloudis et al. 2023.

The mapped Soil Moisture Index (SMI) distributed values (Figure 50) illustrate spots of high soil moisture values (the blue areas), in the areas outside the mine, representing agricultural land cover. The area outside of the waste rock dumping, i.e., north of the South Lignite Field and within the boundary of mining activities, also has high soil moisture. This is due to small forests as land cover, which were build up over the past years of reclamation activities.

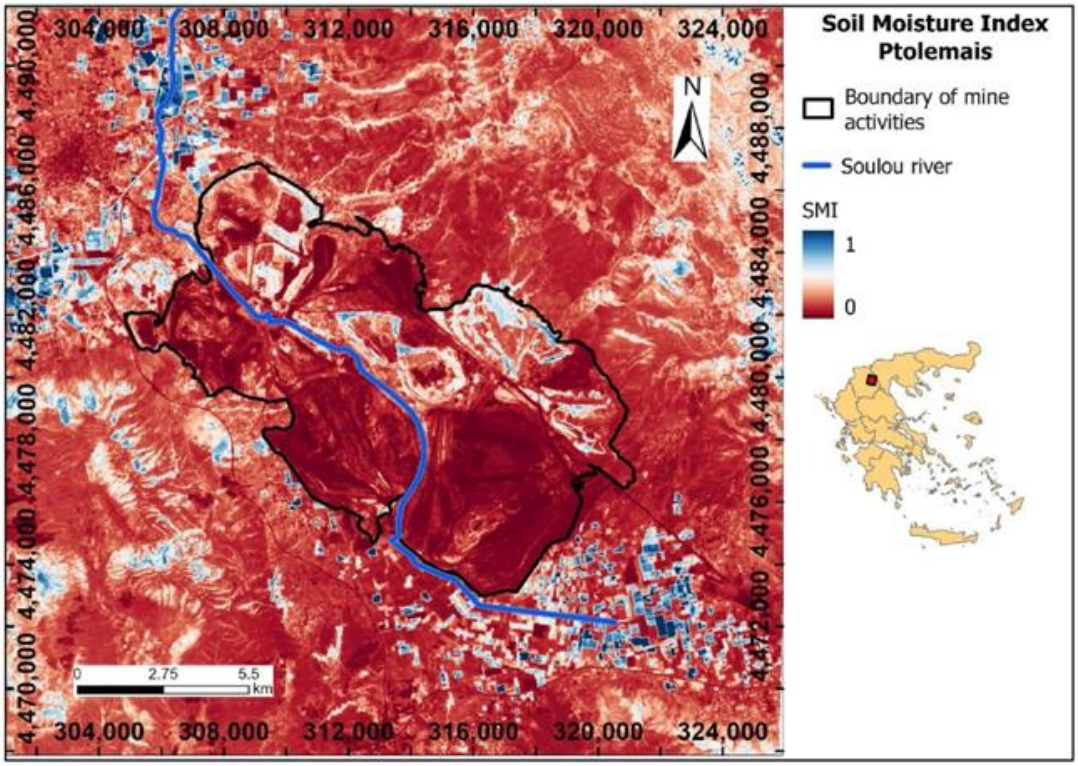

Figure 50 Spatial distribution of SMI in July 2022 (Ptolemais Basin, northern Greece). High soil moisture values are indicated by blue colour, representing agricultural fields and forests. Source: Louloudis et al. 2023.

The slope length (LS) and steepness factor are indicators which calculate the soil erosion based on Digital Elevation Model (DEM). The distribution of LS values Figure 51 for Ptolemais area indicates that water discharge is evident only in the mountains. At the same time, lower calculated values are scattered inside the boundary of the mining activity and in the agricultural area outside the mines. An important issue is the weathering intensity, which is more pronounced around Vermion Mtn.

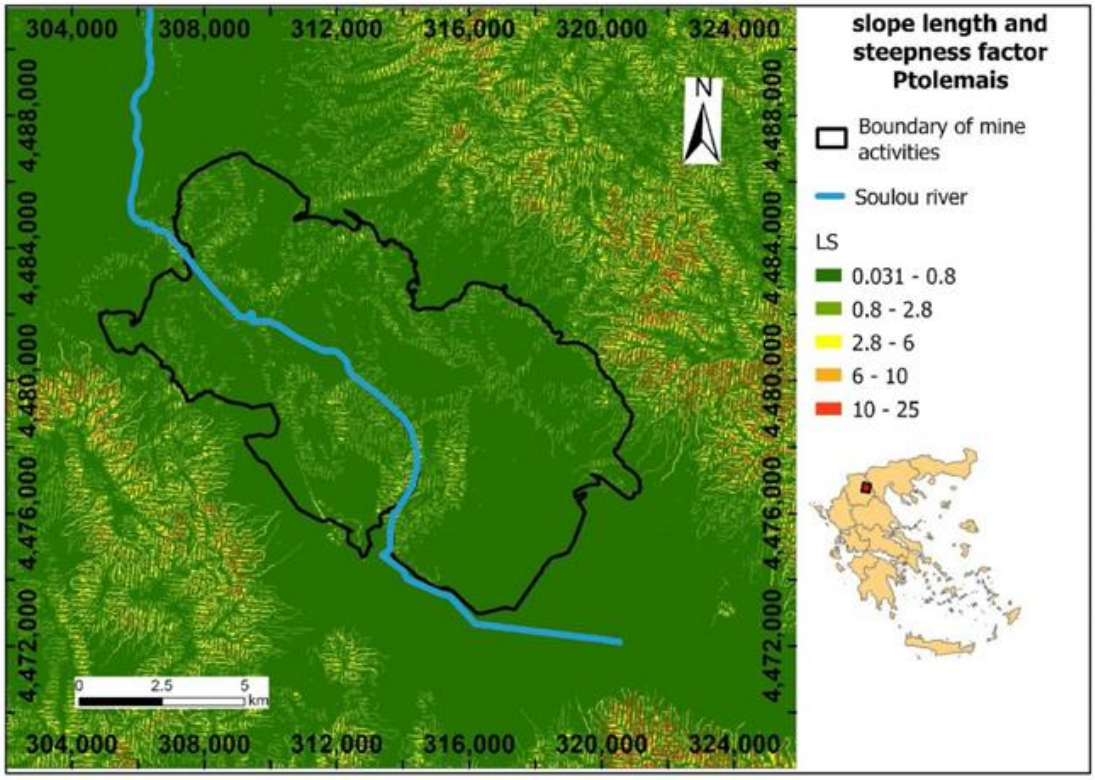

Figure 51 Spatial distribution of LS where high erosion is indicated by red colour (Ptolemais Basin, northern Greece). Source: Louloudis et al. 2023.

4.2.3. Geology of the Ptolemais Lignite Mining Area

From a geological point of view, the Ptolemais lignite basin is dominated by E-W trending normal Quaternary faults (Delogkos et al. 2018). The Ptolemais Basin covers a surface area of approximately 600 km^2. The longitudinal axis of the lignite segment of the Ptolemais Basin, with an NW-SE direction, exceeds 20 km in length, while the maximum width reaches about 20 km. The basin is filled with Late Miocene to Pleistocene Lake sediments, including intercalated lignites and alluvial deposits with a total thickness of up to 600 m. conglomerates. Above lay Quaternary conglomerates of terrestrial and fluvioterrestrial origin (Krassakis et al. 2022) (Figure 52-Figure 54).

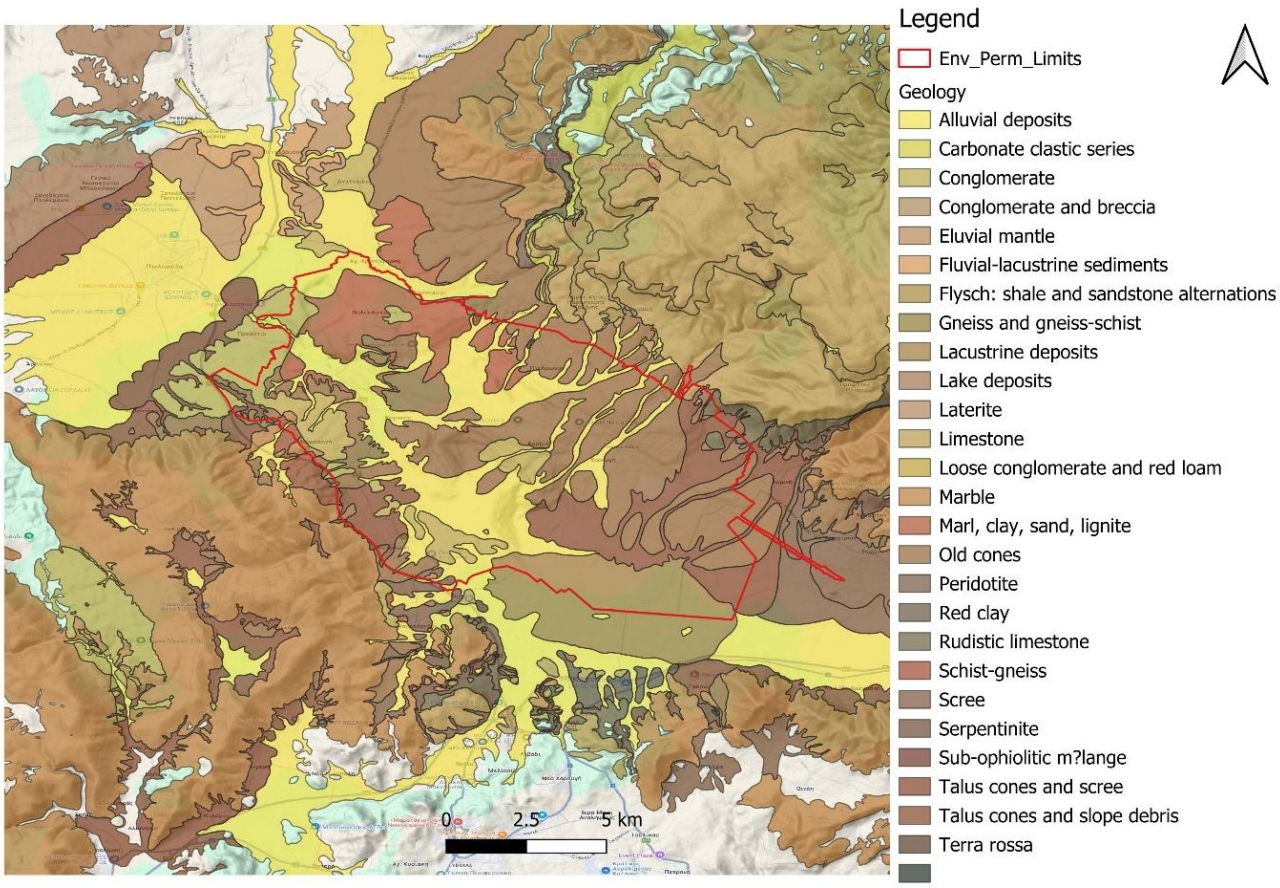

Figure 52 Part of the geological map of Greece. Source: H.S.G.M.E. Geoportal, https://geoportal.eagme.gr/geolmaps/.

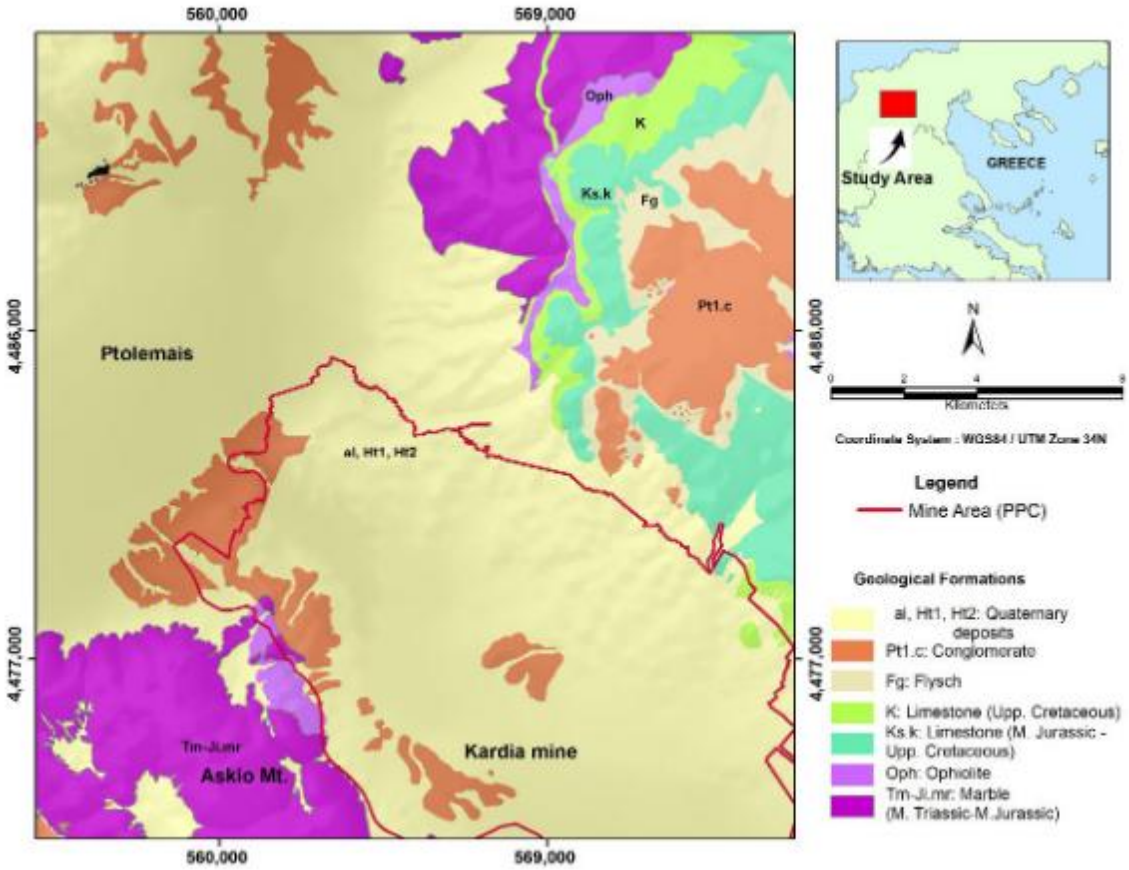

Figure 53 Simplified geological map of the Ptolemais area, located NW and SE of the city of Ptolemais (based and modified on Institute of Geology and Mineral Exploration (IGME) geological sheet, Ptolemais 1:50.000. Source: Koukouzas, 1997.

4.2.4. Agricultural Suitability Assessment

In the work of Servou et al. (2023), a land-use suitability assessment was employed for the Ptolemais mining area, considering topographic criteria and some mining characteristics. The geospatial analysis was employed for four land uses (agriculture, forest, industrial, and recreational), and the topographic criteria included slope, elevation, distance from the road network, distance from villages, distance from rivers, and distance from transmission lines. In the phase of assessing only the topographic criteria, relative importance was assigned to each criterion, and they were overlaid in a GIS environment to determine suitability for each land use. The preliminary suitability assessment was expressed from a rating scale from 1 to 5 (very low suitability to very high suitability). The agricultural land-use suitability allocation map is shown in Figure 54.

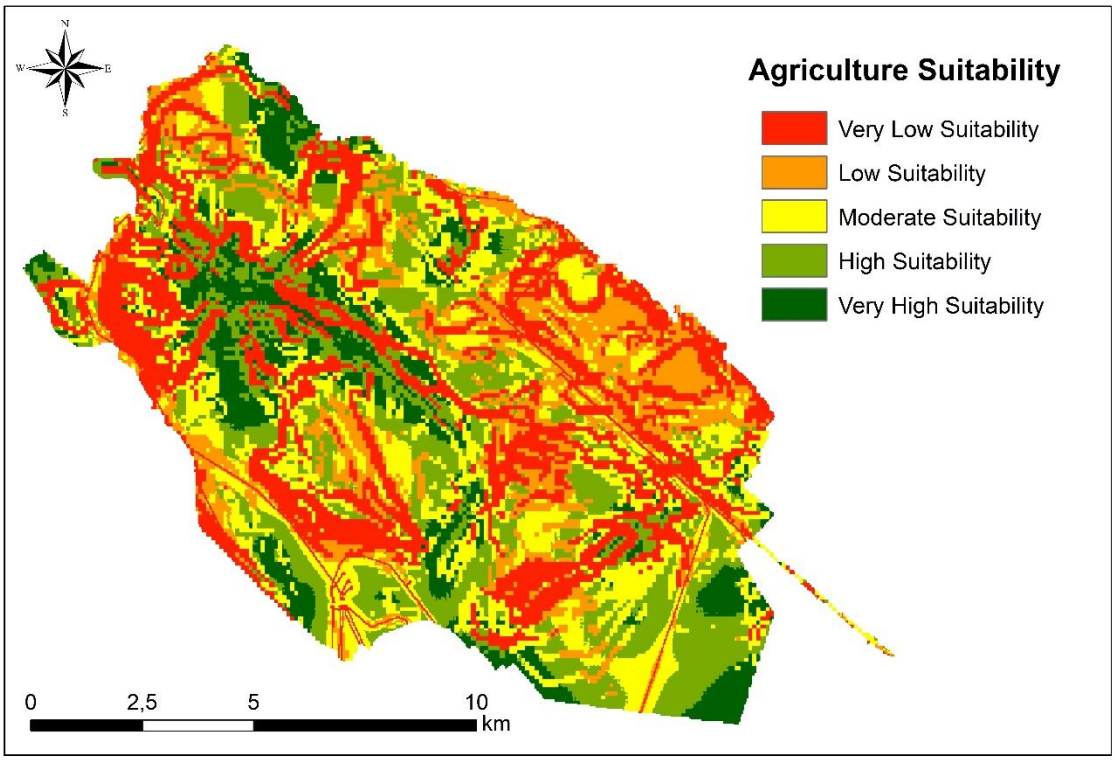

Figure 54 Agricultural suitability map within the Ptolemais mining area based on six topographic criteria.

The suitability for agricultural cultivation in the Ptolemais mining area is monitored diachronically through an extensive monitoring program employed by PPC and includes laboratory analyses concerning the following parameters:

- Available forms (diethylenetriaminepentaacetic acid-DTPA) after micronutrient extraction are used to estimate
- The potential soil availability of Cd, Co, Cr, Cu, Fe, Mn, Ni, Pb and Zn.
- Alternative Cations (Ca^{2+}, ESP, K^{+}, Mg^{2+}, Na^{+}, Cation Exchange Capacity)
- Nutritional ingredients (C_{org}, available B, available K, available P, NH_4^{+}, NO_3, organic substances)
- Mechanical Parameters (granulometric composition-content in sand, clay, silt)
- Total quantities with royal water (Cd, Co, Cr, Cu, Fe, Mn, Ni, Pb, Zn)
- Physicochemical properties ($CaCO_3$, electric conductivity E, and Ph saturation)

The map of Figure 55 shows the soil monitoring sites that PPC currently employs for the abovementioned parameters to investigate soil suitability for agricultural use. Areas that were previously used for agriculture and now host other land uses were also monitored, but they are not depicted on this map.

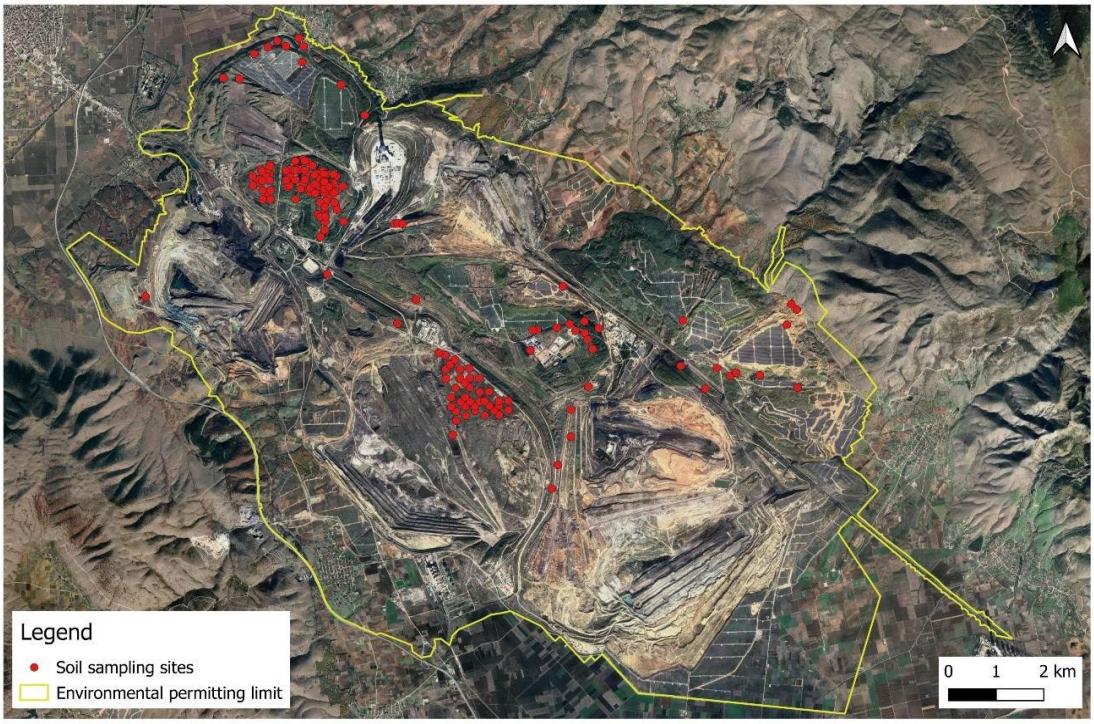

Figure 55 Soil sampling sites that are currently monitored for agricultural land use.

Earlier research by Papadopoulos et al (2015), investigated the soil quality of reclaimed areas and from sites of the greater mining area. The results showed good soil conditions, with no exceedance of the screening values determined by the regulations.

Furthermore, a specific area in the Ptolemais mining area is being monitored within the REECOL project (https://reecol.komag.eu/), which is in progress, where soil parameters are being investigated for their suitability for agricultural cultivation. This area is already reclaimed, with agricultural land, including arable land (e.g., barley), forest (e.g., acacia), and an orchard (apple trees, cherry trees, etc.). The laboratory analyses focused on micronutrient concentrations, mechanical properties (granulometric composition), physicochemical properties, and analyses to determine the soil's carbonate content and fertility.

The reclamation projects in the Ptolemais mining area are employed in parallel with the mining activities. The land-use suitability assessment in a mining area is a multidimensional problem, as mining operations are dynamic, and the respective areas are always susceptible to change. For this, it is considered that mathematical models should be combined with industrial knowledge to obtain more realistic results.

4.2.5. Selected Study area: North Field mine

The selected study area constitutes the dumping area of the exhausted North Field mine and covers 0.61 km^2. The area is covered by waste dumps 100 m thick. It concerns a non-reclaimed area where the configuration and the topsoil and clayey material cover have not yet been completed. Furthermore, this area is close to an area where byproducts (ash and gypsum) from the power plant Ptolemaida V Figure 56) are deposited. This area is intended mainly for agricultural and other uses, so it could be examined for energy crop cultivation and further analysis in the framework of the COFA project. In the broader northern area of the selected polygon, the land where the photovoltaic park is located was previously used for agriculture. Servou et al. (2023) employed a geospatial suitability analysis for several post-mining land uses in the Ptolemais mining area, and the analysis showed that the selected polygon falls within the suitable area for agricultural land use. In addition, the selected area is close to water boreholes, indicating that the water supply would be easy. On the

southern side of the selected area, the already reclaimed orchard is also supplied with water from the broader area's water boreholes. Regarding the origin of the dumping materials, these have come from several sites in the mining area and consist mainly of marls, sands, and clays.

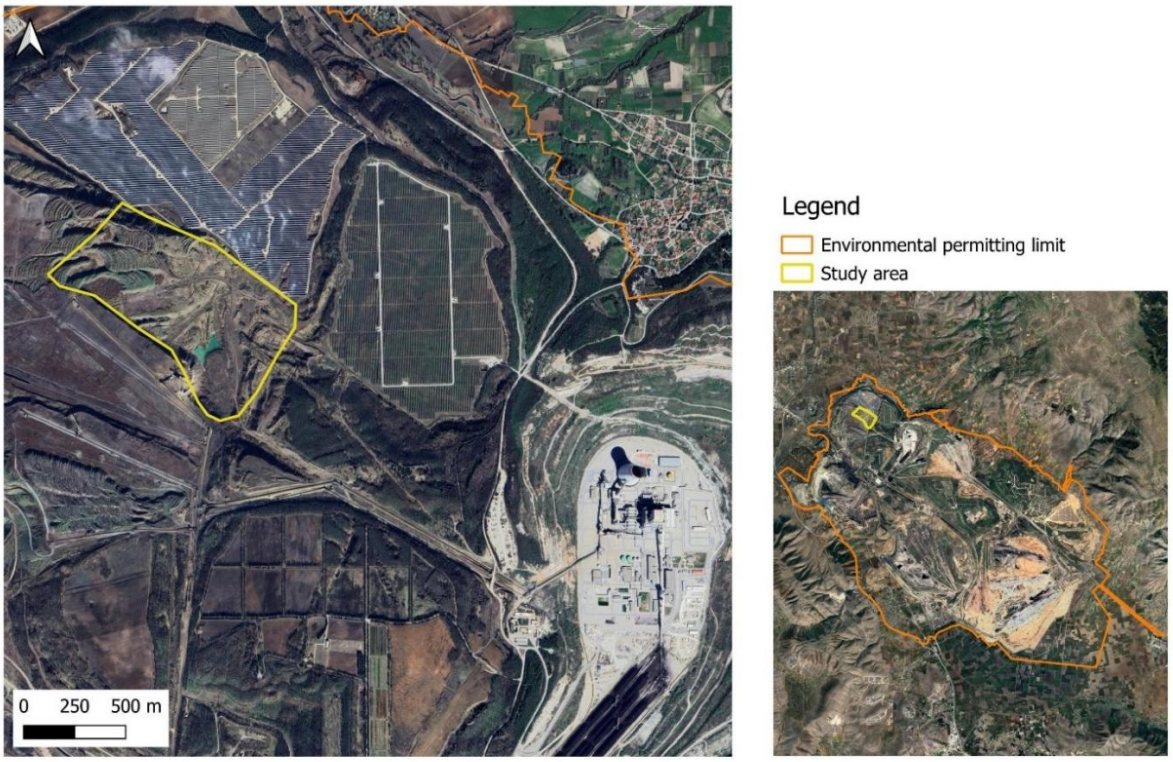

Figure 56 The polygon delineation of the study area in Google satellite basemap

4.3. Konin Lignite Basin (PL)

Additionally, this report includes a partial assessment of the Konin Lignite Basin and its potential for agricultural reclamation. The Konin region was selected due to its long history of lignite mining and its extensive experience in post-mining land reclamation, particularly in agricultural.

The Konin Lignite Basin in central Poland is a mature mining region now entering an intensive reclamation phase, with strong emphasis on water, forest and agricultural land uses (Kasztelewicz et al., 2025; Gilewska et al., 2018; Frydrychowicz et al., 2024; Kasztelewicz 2014). Long-term research in Konin shows that, with appropriate treatments, post-mining technosols can reach good physical properties and agricultural productivity, which supports the aim to justify agricultural reclamation at regional and site scale (Gilewska et al., 2018; Kołodziej et al., 2016).

4.3.1. General Characteristic of the Konin Lignite Basin

Konin is widely regarded as the cradle of Polish lignite mining, with exploitation probably starting in the 12th century and industrial open-cast mining developing in the mid-20th century (Kasztelewicz et al., 2025; Frydrychowicz et al., 2024). In 12 opencasts, about 646–650 million tonnes of lignite were extracted, requiring removal of ~3.5-3.6 billion m³ of overburden and pumping >6 billion m³ of water (Kasztelewicz et al., 2025; Frydrychowicz et al., 2024). This created a highly transformed anthropogenic landscape (Figure 57) of external dumps, deep final pits and mining lakes, now subject to multi-directional reclamation (water, forest, agriculture, recreation). Konin is also a national leader in reclamation surface: by 2010, ~3909 ha were reclaimed to agriculture and 2402 ha to forest, plus large hydrological and recreational areas (Figure 58; Kasztelewicz 2014).

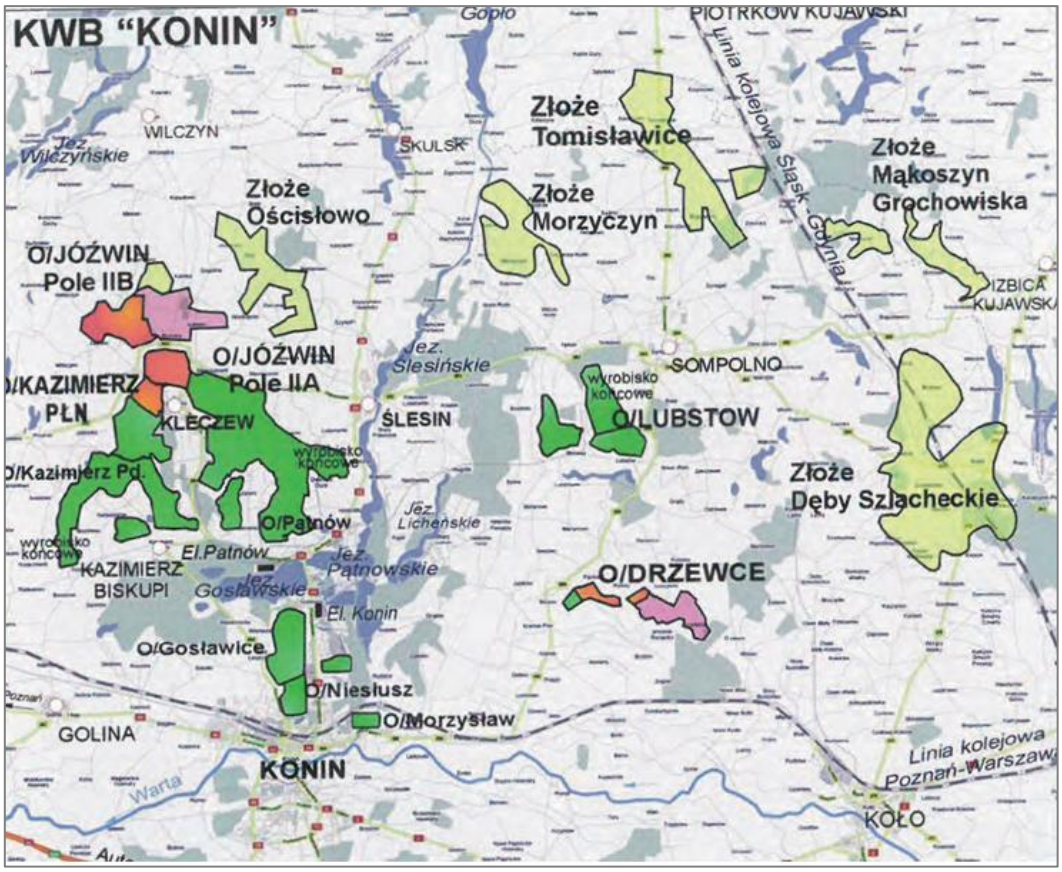

Figure 57 Mining operations and deposits in Konin Lignite Basin. Source: Bajcar et al., 2020; Kasztelewicz et al, 2010.

Table 2 Main reclamation directions in Konin
(Based on: Gilewska et al., 2018; Frydrychowicz et al., 2024; Kasztelewicz 2014; Kołodziej et al., 2016; Pratiwi et al., 2021)

Reclamation direction	Completed area (approx.)	Role in regional transition
Agricultural	3275-3909 ha	Creates new arable land, supports regional food and biomass production
Forest	1470-2402 ha	Biodiversity, carbon storage, slope stabilisation
Water (lakes)	~1517 ha existing; >600 ha lakes already built	Recreation, retention, new microclimates

Figure 58 Reclamation of mining sites in the Konin Lignite Mine. Source: Kasztelewicz et al., 2010.

4.3.2. Geological Characteristic of the Konin Lignite Mine (KLM)

The Konin Lignite Mine (KLM) area tectonically belongs to the central part of the Szczecin–Miechów Synclinorium, specifically to the Mogilno-Łódź segment and the northern part of the Konin Elevation (Wachocki et al., 2025). Most open pits are situated in shallow tectonic depressions only several tens of meters deep, whereas the Lubstów pit is an exception, located in one of the deepest structures of the Polish Lowlands, reaching depths of over 220–240 m (Wachocki et al., 2025).

Beneath the Neogene deposits, Mesozoic rocks were encountered in all pits, mainly Upper Cretaceous marls and carbonate sandstones, locally also glauconitic sands of the Lower Oligocene (Wachocki et al., 2025).

Within the KLM, two main lignite seams were exploited. The older LLS-2 (second Lusatian lignite seam) of the Ścinawa Formation (upper Lower to lower Middle Miocene) reached a maximum thickness of 86.2 m and was mined exclusively in the Lubstów pit between 1982 and 2009 (Kasztelewicz et al., 2025; Wachocki et al., 2025). The younger MPLS-1 (first Mid-Polish lignite seam) forms the lower part of the Poznań Formation and is dated to approximately 15.1–14.3 Ma; it has an average thickness of 6.6–6.9 m and was exploited in the remaining eleven pits (Kasztelewicz et al., 2025; Wachocki et al., 2025).

The overburden consists of 40–60 m thick Quaternary glaciogenic sediments of Würmian age, including features such as moraine hills and subglacial lakes (Kasztelewicz et al., 2025).

Open-pit mining enabled direct observation of significant geological structures, including cleat systems, crevasse-splay cones, paleochannels, and paleosols within the Poznań Clays. The cleat systems and crevasse splays in the MPLS-1 seam are among the best developed in the world (Wachocki et al., 2025).

4.3.3. Soil Characteristics and Implications for Agricultural Reclamation

The map (Figure 59) shows the spatial distribution of soil texture types in Poland according to the USDA classification. Most of the territory, especially in central and northern Poland, is dominated by light pink and grey-pink colours representing mainly sandy clay-loam and sandy loam, with local occurrences of blue-grey loamy sand. These soil types form the main cover of the landscape. In western Poland and in scattered areas elsewhere, light orange patches of sand appear, forming smaller and irregular areas. The southern belt is distinctly different, with a continuous zone dominated by dark green (silt) and yellow-green (silt-loam), locally transitioning into brownish-orange (loam). This creates a clearly defined strip along the southern part of the country. Bright green (clay-loam) occurs only in small patches, mainly in the northeast and southeast, while cream-colored clay is very rare and limited to minor areas. Red areas (sandy clay) and darker tones representing strongly clayey soils (silty clay, silty clay-loam) are almost absent or occur only in very small amounts. Overall, the map shows a clear pattern: sandy soils dominate in the north and centre, while finer-textured silty and loamy soils prevail in the south.

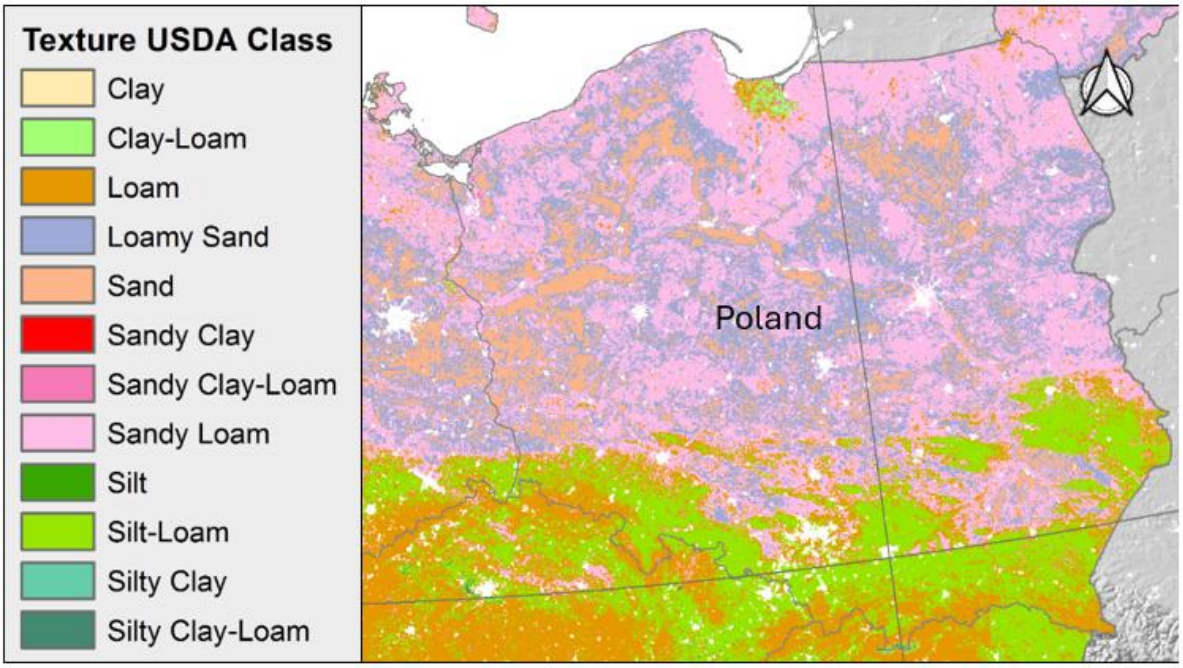

Figure 59 Texture USAD Class for Poland. Source: esdac.jrc.ec.europa.eu.

Long-term experiments on Konin internal dumps (e.g., Pątnów) show that post-mining soils are mainly sandy loam or loamy sand, with high macroporosity, good available water but sometimes sub-optimal permeability (Gilewska et al., 2018; Kołodziej et al., 2018). Different reclamation variants (black fallow, cereal monoculture, cereal + lignite dust, alfalfa/grass mixture, spontaneous succession) all produced physically acceptable topsoils, but spontaneous succession and perennial cover gave the best soil structure and organic carbon accumulation (Gilewska et al., 2018; Kołodziej et al., 2018). Agricultural reclamation in Konin and Adamów has upgraded initial low-quality soils (classes V–VI) to classes III–IV by targeted chemical repair (liming, fertilisation) and deep agrotechnical treatments, enabling successful cultivation of maize, alfalfa, cereals and fodder crops (Gilewska et al., 2018; Kołodziej et al., 2018; Kasztelewicz, 2014).

4.3.4. Why Agricultural Reclamation is Justified at Regional Scale

At the basin scale, Konin already demonstrates that large areas of post-mining land can safely transition to agriculture while maintaining acceptable soil water and air relations (Gilewska et al., 2018; Kasztelewicz, 2014; Kołodziej et al., 2016). The reasons for selecting sites of interest in the Konin Lignite Basin is a combination of:

- extensive reclaimed agricultural area,
- documented long-term soil improvement under vegetation, and
- flexible water management via numerous pit lakes and dumps (Bajcar et al, 2022).
- provides a strong evidence-based justification to select further sites (based on DEM, slope, LST, NDVI, NDMI/NDWI, and urban pressure) as candidates for agricultural end-use within the regional reclamation strategy.

Konin is a heavily transformed but well-studied lignite basin with a long reclamation record. Its geology and glacial overburden explain the dominance of sandy, well-drained substrates, while decades of trials show these technosols can reach good physical quality and crop productivity when reclamation is properly designed.

Although the Konin Lignite Basin provides an excellent example of successful post-mining agricultural reclamation, a regional-scale assessment of agricultural suitability was not undertaken in this study. The majority of mining areas within the basin have already completed or nearly completed their reclamation programmes, and their final land-use directions have been established and implemented over the past several decades. Consequently, a regional suitability assessment would have limited practical value for supporting future reclamation planning and decision-making.

Instead, the analysis focuses on the Jóźwin IIB open-pit, which is currently undergoing closure and reclamation. As one of the last active post-mining landscapes in the Konin region, Jóźwin IIB represents a unique opportunity to evaluate agricultural reclamation potential before the final land-use configuration is fully established. The site remains subject to ongoing geomorphological transformation, water management activities, and land-use planning decisions, making it particularly suitable for assessing the applicability of remote sensing and terrain-based indicators in reclamation planning.

Furthermore, the Konin region already possesses extensive scientific documentation demonstrating the feasibility of agricultural reclamation on post-mining technosols. Long-term field experiments and reclamation projects have confirmed that reclaimed mining areas can successfully support agricultural production following appropriate soil reconstruction and management measures. Therefore, rather than reassessing agricultural suitability across areas where reclamation outcomes are already known, this study concentrates on Jóźwin IIB as a representative case where suitability assessment may still provide practical guidance for future reclamation activities.

The selection of Jóźwin IIB is additionally justified by the coexistence of two major post-mining land-use directions within the same site. While the final excavation is planned to be transformed into an anthropogenic lake through water reclamation, extensive internal dumps remain available for agricultural reclamation. This creates an opportunity to evaluate how topographic conditions, environmental indicators, and spatial constraints influence the allocation of land between water and agricultural end uses during the final stages of mine closure.

4.3.5. Use of Digital Elevation Model at Konin Lignite Mine

To further evaluate the suitability of post-mining areas for agricultural end-use within the Konin Lignite Basin, a detailed Digital Elevation Model (DEM) and slope analysis were performed for the Jóźwin IIB open pit, one of the largest mining excavations currently undergoing closure and reclamation. The site represents a valuable case study because reclamation activities have been implemented progressively during the mining operation, following the long-established reclamation practices developed in the Konin region. This approach allows the assessment of landform characteristics that will ultimately determine the feasibility of future agricultural use.

- **Elevation of the Konin Lignite Mine**

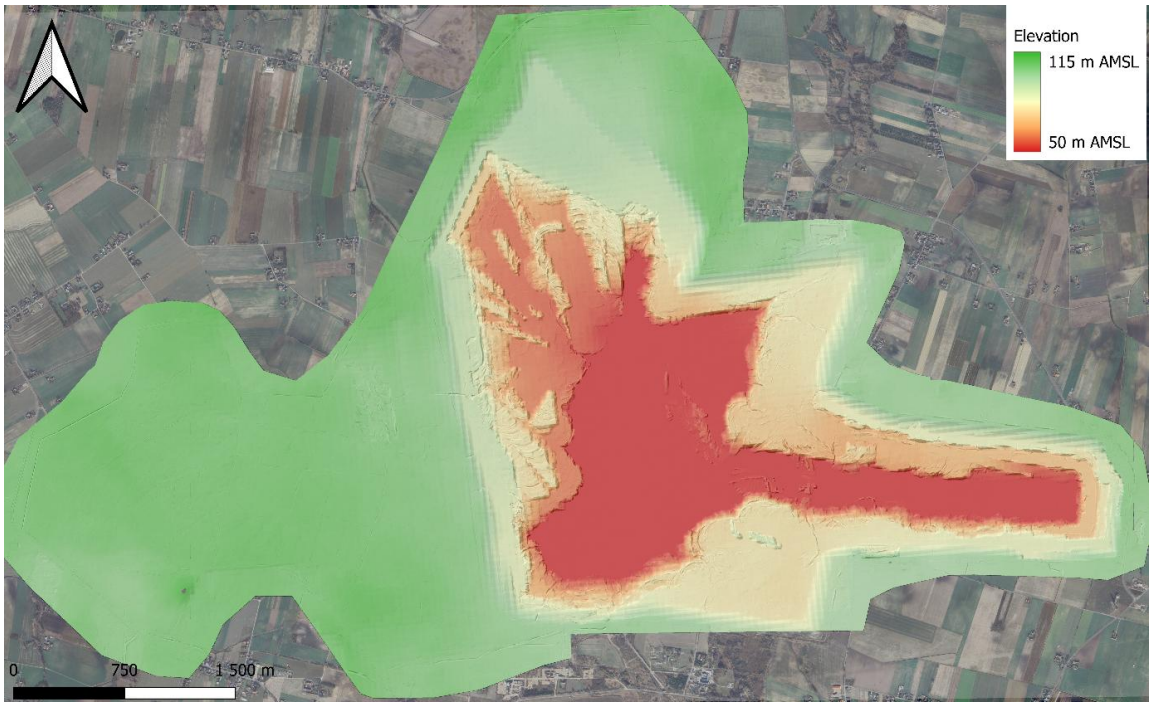

Figure 60 Elevation differences in Jóźwin IIB open-pit. Source: Polish Airborne LiDAR (ALS), data provided by Head Office of Geodesy and Cartography (GUGiK) via Geoportal.gov.pl.

The DEM analysis reveals a strongly diversified post-mining landscape with elevations ranging from approximately 50 m to 115 m above mean sea level. The lowest elevations correspond to the final excavation, while the highest areas are associated with reclaimed spoil heaps and surrounding reconstructed terrain. Such elevation differences reflect both the original mining geometry and subsequent earthworks conducted during reclamation.

- **Steepness of slope at Konin Lignite Mine**

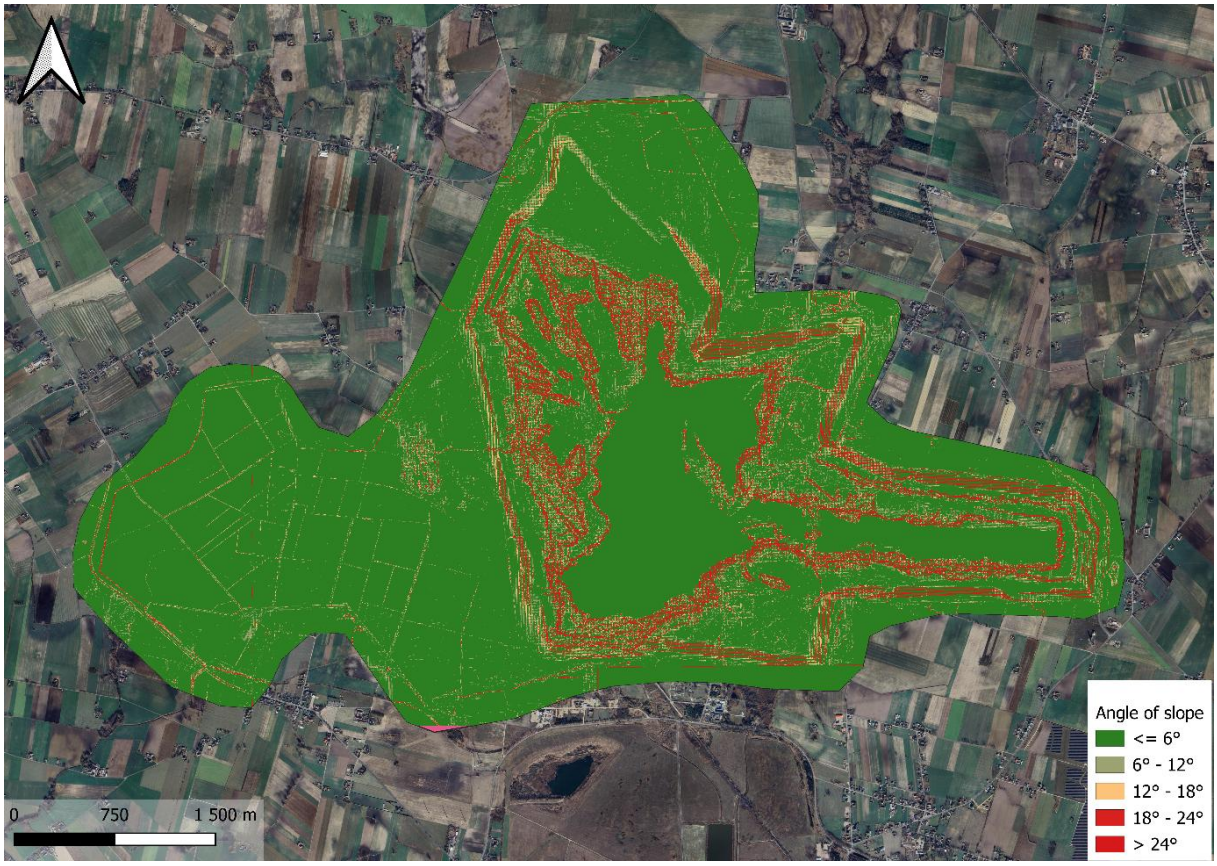

Figure 61 Slope steepness in Jóźwin IIB open-pit. Source: Polish Airborne LiDAR (ALS), data provided by Head Office of Geodesy and Cartography (GUGiK) via Geoportal.gov.pl

Slope analysis indicates that the majority of the reclaimed area is characterized by gentle slopes below 6°, which dominate the external and internal dump surfaces. Areas with moderate slopes (6-12°) occur mainly along transitional zones between reclamation levels, whereas steeper slopes exceeding 18° and locally 24° are concentrated around the margins of the final excavation and along remnants of former mining benches.

From the perspective of agricultural reclamation, these results are highly favourable. The predominance of surfaces with slopes below 6° suggests that a substantial proportion of the area is suitable for mechanised agricultural operations, including crop cultivation, biomass production, and grassland establishment. Such terrain minimizes erosion risk, facilitates field management, and allows efficient use of agricultural machinery. The observed morphology is consistent with the reclamation objectives historically implemented in the Konin mining district, where extensive areas of former spoil dumps have been successfully converted into productive agricultural land.

Nevertheless, several geomorphological constraints remain. The steep slopes surrounding the final excavation exhibit increased susceptibility to erosion and are less suitable for intensive agricultural use. These areas may require alternative reclamation measures, including permanent vegetation cover, afforestation, or ecological buffer zones. In addition, local relief variations may influence surface runoff patterns and require careful water management planning during the final stages of reclamation.

The interpretation of these results must also consider the planned final land use of the Jóźwin IIB excavation. Unlike many reclaimed spoil dumps intended primarily for agricultural production, the final pit is designated for water reclamation through the creation of a large anthropogenic lake. Consequently, the deepest portions of the excavation will not be available for agricultural use. Instead, agricultural reclamation will be concentrated on the gently sloping reclaimed areas

surrounding the future reservoir. In this context, the slope analysis confirms that the majority of these surrounding surfaces possess favourable topographic conditions for agricultural development.

The planned lake may further enhance the long-term value of adjacent agricultural land by improving local water retention, moderating microclimatic conditions, and increasing landscape diversity. Therefore, the future land-use structure of the Jóźwin IIB site can be considered complementary rather than competitive, combining water reclamation within the final excavation with agricultural reclamation on the surrounding reclaimed terrain.

Overall, the DEM-based assessment demonstrates that Jóźwin IIB exhibits a high potential for agricultural reclamation outside the final pit area. The dominance of low-gradient surfaces, together with the extensive reclamation experience gained throughout the Konin Lignite Basin, provides strong evidence that agricultural land use can form an important component of the site's post-mining development strategy.

- **Selection of the Internal Dumping Ground for Detailed Assessment**

While the Digital Elevation Model and slope analyses were conducted for the entire Jóźwin IIB mining area, the results clearly indicated that only a portion of the site remains suitable for future agricultural reclamation. The deepest parts of the final excavation are designated for water reclamation and the creation of an anthropogenic lake, whereas several peripheral areas are characterised by steep slopes or ongoing geomorphological transformations that limit their agricultural potential.

Based on the DEM analysis, a selected section of the internal dumping ground located in the northern part of the Jóźwin IIB open pit was identified as the most suitable area for further agricultural suitability assessment. This area is characterised by relatively gentle terrain, limited relief variability, and its location outside the planned final water reservoir. Moreover, the area has already undergone initial reclamation measures, including the establishment of vegetation cover as part of the progressive reclamation process carried out during the final stages of mining operations. As a result, it represents a large, contiguous reclaimed surface with conditions suitable for further agricultural development.

The selected internal dump therefore constitutes a representative example of land that may realistically be allocated to agricultural reclamation during the final stage of mine closure. Focusing the subsequent analysis on this area enables a more detailed evaluation of environmental conditions directly relevant to future agricultural use.

- **Vegetation and Moisture Conditions of the Selected Internal Dump**

To complement the topographic assessment, vegetation and surface moisture conditions were analysed using Sentinel-2 satellite imagery. Two indicators were calculated for the selected internal dump: the Normalized Difference Vegetation Index (NDVI) and the Normalized Difference Water Index (NDWI). These indicators provide information on vegetation development and moisture availability, both of which are important factors influencing the agricultural potential of reclaimed post-mining land.

The NDVI results indicate a clear spatial differentiation of vegetation development across the analysed area (Figure 62). The northern and north-eastern parts of the internal dump exhibit the highest NDVI values, locally exceeding 0.8, indicating dense and well-established vegetation cover. These areas correspond to surfaces that have already undergone reclamation treatments and vegetation establishment, demonstrating favourable conditions for future agricultural use. In contrast, lower NDVI values occur mainly in the southern and south-western portions of the analysed area, where vegetation remains less developed and the substrate is still partially exposed. The observed pattern suggests that large parts of the selected internal dump already provide environmental conditions conducive to plant growth and biomass production, supporting their suitability for agricultural reclamation.

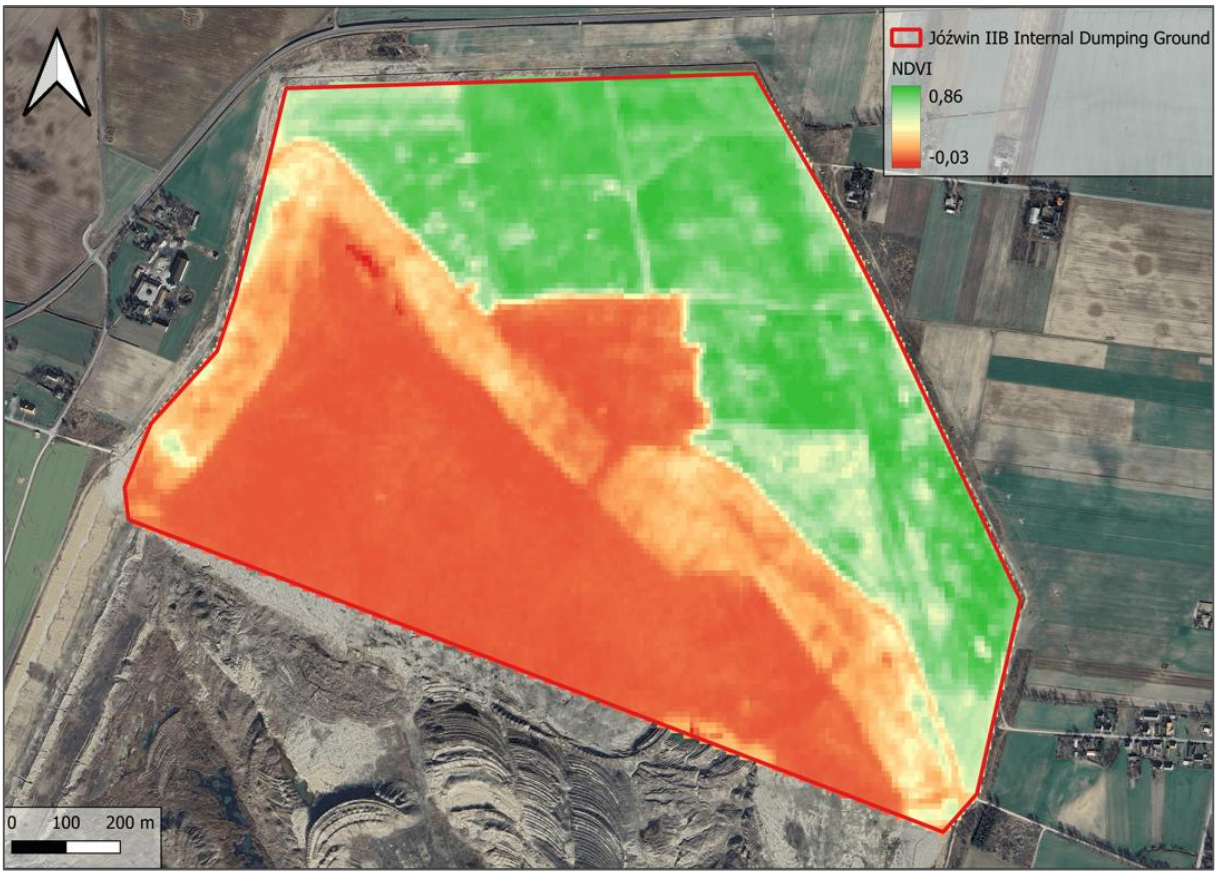

Figure 62 NDVI distribution within the selected Jóźwin IIB internal dumping ground, September 2025. Source: Own elaboration based on Copernicus Sentinel-2 L2A imagery (ESA), processed in Google Earth Engine.

The NDWI analysis reveals a complementary pattern (Figure 63). Higher NDWI values occur predominantly within the central and southern parts of the analysed area, indicating increased surface moisture availability, while lower values are concentrated in the northern sector, suggesting relatively drier conditions. Overall, the moisture distribution remains within the range typically observed for reclaimed and vegetated post-mining surfaces and does not indicate the presence of extensive waterlogged areas that could restrict agricultural use.

Particular attention should be given to several localised zones exhibiting distinctly elevated NDWI values within the selected internal dump. These small blue-coloured anomalies correspond to areas where water is accumulating within subtle terrain depressions formed during dumping and reclamation activities. Such features are commonly observed on reclaimed spoil heaps, where local microtopography influences runoff and infiltration processes. The presence of these moisture accumulation zones indicates the development of natural water retention features capable of storing water after precipitation events and gradually releasing it to the surrounding soil.

From an agricultural reclamation perspective, these localised wet areas may provide additional benefits rather than constraints. They can contribute to improved water availability during dry periods, support vegetation establishment, and increase the resilience of future agricultural systems to seasonal drought. At the same time, their limited spatial extent suggests that they are unlikely to interfere with mechanised agricultural operations or significantly reduce the area available for cultivation. Instead, they may serve as small-scale retention zones enhancing the overall environmental quality of the reclaimed landscape.

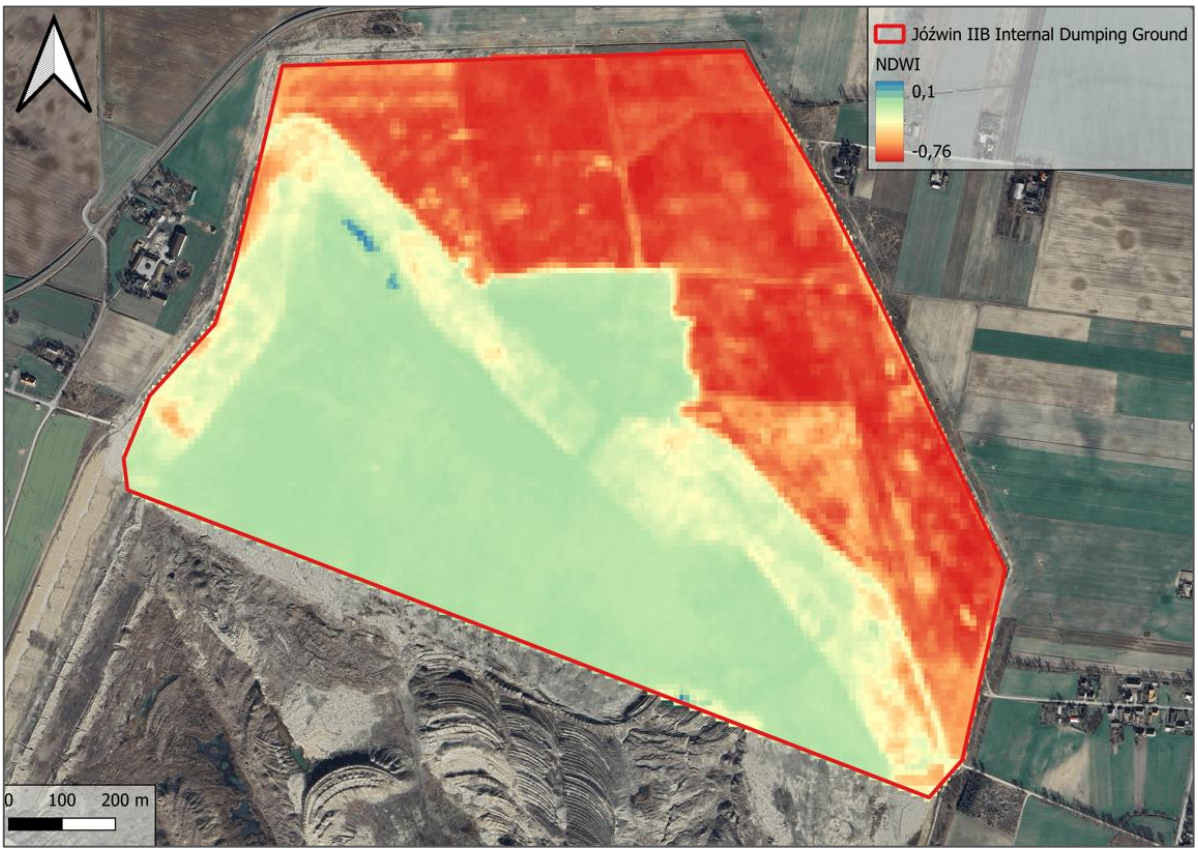

Figure 63 NDWI distribution within the selected Jóźwin IIB internal dumping ground, September 2025. Source: Own elaboration based on Copernicus Sentinel-2 L2A imagery (ESA), processed in Google Earth Engine.

When interpreted together, the NDVI and NDWI analyses indicate that the selected internal dumping ground already exhibits environmental conditions favourable for agricultural reclamation. The combination of well-developed vegetation cover, moderate moisture availability, and the presence of local natural retention features suggests that the area possesses a high potential for future agricultural use. These findings further demonstrate the value of integrating terrain analysis with remote sensing indicators when identifying priority areas for agricultural reclamation within post-mining landscapes.

4.4. Upper Silesian Coal Basin (PL)

4.4.1. Soil Characteristics and Implications for Agricultural Reclamation

Waste rock dumps are usually much smaller than those formed at open-pit mines and often are shaped with steep slopes, which limits their use for agricultural purposes. The detailed analyses in the REECOL project indicate that the main cause of limited vegetation growth on waste rock dumps is the limited availability of phosphorus and, probably, nitrogen, as well as the low content of easily decomposable organic matter.

Another degrading factor is often the improper physical structure of the substrate. The content of skeleton particles >2 mm is above 60%, and it is much higher than in agricultural native soil. This could have a negative impact on the substrate's water holding capacity. This soil structure makes it impossible to perform agricultural operations such as plowing. Waste from hard coal mining has a dark color, which causes the unvegetated surface of the spoil heap to heat up significantly during periods of intense sunlight. As a result, vegetation is exposed to severe thermal stress even in the early stages of development (as early as April and May). High surface temperatures also cause water deficits in plants, especially during periods of heat and drought. Despite these factors that limit plant

growth, it appears feasible to reclaim these areas for agricultural use, particularly for the cultivation of energy crops. This is evidenced by the successful reclamation of Carboniferous rock dumps for forestry purposes. One positive aspect is that waste dumps from hard coal mining in the Upper Silesia region are characterized by low levels of trace substances (e.g., heavy metals) that could pose an environmental and health risk.

To identify potential areas for energy crop cultivation, a spatial analysis of post-mining lands stored in the OPI-TPP project database was conducted, taking into account key environmental and land-use constraints. The analysis included the delineation of areas occupied by forests and tree cover, water bodies (ponds, lakes, and other reservoirs), terrains with slopes exceeding 12%, and impervious surfaces.

Based on the adopted criteria, land classification was carried out, considering both individual constraints and their co-occurrence in the form of hybrid configurations (e.g., areas simultaneously forested and characterized by steep slopes). This approach enabled a more precise assessment of the suitability of individual areas. The remaining lands, not affected by any of the analyzed constraints, were classified as so-called “clean areas.”

The results of the conducted analysis indicate that, despite the significant level of degradation typical of post-mining areas, it is possible to identify zones with real potential for development for energy crop cultivation. Preliminary results of the analysis indicate that, within post-mining spoil heaps in the Silesian Voivodeship, 14 sites have been identified that contain areas larger than 10 hectares with potential suitability for energy crop cultivation.

Preliminary results of the analysis indicate that, within post-mining spoil heaps in the Silesian Voivodeship, 14 sites have been identified that contain areas larger than 10 hectares with potential suitability for energy crop cultivation.

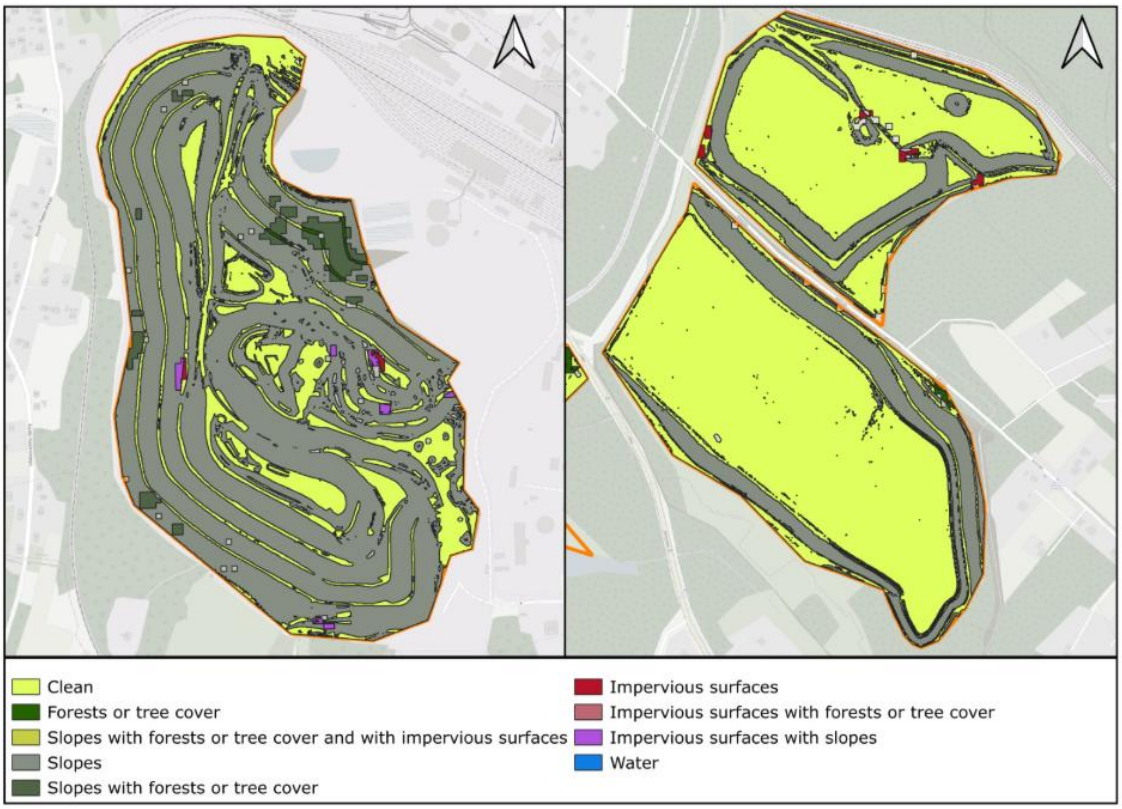

Figure 64 Example spatial analysis of the landfill site – high potential (left), low potential (right).

An example of a spatial analysis of the preliminary suitability of a landfill site for agricultural reclamation is depicted on Figure 64 – on the right, a site with high potential; on the left, one with low potential.

5. Conclusion and Recommendations

This deliverable presents a methodological framework and spatial analysis of agricultural reclamation suitability in selected post-mining areas. By combining main indicators: terrain morphology, land surface temperature, and water conditions, with supplementary indicators including soil texture, vegetation cover, land use, and surface imperviousness, the study provides a layered basis for identifying land with potential for agricultural and energy crop production.

The results demonstrate that post-mining landscapes are highly heterogeneous in terms of their reclamation potential. While certain areas exhibit conditions broadly compatible with agricultural use, others remain constrained by steep slopes, residual soil dysfunctions, or existing land uses. The spatial variability found in all study areas emphasizes the need to evaluate individual sites individually, rather than relying on general reclamation planning.

Suitability maps created within this output can serve as a decision support tool for subsequent field surveys and experimental activities. The proposed candidate sites for energy crop cultivation represent preliminary suggestions based on remote sensing and GIS data. Further steps should consider integrating the outcomes of D3.1 with the soil dysfunction classifications established in D3.2 to refine the overall assessment. This summary of Deliverables D3.1 and D3.2 will be further developed in the subsequent Deliverable D3.3, which focuses on the analysis of soil regeneration and the development of a methodology for agricultural reclamation.

It is recommended that future analyses expand the spatial coverage to include all project study areas. The methodology developed here may also serve as a transferable template for suitability assessments in other post-mining regions beyond the project scope.

6. References

Bajcar, A., Szczepiński, J., & Rogosz, B. (2022). Bathymetry Surveys of Post-Mining Pit Lakes Formed after Exploitation of Lignite. *International Conference on Raw Materials and Circular Economy*. https://doi.org/10.3390/materproc2021005117.

Ballabio, C., Lugato, E., Fernández-Ugalde, O., Orgiazzi, A., Jones, A., Borrelli, P., ... & Panagos, P. (2019). Mapping LUCAS topsoil chemical properties at European scale using Gaussian process regression. Geoderma, 355, 113912.

Ballabio, C., Panagos, P., & Monatanarella, L. (2016). Mapping topsoil physical properties at European scale using the LUCAS database. Geoderma, 261, 110-123.

Carlson, T. N., & Ripley, D. A. (1997). On the relation between NDVI, fractional vegetation cover, and leaf area index. Remote sensing of Environment, 62(3), 241-252.

ČERMÁK, Petr a ONDRÁČEK, Vratislav. (2006). Reclamation of anthropogenic soils of the spoil heaps of the North Bohemian Brown Coal Basin: a methodological guide. Praha: Research Institute for Land Reclamation and Soil Protection, ISBN 80-239-8078-5.

Chlupáč, I., Brzobohatý, R., Kovanda, J., & Stráník, Z. (2002). The geological past of the Czech Republic. Academia. ISBN 80-200-0914-0

Chodak, M. (2013). Methods of reclamation and management of post-exploitation areas in hard rock mining. Poltegor-Institute of Surface Mining Publishing.

Copernicus / ESA. (n.d.). Sentinel 2 L2A Scene Classification Map – General description. Sentinel Hub custom scripts. Retrieved from https://custom-scripts.sentinel-hub.com/custom-scripts/sentinel-2/scene-classification/

Czech Office for Surveying, Mapping and Cadastre. (2016). ZABAGED® – Elevation – Digital elevation model 5th generation (DMR 5G) [Data file]. Geoportal ČÚZK. https://geoportal.cuzk.cz/Default.aspx?lng=CZ&mode=TextMeta&side=vyskopis&metadataID=CZ-CUZK-DMR5G-V

Davis, R. O. E., & Bennett, H. H. (1927). Grouping of soils on the basis of mechanical analysis (No. 419). U.S. Department of Agriculture.

Delogkos, E., Childs, C., Manzocchi, T., & Walsh, J. J. (2018). The nature and origin of bed-parallel slip in Kardia Mine, Ptolemais Basin, Greece. Journal of Structural Geology, 113, 115–133.

DIAMO. (2025). Lake Most. https://www.diamo.cz/cs/milada-most/jezero/most

Diek, S., Fornallaz, F., Schaepman, M. E., & de Jong, R. (2017). Barest pixel composite for agricultural areas using Landsat time series. Remote Sensing, 9(12), 1245. https://doi.org/10.3390/rs9121245

European Space Agency. (2024). Release of Sen2Cor 2.12. STEP ESA. https://step.esa.int/main/release-of-sen2cor-2-12/

Fraštia, M., & Řehoř, M. (2014). Smoothing out the consequences of mining activities – reclamation of the Radovesice spoil heap. Severočeské doly / Research Institute for Brown Coal.

Frydrychowicz, D., Galantkiewicz, E., Kasztelewicz, Z., & Widera, M. (2024). 80 lat Kopalni Węgla Brunatnego Konin Część I – historia rozpoznania złóż i ich eksploatacja. *Przegląd Geologiczny*. https://doi.org/10.7306/2024.34.

Gao, B. C. (1996). NDWI—A normalized difference water index for remote sensing of vegetation liquid water from space. Remote Sensing of Environment, 58(3), 257–266.

Gilewska, M., & Otremba, K. (2018). The some aspects of agricultural reclamation the post-mining grounds of the Konin and Adamów Brown Coal Mines. *Inżynieria Ekologiczna*. https://doi.org/10.12912/23920629/93486.

Grünbaum, D. (2011). Assessment and evaluation of the proposal for the overall reclamation of the Nástup Tušimice Mines area [Master's thesis, VŠB – Technical University of Ostrava, Faculty of Mining and Geology].

Hengl, T. (2006). Finding the right pixel size. Computers & Geosciences, 32(9), 1283–1298.

Huang, S., Tang, L., Hupy, J. P., Wang, Y., & Shao, G. (2021). A review of commentary on the use of the normalized difference vegetation index (NDVI) in the era of popular remote sensing of the earth. Journal of Forestry Research, 32, 1–6. https://doi.org/10.1007/s11676-020-01155-1

Kasztelewicz, Z. (2014). Approaches to Post-Mining Land Reclamation in Polish Open-Cast Lignite Mining. *Civil And Environmental Engineering Reports, 12*, 55 - 67. https://doi.org/10.2478/ceer-2014-0006.

Kasztelewicz, Z., Frydrychowicz, D., Galantkiewicz, E., & Widera, M. (2025). The past, present and future of Konin Lignite Mine in central Poland. *Geologos, 31*, 45 - 59. https://doi.org/10.14746/logos.2025.31.1.04.

Knight, H. G. (1938). New size limits for silt and clay. Soil Science Society of America Proceedings, 2, 592.

Kołodziej, B., Bryk, M., Sſowiſska-Jurkiewicz, A., Otremba, K., & Gilewska, M. (2016). Soil physical properties of agriculturally reclaimed area after lignite mine: A case study from central Poland. *Soil & Tillage Research, 163*, 54-63. https://doi.org/10.1016/j.still.2016.05.001.

Koukouzas, C. (1997). Geological map of Greece, Ptolemais sheet, scale 1:50 000 [Map]. IGME.

Krassakis, P., Pyrgaki, K., Gemeni, V., Roumpos, C., Louloudis, G., & Koukouzas, N. (2022). GIS-based subsurface analysis and 3D geological modeling as a tool for combined conventional mining and in-situ coal conversion: The case of Kardia Lignite Mine, Western Greece. Mining, 2(2), 16. https://doi.org/10.3390/mining2020016

Kriegler, F. J., Malila, W. A., Nalepka, R. F., & Richardson, W. (1969). Preprocessing of transformations and their impact on multispectral recognition. Remote Sensing of Environment, 6, 97–132.

Lefebvre, A., Sannier, C., & Corpetti, T. (2016). Monitoring urban areas with Sentinel-2A data: Application to the update of the Copernicus High Resolution Layer Imperviousness Degree. Remote Sensing, 8(7), 606. https://doi.org/10.3390/rs8070606

Lipský, Z. (2022). Mostecko: Characteristics of the area. http://www.zaniklekrajiny.cz/atlas/karakteristika-uzemi-13/151-modelova-uzemi/mostecko/charakteristika-uzemi/765-fyz-charakter-uzemi

Louloudis, G., Roumpos, C., Mertiri, E., Pavloudakis, F., & Karalidis, K. (2023). Remote Sensing Data and Indices to Support Water Management: A Holistic Post-mining Approach for Lignite Mining in Greece. International Journal of Mine Water. 42. 10.1007/s10230-023-00960-4.

Luxa, J., & North Bohemian Mines. (1997). Bílina mines: From the history of mining to the present of mining in the Bílina region. North Bohemian Mines. ISBN 80-238-1766-3.

Mach, K., Dvořák, Z., Boršiová, J., Vaníková, A., & Vaník, J. (2022). *Radovesice dump*. Bílina Natural Science Society. ISBN 978-80-905739-5-6.

Mahmood, M. R., Abrahem, B. I., Jumaah, H. J., Alalwan, H. A., & Mohammed, M. M. (2025). Monitoring drought in large lakes in Iraq using remote sensing and the Normalized Difference Water Index (NDWI). *Results in Engineering*, *25*, 103854.

Main-Knorn, M., Pflug, B., Louis, J., Debaecker, V., Müller-Wilm, U., & Gascon, F. (2017). Sen2Cor for Sentinel-2. *Proceedings of SPIE*, *10427*, 1042704. https://doi.org/10.1117/12.2278218

McFeeters, S. K. (1996). Use of the Normalized Difference Water Index (NDWI) in delineating open water features. *International Journal of Remote Sensing*, *17*(7), 1425–1432. https://doi.org/10.1080/01431169608948714

Montanarella, L. (2013). *LUCAS topsoil survey: Methodology, data and results* [Technical report]. European Commission, Joint Research Centre.

Musiałek, M., Szwaja, A., Kania, M., Pierzchała, Ł., Janson, E., Łabaj, P., Rehor, M., Schmid, P., Roumpos, C., Louloudis, G., Mertiri, E., & Servou, A. (2024). *Document on classification of ecosystem degradation including of degraded land maps* (REECOL Deliverable D3.1). KOMAG. https://reecol.komag.eu/wp-content/uploads/2024/06/REECOL_D3.1_Document-on-classification-of-ecosystem-degradation-including-of-degraded.pdf

Mzid, N., Pignatti, S., Huang, W., & Casa, R. (2021). An analysis of bare soil occurrence in arable croplands for remote sensing topsoil applications. *Remote Sensing*, *13*(3), 474. https://doi.org/10.3390/rs13030474

Papadopoulos, C., Gekaa, C., Pavloudakis, F., Roumpos, C., & Andreadou, S. (2015). Evaluation of the soil quality on the reclaimed lignite mine land in West Macedonia, Greece. *Procedia Earth and Planetary Science, 15*, 928–932.

Parastatidis, D., Mitraka, Z., Chrysoulakis, N., & Abrams, M. (2017). Online global land surface temperature estimation from Landsat. *Remote Sensing*, *9*(12), 1208. https://doi.org/10.3390/rs9121208

Paulo, A. (2008). Przyrodnicze ograniczenia wyboru kierunku zagospodarowania terenów pogórniczych [Natural constraints on the choice of post-mining land use direction]. *Gospodarka Surowcami Mineralnymi*, *24*(2/3).

Pavloudakis, F., Roumpos, C., Karlopoulos, E., & Pagouni, C. (2026). Social impacts of mining: Extending the literature review findings in the case of the lignite mines in Western Macedonia, Greece. *Land*. https://doi.org/10.3390/land15050867

Pike, R. J., Evans, I. S., & Hengl, T. (2009). Geomorphometry: A brief guide. *Developments in Soil Science*, *33*, 3–30.

Pratiwi, P., Narendra, B., Siregar, C., Turjaman, M., Hidayat, A., Rachmat, H., Mulyanto, B., Maharani, R., Rayadin, Y., Prayudyaningsih, R., Wira, T., , Y., Prematuri, R., Susilowati, A., Rahmonov, O., Ozkowski, J., & Kłys, G. (2021). Managing and Reforesting Degraded Post-Mining Landscape in Indonesia: A Review. *Land*. https://doi.org/10.3390/land10060658.

Radovesice spoil heap – an example of successful reclamation under 21st-century conditions. (2022). *Brown Coal Newsletter*, *2022*(2), 3–18.

Řehoř, M. (2007). *Reclamation of land affected by lignite mining with focus on the creation of anthropogenic soil profiles* [Doctoral dissertation, VŠB – Technical University of Ostrava, Faculty of Mining and Geology].

Řehoř, M., Schmidt, P., Hamerla, A., Kruczek, M., Pierchała, L., Bezak, B., Szwaja, A., Musialek, M., Lamot, A., Kamenik, M., Bert, V., & Roumpos, C. (2024). *Document on identification and characteristics of post-mining rehabilitation schemes* (REECOL Deliverable D3.2). KOMAG.

https://reecol.komag.eu/wp-content/uploads/2024/08/REECOL_D3.2_Document-on-identification-and-characteristics-of-postmining-rehabilitation-schemes-1.pdf

Řehoř, M., Tichá, I., & Königová, M. (2025). Soil dysfunctions at sites in the Most Basin. VUHU.

Rikimaru, A., Roy, P. S., & Miyatake, S. (2002). Tropical forest cover density mapping. *Tropical Ecology*, *43*(1), 39–47.

Roumpos, C., Pavloudakis, F., & Agioutantis, Z. (2023). A sustainability approach to optimize the closure of continuous surface lignite mines. In *Yearbook of sustainable smart mining and energy: Technical, economic and legal framework* (Vol. 2). Springer. https://doi.org/10.1007/978-3-031-41873-0_3

Rouse, J. W., Haas, R. H., Schell, J. A., & Deering, D. W. (1973). Monitoring vegetation systems in the Great Plains with ERTS. In *Third ERTS Symposium, NASA SP-351* (Vol. 1, pp. 309–317). NASA.

Salas, E., & Kumaran, S. (2023). Hyperspectral Bare Soil Index (HBSI): Mapping soil using an ensemble of spectral indices in machine learning environment. *Land*, *12*(7), 1375. https://doi.org/10.3390/land12071375

Šarapatka, B. (2014). *Pedology and soil protection*. Palacký University in Olomouc. ISBN 978-80-244-3736-1.

Servou, A., Paraskevis, N., Roumpos, C., & Pavloudakis, F. (2023). A geospatial analysis model for the selection of post mining land uses in surface lignite mines: Application in the Ptolemais mines, Greece. *Sustainability, 15*(19), 14388. https://doi.org/10.3390/su151914388

Simonson, R. W. (1993). Soil color standards and terms for field use: History of their development. In J. M. Bigham & E. J. Ciolkosz (Eds.), *Soil color* (Vol. 31). Soil Science Society of America. https://doi.org/10.2136/sssaspecpub31.c1

Skłodowska, B., & Widera, M. (2021). Vegetation response to environmental changes based on palynological research on the Middle Miocene lignite at the Jóźwin IIB open-cast mine (Konin region, central Poland). *Annales Societatis Geologorum Poloniae*. https://doi.org/10.14241/asgp.2021.07.

Soil Survey Staff. (1951). *Soil survey manual* (USDA Handbook No. 18). U.S. Department of Agriculture.

Strand, G.-H. (2022). Accuracy of the imperviousness density of the high-resolution Copernicus layer (HRL IMD) assessed by point sampling in pixels. *Remote Sensing*, *14*(15), 3589. https://doi.org/10.3390/rs14153589

Swinnen, E., Toté, C., Tavares, J. L., & Lacaze, R. (2021). Copernicus global land service NDVI continuity with Sentinel-3 data. In *2021 IEEE International Geoscience and Remote Sensing Symposium IGARSS* (pp. 6731–6734). IEEE.

Taloor, A. K., Manhas, D. S., & Kothyari, G. C. (2021). Retrieval of land surface temperature, normalized difference moisture index, normalized difference water index of the Ravi basin using Landsat data. *Applied Computing and Geosciences*, *9*, 100051. https://doi.org/10.1016/j.acags.2020.100051

University of Minnesota Soil Judging Team. (2014, September 11). *The historical development of the USDA textural triangle*. University of Minnesota Soil Judging Team Blog. https://umnsoilsteam.blogspot.com/2014/09/the-historical-development-of-usda.html

Vaudour, E., Gholizadeh, A., Castaldi, F., Saberioon, M., Borůvka, L., Urbina-Salazar, D., Fouad, Y., Arrouays, D., Richer-de-Forges, A. C., Biney, J., Shipped, J., & van Wesemael, B. (2021). Sentinel-2 image capacities to predict common topsoil properties of temperate and Mediterranean agroecosystems. *Remote Sensing of Environment*, *251*, 112–114.

Wachocki, R., Chomiak, L., Klęsk, J., Maciaszek, P., Urbański, P., Widera, M., & Zieliński, T. (2025). Geological peculiarities from the Konin Lignite Mine, central Poland: An overview. *Geologos, 31*, 31 - 43. https://doi.org/10.14746/logos.2025.31.1.03.

Whitney, M. (1911). *The use of soils east of the Great Plains region* (USDA Bureau of Soils Bulletin No. 78). U.S. Department of Agriculture.

Widera, M., Dziamara, M., Klęsk, J., & Wachocki, R. (2024). Four in one: a new crevasse-splay complex in the middle Miocene of central Poland. *Annales Societatis Geologorum Poloniae*. https://doi.org/10.14241/asgp.2024.04.

Wood, J. (1996). *The geomorphological characterisation of digital elevation models* [Doctoral dissertation, University of Leicester].

Annex 1 Legend of the Geological Map for the Most Basin (ČSG)

Geologická mapa 1 : 50 000

Tektonické linie GeoČR50

- zlom zjištěný
- zlom předpokládaný
- zlom zakrytý
- pokles zjištěný
- mylonitizace

Horniny GeoČR50

kvartér

KENOZOIKUM

KVARTÉR

- 1 navážka, halda, výsypka, odval
- 3 vytežené prostory
- 2033 výplavový kužel
- 4 nivní sediment
- 5 nivní sediment
- 6 nivní sediment
- 7 smíšený sediment
- 2061 sediment deluvioeolický
- 8 karbonát sladkovodní
- 9 slatina, rašelina, hnilokal
- 10 hlína, písek, štěrk
- 12 písčito-hlinitý až hlinito-písčitý sediment
- 13 kamenitý až hlinito-kamenitý sediment
- 14 hlinito-kamenitý, balvanitý až blokový sediment
- 34 suťový kužel, osyp
- 15 navátý písek
- 16 spraš a sprašová hlína
- 17 spraš a sprašová hlína
- 19 sprašová hlína
- 20 sediment deluvioeolický
- 22 písek, štěrk
- 23 sediment fluviální
- 35 písek, štěrk
- 2459 písčité štěrky
- 24 písek, štěrk
- 26 písek, štěrk
- 2067 písek, štěrk
- 2068 písek, štěrk
- 25 písek, štěrk
- 2069 písek, štěrk
- 2070 písek, štěrk
- 2071 písek, štěrk
- 2072 písek, štěrk
- 2073 písek, štěrk
- 2074 písek, štěrk
- 2075 písek, štěrk
- 2076 písek, štěrk
- 2077 písek, štěrk
- 2078 písek, štěrk
- 36 nevytříděné štěrky
- 27 písek, štěrk
- 28 písek, štěrk
- 31 písek, štěrk
- 38 jíl, písek, štěrk
- 48 karbonát sladkovodní (vápenec, travertin, pramenit, pěnovec

NEOGÉN–KVARTÉR

- 51 písčitá eluvia

kvartér - terciér

KENOZOIKUM

NEOGÉN–KVARTÉR

- 39 štěrk
- 49 písek, štěrk

terciér

podkrušnohorské pánve a přilehlé vulkanické hornatiny

KENOZOIKUM

NEOGÉN

- 62 písčité štěrky
- 63 písčité štěrky mrazové provířené
- 64 písčité štěrky
- 65 křemence, křemenné krusty
- 66 vypálené jíly, porcelanity
- 67 písčité štěrky
- 77 jíly, písky, písčité jíly
- 74 hnědé uhlí, uhelné jíly
- 76 písky
- 79 uhlí, jílovité uhlí, jíly, písky
- 2038 uhlí
- 81 jíly, písčité jíly
- 84 vápnité jíly, vápence
- 85 vulkanoklastika s polohou karbonátu
- 86 jíly, písky, redeponovaný vulkanogenní materiál
- 92 fluviální písčité štěrky

93	písky, jíly, štěrkopísky
94	písčité štěrky
96	cyprisové jílovce a písčitá facie: šterčíky, štěrky (čankovské písky)
97	jílovce, jíly, pelokarbonáty, písky
98	uhlí, jíly, slojová pásma Antonín a Anežka
2042	sodalitický fonolit
2043	sodalitický fonolit

PALEOGÉN

89	tufy, redeponovaná pyroklastika, jíly, uhelné jíly, písčité jíly, pelosiderity
2034	písky, jíly
260	sediment. klastika a tufity s diatomity a uhlím
103	pískovce, křemence, slepence, písky, štěrkopísky, uhelné proplástky, jíly, lokalně u Podbořan křemencové krusty
90	šedé, rudohnědé jíly, bělavé písky, křemence, písčité jíly

TERCIÉR (PALEOGÉN-TERCIÉR)

258	tufity, ojedinele s polohami diatomitu a nebo uhelných sedimentů
100	jílovce, uhelné proplástky, tufity, písky, pelosiderity
101	vulkanity nečleněné
102	uhlí, jíly slojového pásma Josef
272	vápencové vložky ve vulkanoklastikách
277	křemence
157	fosilní zvětraliny vulkanitů nerozlišené
164	trachyty a sodalitické trachyty
185	bazanit autometamorfovaný
186	bazanit pikritický
192	olivinické foidity autometamorfované
194	ol. melaanalcimit
197	ol. biotitický analcimit
201	ol. leucitit, ol. 'apoleucitit'
212	tefrit autometamorfovaný
215	nef.- analcimický a analc.- nefelinický tefrit
219	foidit autometamorfovaný
221	nefelinit s melilitem
222	analcimický nefelinit leukokratní
224	nefelinity a 'leucitity'
226	analcimit s.s.
227	analcimit aglutinovaný nebo brekciovitý
228	nefelinický analcimit (se sodalitem)
231	mikro)theralit, (mikro)essexit bazaltoid.. typu, theralit
232	trachybazalty, mikroessexity trachytoid. typu
233	syenogabbro (žilné)
235	analcim., apoleucit., sodalitické tefrity a trachybazalty
246	trachybazaltická až trachytoidní subvulk. brekcie
247	trachytoidní subvulk. brekcie místy s maarovými sedimenty
248	roztocká trachytoidní subvulk. brekcie s proniky (pseudo)trachytu
255	pyroklastické napadávky doupovského centra
256	uloženiny bahenních proudu (lahary)
257	kontaktne metamorfované tufy a tufity
264	vulkanoklastika (strezovské souvrství)
265	vulkanog.- sedimenty smíšené, epiklastika (novosedelské s.)
266	alkalické lamprofyry a semilamprofyry
267	tmavé žilné horniny
268	světlé žilné horniny

relikty sladkovodního terciéru

KENOZOIKUM

NEOGÉN

60 písky

130 štěrky, písčité štěrky, písky s vložkami jílů

131 písčité štěrky a písky, ojediněle s bloky křemenných pískovců a vložkami jílů

TERCIÉR (PALEOGÉN-TERCIÉR)

124 zvětraliny, kamenito-jílovitá až jílovitá rezidua předkvartérního povrchu

podkrušnohorské pánve a přilehlé vulkanické hornatiny, rozptýlené alkalické vulkanity

KENOZOIKUM

TERCIÉR (PALEOGÉN-TERCIÉR)

160 trachytoidy nerozlišené

161 trachyty

162 amfibolický trachyt

165 trachyty a sodalitické trachyty s nefelínem

166 fonolit

167 sodalitický fonolit

169 bazaltoidy nerozlišené

170 silne alterované (autometamorfované) bazaltoidy

176 olivinický melilitický nefelinit

183 alk. ol. bazalt - bazanit - limburgit

187 analcimický, 'apoleucitický' bazanit

188 anlc.-nefelinický až nef.-analcimický bazanit ('apoleucitický')

191 sodaliticko-nefelinický bazanit

193 olivinický nefelinit, analcimit a 'leucitit'

195 ol. analcimit až analc. bazanit

196 ol. nef. analcimit až ol. analc. nefelinit ('apoleucitický')

200 ol. sodalitit až ol. sodalitický nefelinit

203 limburgit, plagioklásový limburgit

207 analcimický tefrit až bazanit

210 alk. bazalt - tefrit - augitit (analcimický)

211 alk. bazalt s.s.

213 sodalitický, analc.-sod., sod.-analc., analcimický tefrit

214 analcimický, 'apoleucitický' tefrit

218 bezolivinické foidity (s.s.) nerozlišené

220 nefelinit s.s.

225 analcimit, nef.analcimit až analcim. nefelinit

229 sodalitit s.s. (noseanit, hauyinit)

230 nefelinický sodalitit s melilitem

236 trachybazalt

237 trachyandezit (až andezit: 25-34, 35-12)

241 subvulkanické a explozivní brekcie

242 subvulkanické bazaltoidní brekcie

243 subvulkanické bazaltoidní brekcie

245 bazalt. až trachybaz. subvulk. brekcie místy s maarovými sedimenty

249 vulkanoklastika nerozlišená

250 pyroklastika nerozlišená

251 vulkanoklastika bazaltoidních hornin

254 hrubozrnné tufy oherských center

156 vulkanity nerozlišené

TERCIÉR (PALEOGÉN-TERCIÉR)–KVARTÉR

179 olivinický bazaltoid nerozlišený

rozptýlené alkalické vulkanity

KENOZOIKUM

TERCIÉR (PALEOGÉN-TERCIÉR)

163 sodalitický trachyt
168 fonolity a sodalitické fonolity
184 bazanity nerozlišené
205 alk. olivinický bazalt až alk. bazalt s.s.
208 nefelinit s olivínem (sodalitický)
217 sodal.-nefelinický tefrit až trachybazalt
223 sodalitický nefelinit
239 nefelinit, fonolit, vulkanoklastika (Loucná)
270 výskyty vulkanitu nejisté lokalizace, žíly neurč. Směru

KENOZOIKUM–MEZOZOIKUM

KŘÍDA–TERCIÉR (PALEOGÉN-NEOGÉN)

174 ol. melilitický nefelinit (sodalitit) až ol. nef.melilitit, ol. sodalitický melilitit

terciér

KENOZOIKUM

NEOGÉN

181 alk.ol.bazalt, nef. bazanit, ol. nefelinit

TERCIÉR (PALEOGÉN-TERCIÉR)–KVARTÉR

182 alkalický olivinický bazalt
189 nefelinický bazanit
198 olivinický nefelinit
209 bezolivinické bazaltoidy nerozlišené
252 pyroklastika bazaltoidních (príp. trachybazaltických) hornin
253 tufy a tufity (místy biotitické nebo s biotitem, príp. s pyroxenem)

křída

česká křídová pánev

MEZOZOIKUM

KŘÍDA

278 pískovce arkózovité, jílovité až křemenné s vložkami a závalky jílovců a prachovců
280 jílovce vápnité až slínovce s vložkami vápnitých pískovců
281 vápnité jílovce, slínovce, vápnité prachovce
282 kontaktně metamorfované vápnité jílovce, slínovce a prachovce
285 prachovce vápnité, glaukonitické
287 silicifikované jílovité vápence a slínovce
290 vápnité jílovce, slínovce a prachovce, podřadně vložky jílovitého vápence
291 vápence jílovité a slínovce (střídání)
295 pískovce křemenné, podřízeně štěrčíkovité pískovce
296 pískovce vápnito-jílovité, glaukonitické
297 slínovce s polohami či konkrecemi vápenců, rytmy či cykly slínovec - vápenec (jílovito vápnité prachovce -lužický vývoj)
302 slínovce, vápnité jílovce místy písčité
303 pískovce křemenné, podřízeně štěrčíkovité
304 pískovce vápnité silně glaukonitické
306 pískovce vápnito-jílovité
307 písčité slínovce až jílovce spongilitické, místy silicifikované (opuky)
310 vápence biodetritické
313 jílovce, prachovce, pískovce křemenné, jílovité, glaukonitické, slepence
315 pískovce křemenné, jílovité, glaukonitické
316 vápence biodetritické
317 jílovce, uhelné jílovce, uhlí, prachovce, pískovce, slepence

KENOZOIKUM–MEZOZOIKUM

2240 fosilní zvětraliny (nerozlišeno)

svrchní karbon a perm

středočeské a západočeské mladší paleozoikum

PALEOZOIKUM

KARBON

415 hnědočervené jílovce, prachovce, pískovce, arkózovité pískovce, slepence
417 arkózovité pískovce, valounové pískovce a slepence, hnědočervené jílovce, prachovce až jemně zrnité pískovce

421 jílovce, aleuropelity, pískovce, ark. pískovce až arkózy, lokálne uhelné slojky (kounovské sousl.)

430 pestrobarevné pískovce, arkózovité pískovce, valounové pískovce a slepence, jílovce, prachovce

441 převážně červenohnědé pískovce, slepence, prachovce a jílovce

435 valounové pískovce, slepence, pískovce, prachovce, jílovce, uhelné sloje,brekcie, tufy a tufity

krušnohorské mladší paleozoikum

PALEOZOIKUM

PERM

410 slepence, pískovce, prachovce, porfyrové tufity

KARBON

411 arkózy, pískovce, jílovce, prachovce, uhelná sloj

vulkanity permokarbonu

PALEOZOIKUM

KARBON

1608 ryolitový tuf a ignimbrit

1609 ryolitový ignimbrit

1610 ryolitový ignimbrit

1611 ryolitový až trachytový ignimbrit až ryolit

1612 ryolitový ignimbrit

1613 ryolitový ignimbrit

1614 ryolit

1615 pískovce ,prachovce, jílovce a vulkanoklastika s tenkými cernouhelnými slojkami

KARBON–PERM

2049 ryolit

lužická (západosudetská) oblast

magmatity lužické oblasti

PROTEROZOIKUM–PALEOZOIKUM

NEOPROTEROZOIKUM, KAMBRIUM–ORDOVIK

844 granodiorit

krkonošsko-jizerské krystalinikum

PALEOZOIKUM

KAMBRIUM

851 metadiabaz, zelená břidlice

854 fylit

PROTEROZOIKUM

NEOPROTEROZOIKUM

863 metadroba, fylit

sasko-durynská oblast (saxothuringikum)

sasko-vogtlandské paleozoikum

PALEOZOIKUM

KAMBRIUM–ORDOVIK

1381 fylit

1388 kvarcit

1390 kvarcit

1391 fylit a fylitická břidlice

1393 fylit

1394 fylit

1395 fylit

2029 kontaktně metamorfované fylity

2030 kontaktně metamorfované fylity

2058 fylity

2059 fylity

1396 fylit

1397 fylit

1399 fylit

1400 fylit

1401 fylit až kvarcitický fylit

1402 kvarcitický fylit

1403 kvarcitický fylit až kvarcit

2031 kontaktně metamorfovaný kvarcitický fylit až kvarcit

2032 kontaktně metamorfovaný kvarcitický fylit až kvarcit
1404 kvarcit
1405 kvarcit
1407 fylit
1410 svor
1411 svor
1412 rohovec
1413 rohovec
1414 erlan
1415 skarn
1416 zelená břidlice, albit-epidotický amfibolit
1417 amfibolit
1418 amfibolit

slavkovské krystalinikum

PALEOZOIKUM

KARBON

1469 migmatit s prevahou ortosložky až hybridní granit

SPODNÍ PALEOZOIKUM

1484 ortorula

PROTEROZOIKUM

NEOPROTEROZOIKUM

1447 pararula
1453 pararula
1456 pararula
1457 pararula
1459 pararula

krušnohorsko-smrčinské krystalinikum

PALEOZOIKUM

SPODNÍ PALEOZOIKUM

1470 metagranit
1471 metagranit až metagranodiorit
1472 ortorula
1474 ortorula
1475 ortorula
1477 ortorula
1478 ortorula
1479 metaaplit ci metapegmatit
1483 ortorula

PROTEROZOIKUM–PALEOZOIKUM

NEOPROTEROZOIKUM–SPODNÍ PALEOZOIKUM

1423 svor
1424 svor
2057 svory
1426 svor
2056 svory
1427 svor
1428 svor
1429 svor
1432 metadroba
1434 vetšinou kvarcitický svor
1436 kvarcitický svor s prechody do kvarcitu
1438 svor
1439 svor a pararula svorového vzhledu
1440 svor a pararula svorového vzhledu
1441 svor a pararula svorového vzhledu
1442 pararula svorového vzhledu
1443 pararula svorového vzhledu
1444 pararula svorového vzhledu
1454 erlan (Ca-skarn)
1465 skarn
2466 svor

SPODNÍ PALEOZOIKUM

1480 ortorula
1481 ortorula
1482 ortorula
1485 ortorula
1486 ortorula
1487 ortorula
1488 granulit, granulitová rula
1489 eklogit

PROTEROZOIKUM

NEOPROTEROZOIKUM

1445 pararula
1448 pararula
1449 pararula
1450 pararula
1451 pararula
1461 metakonglomerát, metakonglomerátová rula
1462 krystalický vápenec a krystalický dolomit
1463 erlan-pararulový stromatit
1467 amfibolit
1468 amfibolit

krušnohorský pluton

PALEOZOIKUM

KARBON

- 1594 žilný křemen
- 1595 pegmatit, aplopegmatit
- 1596 aplit a aplitický granit
- 1597 granitový porfyr
- 1598 granitový porfyr mladší
- 1599 granitový porfyr až syyenitový porfyrit mladší
- 1600 lamprofyr nerozlišený
- 1601 granodioritový porfyrit
- 1602 dioritový porfyrit
- 1603 granit
- 1604 granit
- 1605 granit
- 1606 granitový porfyr
- 1607 ryolit
- 1616 greisenizovaný granit až greisen
- 1617 albitit, feldspatit
- 1618 granit
- 1620 granit
- 1621 středně zrnitý granit
- 1622 granit
- 1623 granit
- 1624 granit
- 2274 granit
- 1625 granit
- 1627 granit
- 1628 granit
- 1629 granit
- 1631 granit
- 1632 granit
- 1633 granit
- 1634 granit
- 1635 granit
- 1636 granit
- 1637 granit
- 1638 granit
- 1639 granit
- 1640 granit
- 1641 granit
- 1642 granit
- 1643 granit
- 1644 granit
- 1645 granit
- 1647 granit
- 1652 granit až granodiorit
- 1653 granit až granodiorit
- 1655 granodiorit až diorit
- 1656 křemenný diorit až diorit
- 1658 diorit
- 1659 gabrodiorit, biotitit
- 1661 kaolinizovaný granit
- 2465 dolerit

krušnohorsko-smrčinské krystalinikum, chebsko-dyleňské krystalinikum

PROTEROZOIKUM–PALEOZOIKUM

NEOPROTEROZOIKUM–SPODNÍ PALEOZOIKUM

- 1421 svor
- 1430 svor
- 1433 svor, obcas kvarcitický
- 1435 kvarcitický svor
- 1437 kvarcit

SPODNÍ PALEOZOIKUM

- 1490 serpentinit

krušnohorsko-smrčinské krystalinikum, slavkovské krystalinikum

PROTEROZOIKUM

NEOPROTEROZOIKUM

- 1446 pararula
- 2044 pararula
- 1452 kvarcitická pararula
- 1458 pararula
- 1464 erlan
- 1466 amfibolit

neznámé stáří

- 1646 granit

mariánsko-lázeňský bazický komplex

PALEOZOIKUM

KARBON–DEVON

- 1363 tremolitická a aktinolitická břidlice
- 1364 serpentinit
- 1365 amfibolit
- 1366 amfibolit
- 1367 amfibolit
- 1369 amfibolit

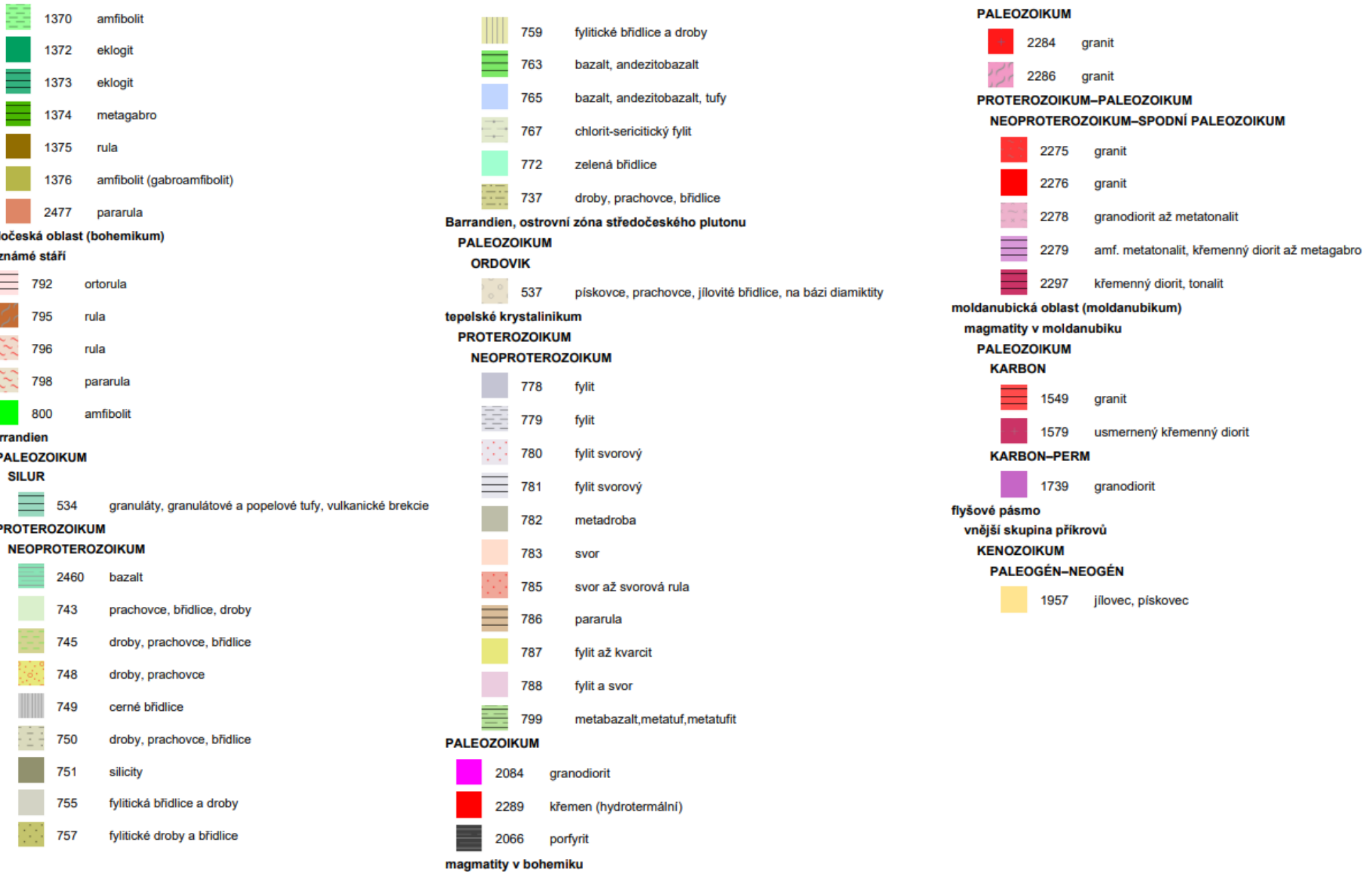
1370 amfibolit
1372 eklogit
1373 eklogit
1374 metagabro
1375 rula
1376 amfibolit (gabroamfibolit)
2477 pararula
středočeská oblast (bohemikum)
neznámé stáří
792 ortorula
795 rula
796 rula
798 pararula
800 amfibolit
Barrandien
PALEOZOIKUM
SILUR
534 granuláty, granulátové a popelové tufy, vulkanické brekcie
PROTEROZOIKUM
NEOPROTEROZOIKUM
2460 bazalt
743 prachovce, břidlice, droby
745 droby, prachovce, břidlice
748 droby, prachovce
749 cerné břidlice
750 droby, prachovce, břidlice
751 silicity
755 fylitická břidlice a droby
757 fylitické droby a břidlice
759 fylitické břidlice a droby
763 bazalt, andezitobazalt
765 bazalt, andezitobazalt, tufy
767 chlorit-sericitický fylit
772 zelená břidlice
737 droby, prachovce, břidlice
Barrandien, ostrovní zóna středočeského plutonu
PALEOZOIKUM
ORDOVIK
537 pískovce, prachovce, jílovité břidlice, na bázi diamiktity
tepelské krystalinikum
PROTEROZOIKUM
NEOPROTEROZOIKUM
778 fylit
779 fylit
780 fylit svorový
781 fylit svorový
782 metadroba
783 svor
785 svor až svorová rula
786 pararula
787 fylit až kvarcit
788 fylit a svor
799 metabazalt,metatuf,metatufit
PALEOZOIKUM
2084 granodiorit
2289 křemen (hydrotermální)
2066 porfyrit
magmatity v bohemiku
PALEOZOIKUM
2284 granit
2286 granit
PROTEROZOIKUM–PALEOZOIKUM
NEOPROTEROZOIKUM–SPODNÍ PALEOZOIKUM
2275 granit
2276 granit
2278 granodiorit až metatonalit
2279 amf. metatonalit, křemenný diorit až metagabro
2297 křemenný diorit, tonalit
moldanubická oblast (moldanubikum)
magmatity v moldanubiku
PALEOZOIKUM
KARBON
1549 granit
1579 usmernený křemenný diorit
KARBON–PERM
1739 granodiorit
flyšové pásmo
vnější skupina příkrovů
KENOZOIKUM
PALEOGÉN–NEOGÉN
1957 jílovec, pískovec

Annex 2 Legend of the Pedological Map for the Most Basin (ČSG)

Půdní mapa 1 : 50 000

Půdní typologie (TKSP ČR)

LIm	litozem modální
LIb'	litozem modální eutrofní
LIc	litozem karbonátová
LIhr	litozem hořečnatá
RNm	ranker modální
RNa'	ranker modální mesobazický
RNb'	ranker modální eutrofní
RNn	ranker melanický
RNnb'	ranker melanický eutrofní
RNk	ranker kambický
RNkd'	ranker kambický oligotrofní
RNka'	ranker kambický mesobazický
RNkb'	ranker kambický eutrofní
RNkz'	ranker kambický podzolovaný
RNkd	ranker kambický dystrický
RNz	ranker podzolový
RNd	ranker dystrický
RNs	ranker suťový
RNsb'	ranker suťový eutrofní
RNt	ranker litický
RNtx'	ranker litický hořečnatý
RNtb'	ranker litický eutrofní
RNtz'	ranker litický podzolovaný
RZm	rendzina modální
PRm	pararendzina modální
PRn	pararendzina melanická
PRk	pararendzina kambická
PRkg	pararendzina kambická oglejená
PRg	pararendzina oglejená
PRv	pararendzina vyluhovaná
PRt	pararendzina litická
PRp	pararendzina pelická
RGm	regozem modální
RGg	regozem oglejená
RGgr	regozem oglejená arenická
RGq	regozem glejová
RGc	regozem karbonátová
RGy	regozem psefitická
RGr	regozem arenická
RGp	regozem pelická
FLm	fluvizem modální
FLk	fluvizem kambická
FLky	fluvizem kambická psefitická
FLa	fluvizem antropická
FLg	fluvizem oglejená
FLq	fluvizem glejová
FLqc	fluvizem glejová karbonátová
FLc	fluvizem karbonátová
FLcr	fluvizem karbonátová arenická
FLy	fluvizem psefitická
FLr	fluvizem arenická
KOm	koluvizem modální
SMm	smonice modální
CCm	černice modální
CCo'	černice modální zrašelinělá
CCf	černice fluvická
CCfq	černice fluvická glejová
CCfc	černice fluvická karbonátová
CCq	černice glejová
CCqc	černice glejová karbonátová
CCc	černice karbonátová
CCr	černice arenická
CEm	černozem modální
CEl	černozem luvická
CElx	černozem luvická černická
CEx	černozem černická
CExc	černozem černická karbonátová
CExr	černozem černická arenická
CEc	černozem karbonátová
CEcp	černozem karbonátová pelická
CEcr	černozem karbonátová arenická
CEve	černozem vertická
CEp	černozem pelická
CEr	černozem arenická
SEm	šedozem modální
HNm	hnědozem modální

HNl	hnědozem luvická
HNlg	hnědozem luvická oglejená
HNg	hnědozem oglejená
HNp	hnědozem pelická
LUm	luvizem modální
LUg	luvizem oglejená
LUd	luvizem dystrická
LUr	luvizem arenická
KAe'	kambizem modální eubazická
KAb'	kambizem modální eutrofní
KAgb'	kambizem oglejená eutrofní
KAqb'	kambizem glejová eutrofní
KAtb'	kambizem litická eutrofní
KAsb'	kambizem rankerová eutrofní
KAm	kambizem modální
KAg'	kambizem modální slabě oglejená
KAx'	kambizem modální hořečnatá
KAl	kambizem luvická
KAlb'	kambizem luvická eutrofní
KAlg	kambizem luvická oglejená
KAlgb'	kambizem luvická oglejená eutrofní
KAf	kambizem fluvická
KAge'	kambizem oglejená eubazická
KAg	kambizem oglejená
KAq	kambizem glejová
KAv	kambizem vyluhovaná
KAp	kambizem pelická
KAt	kambizem litická
KAs	kambizem rankerová
KAa'	kambizem modální mesobazická
KAla'	kambizem luvická mesobazická
KAlga'	kambizem luvická oglejená mesobazická
KAga'	kambizem oglejená mesobazická
KAqa'	kambizem glejová mesobazická
KApa'	kambizem pelická mesobazická
KAgpa'	kambizem oglejená pelická mesobazická
KAta'	kambizem litická mesobazická
KAsa'	kambizem rankerová mesobazická
KAd'	kambizem modální oligotrofní
KAd	kambizem dystrická
KAdz'	kambizem dystrická podzolovaná
KAdx'	kambizem dystrická hořečnatá
KAgd	kambizem oglejená dystrická
KAgdx'	kambizem oglejená dystrická hořečnatá
KAqd	kambizem glejová dystrická
KAdp	kambizem dystrická pelická
KAdt	kambizem dystrická litická
KAdtx'	kambizem dystrická litická hořečnatá
KAds	kambizem dystrická rankerová
KAdsz'	kambizem dystrická rankerová podzolovaná
KAdr	kambizem dystrická arenická
KAdrz'	kambizem dystrická arenická podzolovaná
KAr	kambizem arenická
KArz'	kambizem arenická podzolovaná
KAra'	kambizem arenická mesobazická
KAgr	kambizem oglejená arenická
KAy	kambizem psefitická
KAgy	kambizem oglejená psefitická
PEm	pelozem modální
PEg	pelozem oglejená
KPm	kryptopodzol modální
KPg	kryptopodzol oglejený
KPq	kryptopodzol glejový
KPt	kryptopodzol litický
KPs	kryptopodzol rankerový
KPr	kryptopodzol arenický
KPgr	kryptopodzol oglejený arenický
PZm	podzol modální
PZz'	podzol modální železitý
PZo'	podzol modální zrašelinělý
PZk	podzol kambický
PZo	podzol histický
PZg	podzol oglejený
PZgh'	podzol oglejený humózní
PZgo'	podzol oglejený zrašelinělý
PZgr	podzol oglejený arenický
PZq	podzol glejový
PZqo'	podzol glejový zrašelinělý


PZqo podzol glejový histický
PZs podzol rankerový
PZr podzol arenický
PZro' podzol arenický zrašelinělý
PGm pseudoglej modální
PGa' pseudoglej modální mesobazický
PGl pseudoglej luvický
PGk pseudoglej kambický
PGkdu' pseudoglej kambický dystrický mělce umbrický
PGkp pseudoglej kambický pelický
PGq pseudoglej glejový
PGqu' pseudoglej glejový mělce umbrický
PGd pseudoglej dystrický
PGdk' pseudoglej dystrický kaolinický
PGp pseudoglej pelický
SGm stagnoglej modální
SGo' stagnoglej modální zrašelinělý
SGo stagnoglej histický
GLm glej modální
GLa' glej modální mesobazický
GLo' glej modální zrašelinělý
GLz' glej modální podzolovaný
GLx' glej modální hořečnatý
GLf glej fluvický
GLfo' glej fluvický zrašelinělý
GLfo glej fluvický histický


GLe glej povrchový
GLq glej akvický
GLk glej kambický
GLo glej histický
GLor glej histický arenický
GLr glej arenický
ORfi organozem fibrická
ORme organozem mesická
ORsa organozem saprická
ORq organozem glejová
AN antropozem
ANg antropozem oglejená
ANsk antropozem skeletovitá
vodní plochy